ATTRIBUTION OF ATLANTIC MULTIDECADAL VARIABILITY TO EXTERNAL FORCING, INTERNAL VARIABILITY, AND WEATHER NOISE

by

Ioana Colfescu

A Dissertation
Submitted to the
Graduate Faculty
of
George Mason University
in Partial Fulfillment of
The Requirements for the Degree
of
Doctor of Philosophy
Climate Dynamics

Committee:

_____	Dr. Edwin K. Schneider, Dissertation Director
_____	Dr. Timothy DelSole, Committee Member
_____	Dr. David M. Straus, Committee Member
_____	Dr. Tim Sauer, Committee Member
_____	Dr. Paul Schopf, Department Chair
_____	Dr. Donna M. Fox, Associate Dean, Office of Student Affairs and Special Programs, College of Science
_____	Dr. Peggy Agouris, Dean, College of Science
Date: _____	Summer Semester 2014 George Mason University Fairfax, VA

Attribution of Atlantic Multidecadal Variability to External Forcing, Internal Variability, and Weather Noise

A Dissertation submitted in partial fulfillment of the requirements for the degree of Doctor of Philosophy at George Mason University

by

Ioana Colfescu
Master of Mathematics
Bucharest University, Faculty of Mathematics and Computer Science, 2007
Bachelor of Science
Bucharest University, Faculty of Mathematics and Computer Science, 2005

Director: Edwin K. Schneider, Professor
Department of Climate Dynamics

Summer Semester 2014
George Mason University
Fairfax, VA

DEDICATION

This thesis is dedicated to my family and to my grandma, Meme , who would have been happier than words can say to see this thesis.

I also thank so much to my colleagues for sharing their culture and time with me. I feel lucky and privileged to have learned so much about how other people live and how they see life. In particular I thank to Abheera for these years full of 'moments of friendship' and to Sara for a wonderful summer together (not yet over) and for the potatoes salads.

My biggest gratitude goes equally to my family, my advisor and to Penny who's kindness and warmth made me so many times feel at home in America.

I thank my parents for teaching me to never give up no matter what, by showing their own example and their immense capacity to go on despite of anything: multumesc mama si Pape ! I thank to my sister for being there for me when I needed it despite of everything.

I thank with all my heart to my husband for five long years of unconditional love across states and continents, ships and planes, for support, help with my scripts, patience with my tantrums and for loving me as I'm: ti amo moltissimo!

I thank to my advisor for teaching me to be curious and find a proof before believing anything – this is useful anywhere in life not only in my scientific career. I also thank my advisor for never discouraging me thus helping me gain the self confidence I didn't have, for the moments I spent with his family and at his concerts – these all were wonderful experiences which cured my home sickness and made me feel happy.

I thank to America for all the invaluable life lessons I learned while living here and for the good contributions it had in my transformation and personal growth in the last years. I'm quite sure there is no other place in the world where you can learn so much about diversity, with all the facets that this word could imply. These PhD years are for sure some of the best years of my life!

ACKNOWLEDGEMENTS

I thank so much to all my Professors at George Mason for always so enthusiastically sharing their knowledge with me. I thank a lot to Dr. Klinger and Dr. Straus for being really supportive with my transition to the PhD student life in my first year and for convincing me not to give up in those first months. It really worth not giving it up ! I thank a lot to Dr. Del Sole for being such a wonderful example of the fact that it is possible to teach a Statistics class and make students love it. I thank to Dr. Shukla for encouraging me in the last months of my PhD and for sharing some of his life experience with us students and to Dr. Krishnamurthy for the useful experience I gained while working under his supervision in Trieste in the summer of 2012. I also thank a lot to Dr.Sauer for being part of my committee and for his curiosity and patience in understanding the Atmospheric Sciences related topics in my thesis. I'm very grateful to Dr. Kirtman and Dr. Dughong Ming for the substantial help regarding the technical/modeling part of my thesis.

I don't have enough words to thank to my advisor for all he thought me, for his infinite patience, understanding and kindness and above all for teaching me to always be honest about the results of my research and that I do science to find answers not to proof things which I believe in or imagine with no proof: Professor, it was an honor, a privilege and a joy to work with you and my biggest hope for the future is to be a Scientist like you are!

The contributions of Colfescu et al. (2013) were supported by NSF grants ATM-0653123 and AGS-1137902. Schneider was also supported by NSF grants ATM-0830068 and ATM-0830062, NOAA grant NA09OAR4310058, and NASA grant NNX09AN50G. NASA provided computer resources on the Pleiades computer, and resources were also provided by the NCAR CISL. Our work is part of the CLIVAR International Climate of the Twentieth Century Project (C20C). Data analyses and plotting were done using GrADS.

TABLE OF CONTENTS

LIST OF TABLES

LIST OF FIGURES

LIST OF EQUATIONS

LIST OF ABBREVIATIONS

500 hPa height	Z500
Antarctic Oscillation	AAO
Arctic Oscillation	AO
Atlantic Meridional Overturning Circulation	AMOC
Atlantic Multidecadal Variability	AMV
Atmospheric General Circulation model	AGCM
Atmospheric Model Intercomparison Project 3	AMIP3
Center for Ocean Land Atmosphere	COLA
Community Atmosphere Model 3	CAM3
Community Climate System Model Ensemble	CGCM_ens
Community Climate System Model version 3	CCSM3
Coupled General Circulation Model	CGCM
Coupled Model Intercomparison Project 3	CMIP3
December January February	DJF
El Nino Southern Oscillation	ENSO
Empirical Orthogonal Function	EOF
Hadley Center Atmospheric Model 3	HadAM 3
Interactive Ensemble	IE
Interactive Ensemble - Coupled General Circulation Model	IE-CGCM
Intergovernmental Panel for Climate Change	IPCC
Max Plank Institute	MPI
Max Plank Institute Atmospheric General Circulation Model version 5	ECHAM 5
National Centers for Environmental Prediction	NCEP
North Atlantic	NA
North Atlantic Oscillation	NAO
North Pacific	NP
Ocean General Circulation Model	OGCM
Pacific Decadal Oscillation	PDO
Pacific North American Pattern	PNA
Principal Component	PC
Probability Density Function	PDF
Schneider and Fan 2007	SF2007
Sea Level Pressure	SLP
Sea Surface Temperature	SST
Southern Hemisphere	SH
Special Report Emission Scenario A1B	SRES A1B

Standard Deviation ..... SD
Total Heat Flux ..... THF
Total Heat Flux Noise ..... THFN
Two Meter Air Temperature ..... TS
Weather Noise ..... WN

ABSTRACT

ATTRIBUTION OF ATLANTIC MULTIDECADAL VARIABILITY TO EXTERNAL FORCING, INTERNAL VARIABILITY, AND WEATHER NOISE

Ioana Colfescu, Ph.D.

George Mason University, 2014

Dissertation Director: Dr. Edwin K. Schneider

Detection of externally forced climate change and attribution of the causes of the externally forced and internally generated climate variability during the last century are the central scientific issues of current climate science and the subject of important controversies. This thesis systematically addresses fundamental problems in detection and attribution.

A novel three-tier model ensemble strategy is developed and applied in the model world to address these issues. At the top tier, an ensemble of CGCMs with the same external forcing applied to each member is used to separate the results from each ensemble member into the externally forced and internally generated components. At the second tier, an ensemble of atmospheric GCMs (AGCM) with each member forced by the same SST, taken from a member of the CGCM ensemble, is used to separate the atmospheric variability in that CGCM member into SST-and-externally-forced and weather noise

components. The third tier, uses an interactive ensemble version of the CGCM, in which the AGCM is replaced by an AGCM ensemble, so that atmospheric weather noise in the CGCM is suppressed. Controlled experiments forcing the interactive ensemble with the atmospheric noise diagnosed in the AGCM ensemble tier isolate the role of the weather noise in generating the internal SST variability found in the CGCM Ensemble tier.

The strategy is employed to examine three important detection and attribution issues. The first is why the AGCM ensemble forced by observed SST does not simulate the observed 20^{th} century sea level trends in the Indian Ocean. It has been suggested that this is because of an intrinsic failure of the AGCM Ensemble to correctly represent the SST forced response of the coupled system. The results show that the AGCM and CGCM ensembles are consistent with each other, and suggest that the failure to simulate the observed trends is due to model bias rather than coupling.

Next, the spatial and temporal properties of the weather noise obtained from the CGCM and AGCM ensembles are examined in a preliminary fashion. This is the first attempt to document these properties. The temporal and spatial structures of the weather noise in the CGCM and AGCM simulations are very similar. The temporal structures of the noise spectra are white at timescales larger than approximately 5 months, although the noise is temporally non-Gaussian, while the spatial structures resemble those of major modes of observed climate variability. No change is detected between the statistical properties of the noise in the early and late 20^{th} century.

The Atlantic Multidecadal Variability (AMV) sea surface temperature is decomposed into externally forced and internally generated components using the CGCM ensemble, and the weather noise contribution to the internal component is isolated using the AGCM ensemble and interactive ensemble. The AMV has a strong contribution from the external 20th century forcing. The internal AMV variability is primary forced by the weather noise, but other sources of internal variability are also important. An important contribution to the internal AMV is associated with the internal variability of the oceanic Atlantic Meridional Overturning Circulation, and this contribution is distinct from the weather noise forced component.

PREFACE

This thesis systematically addresses several problems in the attribution of climate variability using the same model framework. Attribution determines the reasons for climate variability, and is a central focus of climate research today. Understanding of the causes of the changing climate since the industrial revolution, and particularly the role of human society, is necessary in order to decide on the efficacy and consequences of actions proposed to address future anthropogenic climate change.

Low frequency climate variability can be classified as either externally forced or internally generated. The externally forced variability is due to both natural and anthropogenic causes. The natural causes include changes in the incoming solar radiation, changes in the atmospheric composition due to volcanoes, and changes in the configuration of the continents and oceans due to geologic processes. Anthropogenic causes include changes in the atmospheric composition and distribution of vegetation due to human influences. Internally generated climate variability has as main sources the intrinsic internal variability of the atmosphere or ocean components, which can be thought of as noise internal to the individual components, and coupled processes involving intrinsically coupled interactions among the components.

Figure INCR1 shows how the total Sea Surface Temperature (SST) variability can be

divided into externally forced and internally generated parts, and the internally generated part can be divided into atmospheric weather noise, ocean weather noise and coupled variability.

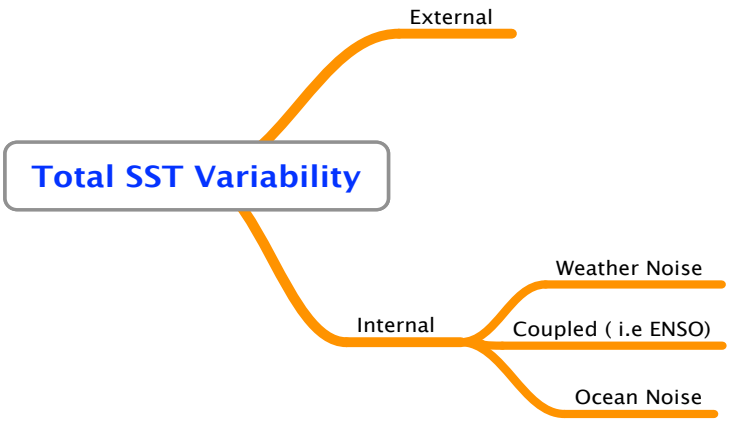

Figure P1. Separation of SST variability into externally forced and internal variability

In the real world, when using observations, isolating these sources is very difficult since there is only one realization of reality. However, using climate models allows us to perform experiments to separate the externally forced climate change from internally generated variability, and to isolate the role of atmospheric noise in forcing internal variability.

A novel three-tier model ensemble attribution strategy is developed and applied in the model world. At the top tier, an ensemble of CGCMs with the same external forcing applied to each member is used to separate the results from each ensemble member into the externally forced and internally generated components. The sources of SST variability

in each ensemble member follow the structure of Fig. P1. By averaging across ensemble members, the internally generated variability in the individual realizations can be sufficiently diminished so that the average ensemble mean represents the model's response to external forcing. Once the externally forced response is obtained, it is subtracted from each model run to find the contribution from internal variability.

At the second tier, an ensemble of atmospheric GCMs (AGCM) with each member forced by the same SST, taken from a member of the CGCM ensemble, is used to separate the atmospheric variability in that CGCM member into SST-and-externally-forced and weather noise components. The weather noise component contributes to the internal SST variability as indicated in Fig. P1, while the SST and externally forced component participates in the both External and Coupled SST variability.

The third tier uses an interactive ensemble version of the CGCM, in which an AGCM ensemble replaces the AGCM, so that atmospheric weather noise forcing of the SST is suppressed, and, as seen from Fig. P1, leaving only coupled processes and oceanic noise as sources for internal variability. Controlled experiments forcing the interactive ensemble with the atmospheric weather noise diagnosed in the AGCM ensemble tier isolate the role of the weather noise in generating the internal SST variability found in the CGCM Ensemble tier.

Using the experimental design described above three main problems of study are addressed. In the **first Chapter** we study why the AGCM ensemble forced by observed

SST does not simulate the observed 20th century sea level trends in the Indian Ocean. It has been suggested that this is because of an intrinsic failure of the AGCM Ensemble to correctly represent the SST forced response of the coupled system.Results from tier 1 and tier 2 simulations show that the AGCM and CGCM ensembles are consistent with each other, and suggest that the failure to simulate the observed trends is due to model bias rather than coupling.

The **second Chapter** investigates in a preliminary fashion the spatial and temporal properties of the weather noise obtained from the tier 1 CGCM and tier 2 AGCM ensembles. This is the first attempt to document these properties, and is relevant to understanding the mechanisms by which climate change affects extreme events. The temporal structure of the noise is consistent with white noise for annual and longer periods, although the probability density functions (PDF) are not Gaussian. No change is detected between the statistical properties of the noise in the early and late 20th century, so that changes in extreme events can be attributed primarily to changes in the mean rather than the noise.

In the **third Chapter** the Atlantic Multidecadal Variability (AMV) sea surface temperature is decomposed into externally forced and internally generated components using the CGCM ensemble. The weather noise studied in the second part is used in the tier 3 interactive ensemble to isolate the weather noise contribution to the internal component (Fig. P1). The AMV has a strong contribution from the external 20th century forcing. The internal AMV variability is primary forced by the weather noise, but other sources of internal variability are also important. An important contribution to the

internal AMV is associated with the internal variability of the oceanic Atlantic Meridional Overturning Circulation, and this contribution is distinct from the weather noise forced component.

CHAPTER 1 : CONSISTENCY OF 20TH CENTURY SEA LEVEL PRESSURE TRENDS AS SIMULATED BY A COUPLED AND UNCOUPLED GCM

ABSTRACT

A coupled CGCM, and an uncoupled AGCM forced with the Sea Surface Temperature (SST) and external forcing of the coupled model, simulate similar two-meter air temperature (TS) trends and also similar sea level pressure (SLP) trends for the latter half of the 20th century. This suggests that the inability of atmospheric models forced by observed SST and external forcing to reproduce observed SLP trends in the Indian Ocean could be due to model bias rather than lack of coupling. The internally generated TS trend in the CGCM is found to be small in comparison to the externally forced component. Intrinsic atmospheric noise explains most of the CGCM's internally generated high latitude SLP trend, while in low latitudes the response of the SLP trend to the internally generated SST trend is important.

1.1 Introduction

Sea level pressure (SLP) trends, as simulated by AGCMs forced by observed SST and estimated external forcing for the latter half of the 20th century, do not agree with observed trends, particularly in the Indian Ocean. Using the HadAM3 AGCM Copsey et al. (2006) found that the simulated SLP trend in the Indian Ocean was negative while the observed trend was positive (Vecchi et al. 2006). The explanations they suggested for this

result were that either the SST forced AGCMs have different responses in comparison to coupled models (even with the same SST), or that the AGCM has a biased response to SST forcing. Although Deser et. al. (2012) found better agreement between the observed DJF tropical SLP trend and the corresponding trend in the CAM3 AGCM, differences from the observed trend appear to have same sign and similar structure as in Copsey et al. (2006). Meng et al. (2011) found a similar inconsistency from forcing the ECHAM5 AGCM with observed SST, although they found no inconsistency in a perfect model comparison (AGCM forced by the SST simulated by the CGCM) using the MPI CGCM and the ECHAM5 AGCM. The impact of observed SST trends in the latter half of 20th century on the trends of 500 hPa height (Z500) in Northern Hemisphere winter was analyzed by Schneider. et.al. (2003) using an ensemble of simulations made with the COLA AGCM. The study found that intra-ensemble Z500 trend variability, attributable to intrinsic atmospheric noise, was comparable to the SST forced trend in high latitudes. The SST forced Z500 trend was attributed primarily to forcing by the tropical SST trend.

The mechanism of the internal variability of the SLP trend in CGCM simulations has been addressed by Deser et al. (2012) using CCSM3. The externally forced trend and its internal variability were evaluated from an ensemble of future climate simulations The main source of intra-ensemble variability in the CGCM simulated SLP trends depended on the region of study – in middle and high latitudes the structure of the coupled variability was similar to that of the intrinsic atmospheric variability, while in the tropics the structures in the coupled and uncoupled simulations differed in the tropics, demonstrating an important role for ocean-atmosphere coupling.

Recently Chen.et.al (2013) examined the similarity between the SST forced response in a CGCM current climate control simulation (constant external forcing), and the AGCM component of the CGCM, forced by the CGCM-generated SST in the Community Climate System Model version 3 (CCSM3). The differences they found between the CGCM and AGCM fields were attributed to forcing of SST by intrinsic atmospheric noise in the CGCM, but not the AGCM, essentially as described by the simple model of Barsugli and Battisti (1998).

If coupled and uncoupled models have different responses with/to the same SST, as suggested by Copsey et al. (2006) and if the SST forced AGCM does not correctly simulate the atmospheric response due to lack of coupling, conclusions drawn using SST forced AGCM simulations could be in error. Our study examines the issue of whether atmosphere-ocean coupling is essential to simulate the externally forced SLP trends, and identifies the role of intrinsic atmospheric noise in the coupled internal variability. The experiments use a perfect model framework, eliminating differences between CGCM and AGCM due to model bias and isolating the role of coupling.

1.2 Models and Methods

The experimental design and analysis extend these used by Chen et al. (2013) to include 20th century external forcing, and to examine trends in the latter half of the 20th century. The SLP trends in a CGCM and in an AGCM ensemble forced by the CGCM SST, sea ice, and external forcing are compared in a situation where uncertainty due to model bias is eliminated through the experimental design. Additionally, the design allows

attribution of the trends in the CGCM to external forcing and internally generated variability, and furthermore, for the internally generated variability to be decomposed into two components – a component where coupling to the SST internal variability is important and a noise component. The models used were the coupled model, the Community Climate System Model (CCSM3; Collins et al. 2006a), and its atmospheric component, the Community Atmosphere Model (CAM3; Collins et al. 2006b). The atmospheric model for both the coupled and uncoupled simulations had T42 spectral resolution in the horizontal and 26 levels. The ocean model configuration was an approximately 1º by 1º-horizontal grid and 40 levels.

A CGCM simulation (CONTROL) for the period 1870-1998 with prescribed 20th Century historical forcing represents the observations. Extending the approach of Chen.et.al. (2013), the results for field V in the CGCM, V_{CGCM}, are decomposed into externally forced, V_{CGCM}^{Ext}, and internally generated variability, V_{CGCM}^{Int}.

$$V_{CGCM} = V_{CGCM}^{Ext} + V_{CGCM}^{Int}$$

Equation 1.1

For this study, V represents the SLP or surface air temperature (TS) trends evaluated over the 1950-1996, the period chosen for comparison with the results of Copsey et al. (2006).

Similarly, the internally generated atmospheric variability is separated into the atmospheric response to the internally generated SST variability – coupled variability, $V_{CGCM}^{Int\ Coupled}$ - and the intrinsic atmospheric noise, V_{CGCM}^{Noise}:

$$V_{CGCM}^{Int} = V_{CGCM}^{Int\ Coupled} + V_{CGCM}^{Noise}$$

Equation 1.2

In order to estimate the externally forced trends an ensemble of four additional CCSM3 simulations with prescribed 20th Century historical external forcing was performed for the period 1870-1998. The differing initial conditions of the coupled ensemble members were obtained by choosing arbitrarily from a 500-year pre-industrial control run with external forcing fixed at 1870 levels (archived as run b30.043 in the Community Earth System Model database at the National Center for Atmospheric Research). V_{CGCM}^{Ext} is determined by

$$V_{CGCM}^{Ext} = \langle V_{CGCM_i} \rangle$$

Equation 1.3

where the subscript refers to the ith ensemble member (including CONTROL), and the brackets represent ensemble averaging. V_{CGCM}^{Int} is then found using (1) and (3) by

$$V_{CGCM}^{Int} = V_{CGCM} - V_{CGCM}^{Ext}$$

Equation 1.4

An ensemble of six AGCM simulations forced by the CONTROL SST and external forcing was made in order to decompose V_{CGCM}^{Int} into $V_{CGCM}^{Int\ Coupled}$ and V_{CGCM}^{Noise}, as well as for comparison with the CONTROL trend. We improved the consistency of the SST forcing for the AGCM ensemble compared to Chen et al. (2013) by evaluating it from the CGCM monthly ocean model output rather than from the atmospheric model output. Taking the AGCM ensemble mean, $\langle V_{AGCM_i} \rangle$, as the SST and externally forced trend, $V_{CGCM}^{Int\ Coupled}$ is found by

$$V_{CGCM}^{Int\ Coupled} = \langle V_{AGCM_i} \rangle - V_{CGCM}^{Ext}$$

Equation 1.5

Then V_{CGCM}^{Noise} is calculated from (2) and (5):

$$V_{CGCM}^{Noise} = V_{CGCM}^{Int} - V_{CGCM}^{Int\ Coupled}$$

Equation 1.6

Two statistical tests are applied to the trends. One is a two-sided t-test of the significance of the linear trend with respect to the yearly residuals from the trend (47 degrees of freedom if the the lag-1 autocorrelation of the residuals is small, a condition satisfied for the SLP). The other is a two-sided t-test of the reproducibility of the trend in the ensemble members, where the residuals are trends of the N individual ensemble members minus the ensemble mean trend (N-1 degrees of freedom) as in Deser et al. (2012). This test will be called the "reproducibility" of the trend to distinguish it from the first test.

1.3 Results

SLP_{CGCM}^{Ext} (Figure 1a) shows reproducible positive trends in the Pacific, over India, and in the midlatitude North Atlantic, and reproducible negative trends in high latitudes of both hemispheres. The tropical Indian and Atlantic Oceans have large regions of negative SLP trend, but these are reproducible only in the Indian Ocean near 15°S and in the eastern tropical North Atlantic. TS_{CGCM}^{Ext} (Figure 1c) has significant positive values over most of the globe. Compared with the observed SST trend between ±40° latitude shown by Copsey et al. (2006), the externally forced trend in CCSM3 is similar in the Indian and Atlantic Oceans, but more uniform in the Pacific and weaker in the eastern

Pacific. The internally generated variability in the CGCM ensemble, taken as the unbiased standard deviations (SD) of SLP_{CGCM_i} and TS_{CGCM_i}, Figures 1b and 1d respectively, are small in the tropics and increase with latitude. The increase is more pronounced in the case of the SLP. The increase of SD of SLP_{CGCM_i} with latitude is probably related in part to the internal atmospheric variability of NAO-like or annular modes of trend variability (Schneider et al. 2003, Deser et.al. 2012). However, these modes do not appear to be responsible for the lack of reproducibility of the SLP trends in the middle latitudes of both hemispheres because the annular mode structures are clearly seen in the externally forced response (Figure 1a), and also because the irreproducible regions occur near the nodal surfaces of the annular modes.

SLP_{CGCM} and TS_{CGCM} (Figure 2) have areas of significant trends substantially smaller than the areas of reproducible trends shown in Figure 1.

The AGCM ensemble means SLP trend, $\langle SLP_{AGCM_i} \rangle$ (Figure 3a), has a spatial structure that is similar to SLP_{CGCM} (area-weighted correlation 0.69 globally, 0.84 between ±30° latitude). $\langle SLP_{AGCM_i} \rangle$ is reproducible in regions where SLP_{CGCM} trend is significant, but also in additional regions in the North Atlantic, North Pacific and Indian Ocean and Indian subcontinent. Over land and sea ice, $\langle TS_{AGCM_i} \rangle$ (Figure 3c) increases towards higher latitudes. TS_{CGCM} (Figure 2b) and $\langle TS_{AGCM_i} \rangle$ are similar even in regions where the significance of the trend is low, as long as the trends are reproducible. $\langle SST_{AGCM_i} \rangle$ is reproducible everywhere, of course, since the SST is identical in all of the AGCM ensemble members.

The variability of the intrinsic atmospheric noise trend in the AGCM ensemble is calculated as the SD of SLP_{AGCM_i} and TS_{AGCM_i} (Figure 3b,d). SD of SLP_{AGCM_i} is smaller in the tropical and subtropical regions and increases with latitude. This increase is probably partly the result of internal atmospheric variability related to the NAO and annular modes. SD of TS_{AGCM_i} over land shows the highest values over the Euro-Asian continent, and can be attributed to internal atmospheric variability, perhaps involving land surface feedbacks, since the SST and external forcing is the same in all of the AGCM ensemble members. .

SD of $SLP^{Int}_{CGCM_i}$ (Figure 1b) and SD of SLP_{AGCM_i} (Figure 3b) have similar structures. An f-test shows that the ratio of the intra-ensemble SLP trend variability between the CGCM and AGCM is not different from one at the 10% level except for a few isolated, small regions over land.

SLP^{Noise}_{CGCM} (Figure 4a) and SLP^{Int}_{CGCM} (Figure 4b) have similar structures in middle and high latitudes, but large areas where the sign differs in low latitudes, for example in the Indian Ocean. $SLP^{Int\ Coupled}_{CGCM}$ (Figure 4c) is comparable to or larger than SLP^{Noise}_{CGCM} in low latitudes, and resembles the phase of the Southern Oscillation associated with La Nina there.

TS^{Int}_{CGCM} (Figure 4d) shows cooling in the North and western Pacific, Indian Ocean and North Atlantic and warming over North America. The pattern is associated with a La Nina like structure, with warming in the western equatorial Pacific and cooling in the east, consistent with a positive coupled feedback between $SLP^{Int\ Coupled}_{CGCM}$ and TS^{Int}_{CGCM}. The high (low) temperature centers in the North Pacific (North Atlantic) correspond to

increased (decreased) westerlies inferred from SLP_{CGCM}^{Noise}. The configuration is consistent with the internally generated SST trends in those regions being forced by the SLP noise.

1.4 Conclusions

The role of atmosphere-ocean coupling in the simulation of 1950-1996 TS and SLP trends was investigated in a perfect model setting, using coupled and SST forced simulations with specified 20th century external forcing. We found that the SLP trend of a coupled simulation was well reproduced over most of the globe by the mean trend of an AGCM ensemble forced by the SST from the coupled simulation. Our results show that the major characteristics of the trends are the response to the SST and external forcing in either the coupled or uncoupled models. While differences from the observed SLP trend over the Indian Ocean are seen both here and in the AGCM simulations of Copsey et al (2006), our results explain the error as a bias in the model, seen both with and without coupling rather than an error due to lack of coupling alone. Attribution of the trend errors to atmospheric model bias unrelated to coupling is supported by the model dependence of earlier results, i.e. the apparently better success of CAM3 in simulating the observed tropical SLP trends when forced by observed SST (Deser et al. 2012).

It is important to note that our simulations were made with a single relatively low-resolution model. The results might change in the model world or in comparison to the real world if a set of very much higher horizontal resolution climate models (e.g. Scaife et al. 2011) were used. In such a case qualitative changes in the strength of AGCM and CGCM atmospheric-ocean interactions, especially in the extratropics, should be expected

(Minobe et al. 2008). We recommend that similar perfect model experiments to those presented here be undertaken using other models, and especially high resolution coupled models, in order to determine the model dependence of the results.

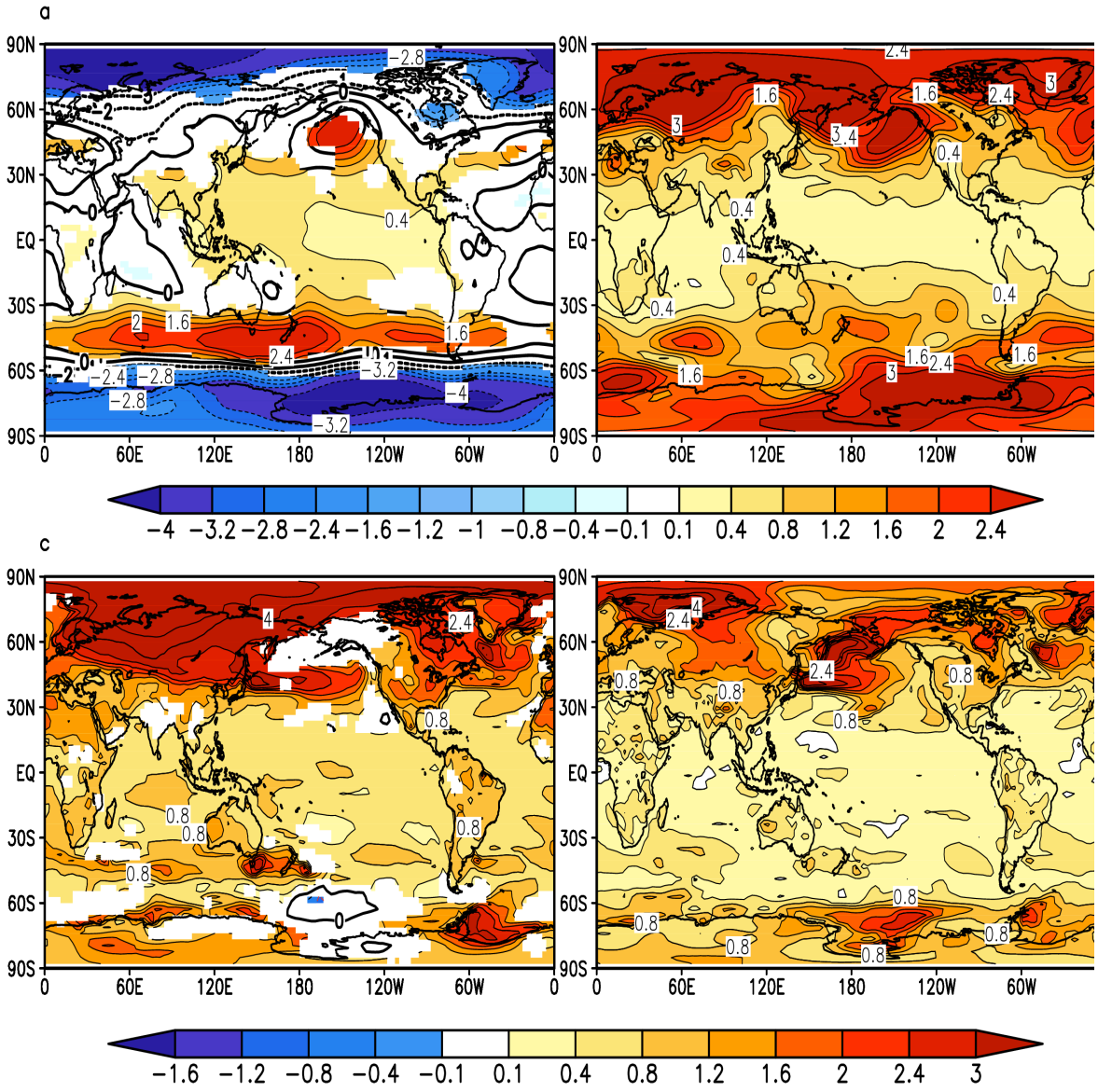

Figure 1.1 a) SLP^{Ext}_{CGCM} c) TS^{Ext}_{CGCM} for 1950-1996. Standard deviation of the trends in the CGCM ensemble for b) SLP and d) TS. Units are hPa per 100 years in a) and b), and K per 100 years in c) where the reproducibility is significant at the 10% level are shaded and other areas are plotted with contours only. Contour lines represent same level as contour shading.

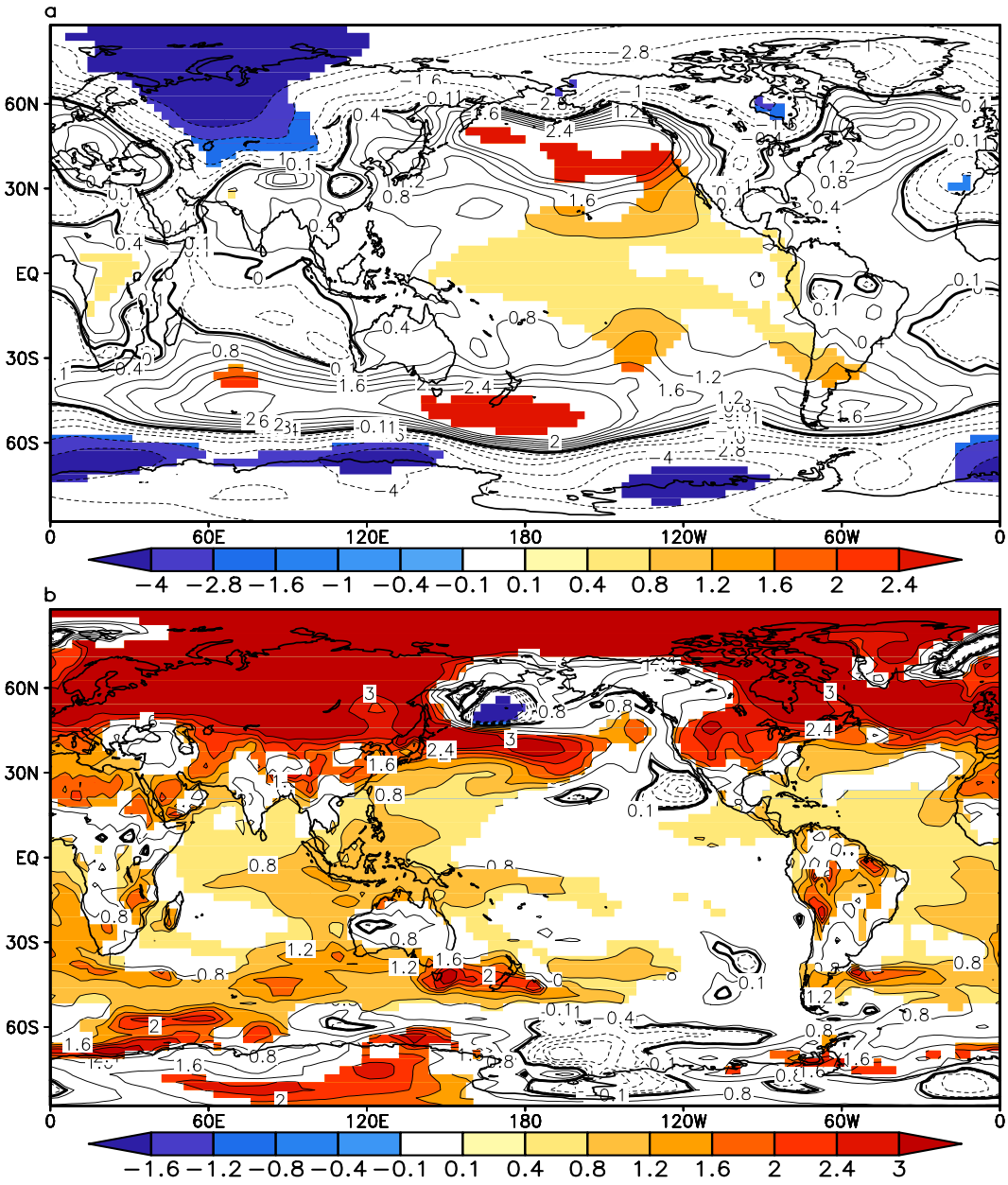

Figure 1.2 CONTROL coupled run linear trends for a) SLP (hPa century^{-1}) and b) TS (°C century^{-1}). Areas where the trend is significant at the 10% level are shaded and other areas are plotted with contours only. Contour lines represent same level as contour shading.

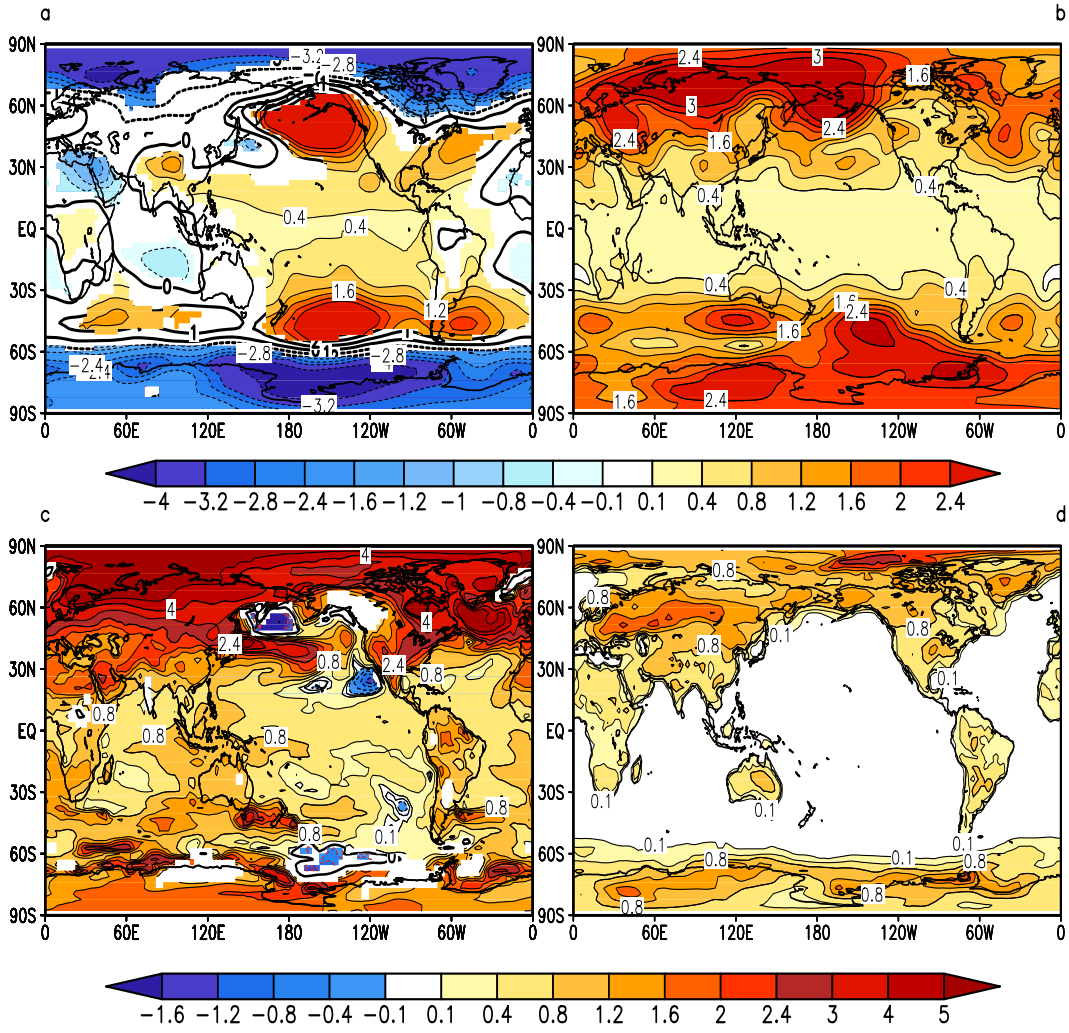

Figure 1.3 a) $\langle SLP_{AGCM_i} \rangle$, *b*) SD of SLP_{AGCM_i}, *c*) $\langle TS_{AGCM_i} \rangle$, *d*) SD of TS_{AGCM_i} for the six-member AGCM ensemble forced by the CONTROL coupled run SST. Units and significance shading as in Fig. 1 for the respective panels. Contour lines represent same levels as contour shading

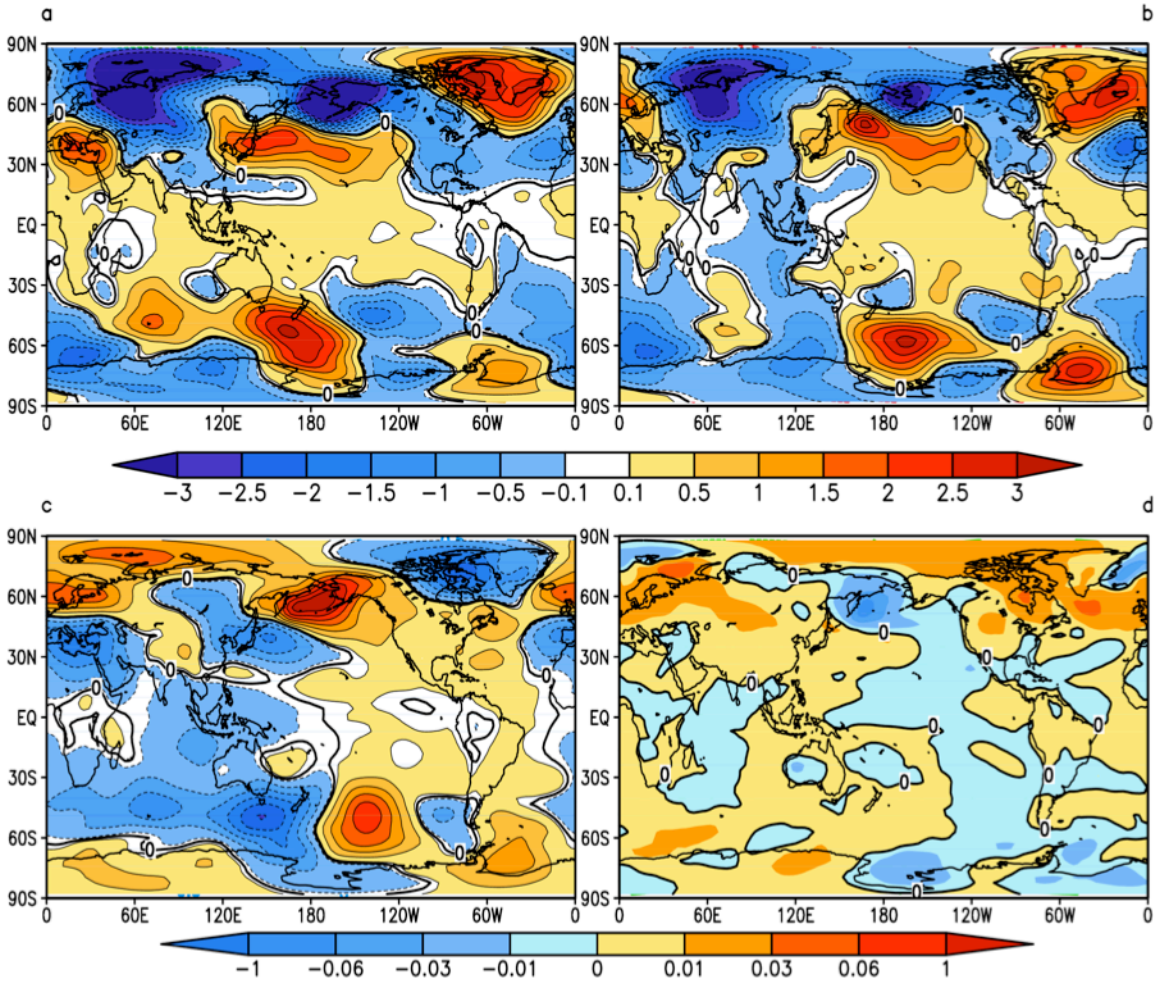

Figure 1.4 Trends in CONTROL: (a) SLP^{Noise}_{CGCM}, (b) SLP^{Int}_{CGCM} (c) $SLP^{Int\ Coupled}_{CGCM}$ (d) TS^{Int}_{CGCM}. Units (hPa century^{-1}) and upper color bar for (a)-(c), (°C century^{-1}) and lower color bar for (d). Contour lines represent same levels as contour shading.

CHAPTER 2 WEATHER NOISE CHARACTERISTICS IN A SERIES OF 20TH CENTURY CCSM3 MODEL SIMULATIONS

Abstract

Three main questions are investigated by the present study: 1) What are the statistical characteristics of model generated atmospheric weather noise? ; 2) Are these properties the same for the early and late 20th century?; 3) Are the characteristics of this noise depended on coupling between the ocean and the atmosphere? The weather noise is determined in post-industrial (1871-1998) Community Climate System Model 3 simulations by removing the SST and externally forced responses from the total fields, where the forced responses are found from atmosphere-only simulations.

The weather noise determined for the net surface heat flux is chosen for analysis. An empirical orthogonal function (EOF) analysis is performed globally, and for various regions. The spatial characteristics the noise are determined from the spatial structures of the EOFs, and by linear regressions of the SLP against the principal components (PCs), while the temporal characteristics are found from power spectra and probability density functions (PDFs) of the PCs.

Our findings show that the temporal and spatial structures of the noise in the CGCM and AGCM simulations are very similar. The temporal structures of the noise are white at timescales larger than approximately 5 months, while the spatial structures resemble

those of major modes of observed climate variability. The comparison between the probability distribution functions for the noise PCs in the early and late periods shows that the main statistical properties of the noise do not change between the two periods. However, some of the noise PDFs, especially those for global patterns, departs substantially from a Gaussian structure, with enhanced probabilities for small anomalies.

2.1. Introduction

An important role for intrinsic atmospheric noise in forcing climate variability, and in particular, SST variability, was proposed by Hasselmann (1976). That single-point model represented forcing of SST by atmospheric noise as a specified white noise heat flux, and demonstrated that the large heat capacity of the ocean filters out the high frequency and leads to a red noise SST response that resembles the spectrum of observed SST variability. Since that time, other stochastically forced single column linear models have been developed to simulate the SST response to atmospheric noise forcing. The approach has also been extended to include the use of linear stochastically forced models for prediction of ENSO SST patterns in two spatial dimensions, including Gaussian white noise forcing to represent neglected process including atmospheric noise (Penland and Magorian1993; Newman et al. 2011). The role of atmospheric noise in ENSO irregularity has been addressed with stochastically forced linear models, for example by Blanke et al. (1997), where the spatial patterns of the monthly noise were estimated by removing the signal linearly and simultaneously related to the monthly SST anomalies. However,

Barsugli and Battisti (1998) demonstrated that if the SST anomalies are forced by the atmospheric noise, which can occur only in a coupled atmosphere-ocean system, the noise and the SST anomalies will be linearly correlated, and it is therefore not appropriate to assume that the noise is uncorrelated with the SST anomalies. In AMIP simulations forced by climatological SST and constant external forcing, that is when there is are no SST anomalies, all of the simulated atmospheric variability can be thought of as intrinsic noise. In this case, a single long simulation can be used to infer the properties of the noise. Schneider and Kinter (1994) examined properties of the noise in this way in multi-century simulations with a low resolution AGCM. They identified Arctic Oscillation (AO) and Antarctic Oscillation (AAO) -like zonally symmetric modes as the leading EOFs of the global sea level pressure. Deser et al. (2012) made a 10,000 year run of the CAM3 AGCM with current day external forcing and climatological SST and used 56-year trends in variables such as SLP in this run as a null hypothesis for the detection of externally forced climate change in CGCM simulations.

A method consistent with the conceptual model of Barsugli and Battisti (1998) is used here to extract the space and time varying noise from an analysis of observations or a climate model simulation. In order to determine the noise in this situation, the SST and externally forced signal needs to be determined and removed. In the following, both the observed/analyzed and simulated fields are referred to as "observations" or "observed". The method was first described and applied by Schneider and Fan (2007). In this approach, the SST forced signal is taken to be the ensemble mean of an ensemble of atmospheric model simulations forced by the observed SST ("AMIP ensemble"; Gates et

al. 1998). The noise in the AMIP ensemble members is uncorrelated with the SST, since the SST is specified and is not affected by the surfaces fluxes from the atmosphere. The noise in an AMIP ensemble member is also uncorrelated with the noise in the other ensemble members. The ensemble averaging then reduces the noise in the AMIP ensemble, but preserves the SST forced signal. The observed noise is then found by removing the time-dependent SST forced signal; however, only the noise in the observations can be related to the observed SST.

Results from applying the AMIP ensemble method to determining the intrinsic atmospheric noise have been reported by Schneider and Fan (2007), where the observations were generated by a long coupled model simulation with constant external forcing using the COLA CGCM; by Fan and Schneider (2012), where the observations were from the 1950-2000 NCEP reanalysis (Kalnay et al. 2006); by Chen et al. (2013) and Chen and Schneider (2014), where it was argued that noise in the a long control simulation of the CCSM3 CGCM was indistinguishable from those the in the associated AMIP ensemble members, and that only the noise in the CGCM was consistent with noise forcing of the SST; and by Colfescu et al. (2013), where the method was extended to evaluating the noise in CCSM3 simulations with estimated 20th century external forcing.

The studies described above did not examine the spatial or temporal properties of the noise in much detail. Here, having gained some confidence that the methodology produces meaningful results, we examine the statistical properties of the intrinsic

atmospheric noise in 20th century CCSM3 CGCM simulations more closely. In particular, the analysis is directed towards comparing the inferred properties of the presumably somewhat realistic CGCM noise to the noise properties are assumed in simplest stochastically forced models:

- Is the noise temporally white, and if not, how can the temporal properties be characterized?
- Is the noise spatially white, and if not, how can the spatial patterns be characterized?
- Is the noise temporally Gaussian, and if not, how can the deviations be characterized?
- Is the noise influenced by the changing external forcing, and if so, how?

In addition, we apply the analysis to a more refined comparison between the statistical properties of the noise in the coupled and uncoupled simulations, since it is a prerequisite for the validity of the method that the noise statistics in the coupled and uncoupled simulations should be indistinguishable.

2.2 Methodology

The experimental design is the same as the one used in Colfescu et al. 2013. The models are the coupled model, the Community Climate System Model (CCSM3) (Collins et al., 2006a) and its atmospheric component, the Community Atmosphere Model (CAM3) (Collins et al., 2006b). As in Colfescu et al. 2013 a CGCM simulation

(CONTROL) covering the 1870-1998 period and including prescribed 20th century historical forcing represents the observations. In order to calculate the weather CGCM weather noise an ensemble of six 20th century externally forced AGCM with SST forcing prescribed from the CONTROL is performed. The SST and externally forced response is defined as the ensemble mean of the atmosphere-only model simulations. The coupled CGCM weather noise (CGCM WN) is obtained by removing the forced component from the observations (CONTROL). The weather noise for each AGCM ensemble is obtained by removing the externally forced component from each AGCM member (AGCM WN).

Monthly weather noise for CGCM WN and AGCM WN are calculated for total heat flux (THF). In order to study the regional differences in weather noise patterns four regions are used as described by Table 1: global domain (GD), Equatorial Pacific (EP), North Pacific (NP) and North Atlantic Ocean (NA).

Table 2.1 Index Names and Areas

Index Name	Index Area
Global Domain(GL)	60S to 60N and 0-360
Equatorial Pacific (EP)	-10S to 10N and 90E to 100W
North Pacific (NP)	20N to 60N and 90E to 100W
North Atlantic Ocean (NA)	20N to 60N and 90W to 40E

First, the main modes of variability of the weather noise are studied by calculating the Empirical functions (EOFs) (Storch and Zwiers 1999, Jolliffe 2000) and the corresponding principal components for THF WN. The first 3 EOFs and the associated PCs are used in this analysis. A spectral analysis of the PCs is performed in order to study the noise behavior in time. The significance of the spectrum is evaluated in each case using a Markov "red noise" confidence spectrum with upper and lower confidence curves of 5% and 99% respectively. In order to study the linkage of the noise with main climate variability modes, regressions of the Sea Level Pressure (SLP) anomalies of noise fields onto the standardized noise PCs are performed for each of the regions listed in Table 2.1. A two-sided t-test of the significance of the linear regressions with respect to the monthly (1536 degrees of freedom if the lag-1 autocorrelation of the residuals is small, a condition satisfied for the monthly data) is performed.

Probability density functions (PDFs) of the nonstandardized noise PCs are studied in order to assess changes in the noise patterns between the first and last 30 years of the period of study. A normal distribution is generated and compared to the PDFs of the standardized noise PCs in order check the similarity of the noise statistics to those of a Gaussian curve.

2.3 Results

2.3.1 Total Heat Flux EOF Analysis

An EOF analysis was carried out for the CGCM WN and AGCM WN THF monthly values, for each of the regions defined by the indexes in Table 2.1.

The global patterns for the first 3 leading EOFs of the noise THF in the CGCM and AGCM are shown Fig. 2.1 left and right.

The first EOFs explain - 6.5% and 6.1 % - for the CGCM and AGCM respectively. The CGCM EOF1 shows an east to west tripole pattern across the Atlantic Ocean with a small variation in the meridional direction. The centers are the Gulfstream, 40N and about 45N in East Atlantic along the European Coast. A wave like pattern with alternating centers of opposite sign, from West to East is seen in the Pacific Ocean. This pattern starts with a center over Kuroshio region and ends with an opposite sign center along the Western US coast. A very similar structure can be seen in the AGCM EOF1 (Fig. 2.1a right). Neither the AGCM nor the CGCM patterns show much variability below 10N and the Southern Hemisphere.

The second EOF (Fig. 2.1b right and left) explains approximately 5% of the total variance for both the AGCM and CGCM and, as in the case of the first EOF, show little to no variability in the Southern Hemisphere. In the Pacific Ocean a dipole like pattern, extended on the meridional direction is seen. In the Atlantic Ocean a tripole pattern, with positive to negative alternative centers can, be seen from South to North. The tripole centers cover a much wider area than the first EOF, extends to both higher and lower latitudes and seem to be propagating from the tropical region. .

The third EOF of is also similar between AGCM and CGCM. The Atlantic AGCM weather noise EOF3 (Fig.2.1 c) shows an east-west dipole in the Atlantic. The third EOF of the is characterized by low to no variability in the Southern Hemisphere, a wave live structure over the Pacific Ocean, and a tripole structure in the Atlantic.

To study if such patterns occurred randomly the THF weather noise EOFs were compared to EOFs of a randomly generated timeseries with an average and standard deviation same to the noise (not shown). The comparison showed that in the northern hemisphere, in particular in the North Pacific and North Atlantic the spatial structures seen in Figure 3.1 cannot be found in the randomly generated weather noise..
The global patterns have substantial amplitudes in both the Atlantic and Pacific. Thus the noise in the two oceans appears to be tied together somehow.

2.3.2 Regional EOFs of Total Heat Flux

The spatial patterns of EOFs 1-3 for the North Atlantic CGCM and AGCM weather noise are shown in Fig. 2.2. Again, all three EOFs for the AGCM and CGCM are very similar. The pattern of EOF1 is in agreement with that of global EOF2 (Fig. 2.1ba), showing a meridional tripole over the North Atlantic with centers around the subpolar and subtropical gyres. The second EOF (Fig. 2.2b) shows also a dipole pattern in the zonal direction with one of the centers in the Western Atlantic and the other in the central and Eastern Atlantic. The third EOF is a tripole with zonal-meridional orientation, in both the CGCM and AGCM (Fig. 2.2 c). The Pacific regional EOF1 (Fig. 2.3a) shows in both the CGCM and AGCM a pattern with a negative center over the western Pacific Ocean, North of 20N and with opposite sign in Eastern Pacific. The presence of a PDO like pattern here is in agreement with Newman et al. 2003 which shows that the PDO is caused by a "reddening" of the El Niño–Southern Oscillation (ENSO) combined with

stochastic atmospheric – weather noise – forcing. Pacific EOF1 is similar to the Pacific structure in global noise EOF2.

The second NP EOF, Fig.2.3 b looks like a southward propagating wavelike structure in both AGCM and CGCM, similar to the Pacific structure in global EOF3. The third EOF (Fig. 2.3 c) shows a wave train with four centers arcing across the Pacific, similar to the structure in global noise EOF1

The EOFs in Fig. 2.4 show the main modes of noise variability found for the ENSO region. Again, CGCM and AGCM noise are indistinguishable. EOF1 (Fig. 2.4 a) has a monopole pattern concentrated over the western Pacific EOF2 is a north-south dipole centered on the equator and concentrated west of the dateline. EOF 3 has an east-west dipole structure more west of the dateline more or less symmetric about the equator.

The EOF pattern analysis shows that the AGCM and CGCM noise EOFs are almost identical globally and regionally, and that the noise in the Atlantic and Pacific may have some connection.

2.3.4 Regressions of noise SLP on noise THF PCs

In order to have an understanding of what atmospheric structures are linked to the noise heat flux variability shown by the EOF patterns, regressions of the SLP noise anomalies onto the standardized THF noise PCs were carried out. For all the three global patterns, those found in the CGCM and AGCM correspond very well. Wave like patterns can be seen in the Pacific and both north-south and east-west oriented structures in the Atlantic.

For the southern hemisphere there is little to no variability pattern thus, the SH hemisphere patterns are not shown.

The SLP regressions on the North Atlantic THF noise PCs (Fig. 2.6) show that most of the Pacific variability is suppressed and a west to east wave like pattern can be seen in the Atlantic. As expected from the global EOFs, the SLP regressions on the regional Pacific THF noise index (Fig. 2.7) show a wave like patterns for all 3 PCs, both CGCM and AGCM. The regressions of SLP on the noise PCs of the "ENSO" region (Fig. 2.8) shows very low to no variability in the first PC (Fig 2.8 a, d) and wave like patterns in PC2 and PC3 in both models.

Thus, the regressions of the SLP onto the THF noise PCs show that the THF noise in the first three modes of EOF decomposition is associated to small-scale SLP structures.

2.3.3 Noise SLP patterns

An EOF analysis was also made of the noise SLP in the CGCM and AGCMs. The first; three global patterns for the CGCM (Fig. 2.9) and AGCM (Fig. 2.10) are very similar. The first pattern has centers of opposite sign in the Pacific and Polar Regions and has some resemblance to the Arctic Oscillation pattern. The second pattern is a southern hemisphere analog first pattern and resembles the Antarctic Oscillation. The third pattern has centers of opposite sign in the North Atlantic and the polar region and resembles the North Atlantic Oscillation. These patterns are having much larger spatial scale than those associated with the THF.

The regressions of noise SLP for CGCM and AGCM on the NA PCs indexes are shown in Fig. 2.11 and 2.12 respectively, and those on the NP PCs shown in Figs. 2.13 and 2.14.

CGCM and AGCM patterns closely correspond in both cases. The patterns are again much larger scale than those associated with the first the THF patterns, and are localized to the regions that the EOF decomposition was performed in.

The regressions on ENSO regions noise SLP PCs (Fig 2.15 and 2.16) have patterns that have large projections globally, in both hemispheres. The first pattern is symmetric about the equator with large projections, representing a mass exchange between low and high latitudes. The second is more or less antisymmetric about the equator, and the third represent redistribution of mass between the North Polar Region and the rest of the globe.

2.3.4 Power spectrum Analysis

A power spectral analysis of the first three PCs for the THF noise has been carried out and the power spectra for AGCM PC1 from a single member of the AGCM ensemble is shown in Fig 2.17 and those for CGCM in Fig. 2.18. The significance of the spectrum is evaluated in each case using a Markov "red noise" confidence spectrum with upper and lower confidence curves of 5% and 95% respectively. There is a significant peak in the AGCM spectrum at about 39 month period in NA and another at about 100 month in GL, but these are do not appear in the spectra of the other AGCM members. Then for periods longer than 1 year the AGCM spectra are generally consistent with the temporal white noise. The CGCM ENSO spectrum has significant peaks at 63 and 30 months. We have not yet examined the other CGCM runs to see if these peaks are robust. Otherwise, the CGCM spectra are consistent with white noise.

2.3.5 Probability Density Functions

The probability density function (PDF) provides a probabilistic description of the PCs , in particular the tails are critical in quantifying the density of occurrence of extreme values. The PDF shape, displacements and tails are investigated in order to study if:

1) A shift in the noise standard deviation took place between 2 different periods – 1871-1901 and 1951 -1998 – and second if the noise PDFs are in agreement with a randomly generated (Gaussian) curve i.e if the PDF of the noise PCs are approximately symmetric and bell-shaped. In order to study the changes between the 2 different periods the non-standardized PCs were used while for comparison to the Gaussian curve the standardized PCs were used.

For both periods the PDF was calculated, for every region of study. In Fig 2.19 the PDFs for the CGCM are shown. Although there are differences, the PDFs do not show substantial changes between the two periods.

The standardized PDFs are shown in Fig 2.21, in red for 1871-1901, in blue 1951-1991 and in black for the Gaussian curve.

Briefly, the properties for assessing if a PDF is a Gaussian are:

- The highest point occurs at $x = \sigma$.
- It is symmetric about the mean.
- It has inflection points at $\mu-\sigma$ and $\mu+\sigma$.
- The curve is asymptotic to the horizontal axis at the extremes.
- The total area under the curve equals one.

For the PDFs analyzed (Fig 2.20 and Fig 2.21) the last condition is satisfied – namely the area under the curves is approximately 1 by construction. The curves are asymptotic to the horizontal axes for the extreme values however there is no perfect symmetry of the curves around the mean and the inflection points are not at $\mu-\sigma$ and $\mu+\sigma$.

When comparing to a Gaussian, both CGCM show that the global PDFs – panels j,k,l of the plots – are not a Gaussian due to the fact that the median and around median probabilities are much higher than for a Gaussian curve. Outside +1 and -1 standard deviation the PCs (red and blue curves) the PDFs of the noise are close to the Gaussian curve therefore is probably the median values in the noise , not the extreme ones, that make the noise to diverge from a Gaussian curve. Similar behavior is seen for the Atlantic PC1 and PC2 PDFs in the AGCM however, the corresponding PCs in the CGCM (Fig 2.20 g and h) are very close and could be approximated to the Gaussian curve. For the ENSO region both the CGCM and AGCM PCs 1 and 2 – Figures 1.20 and 1.21 d , e , f - are very close to the Gaussian curve and could be considered approximately Gaussian while PC3 shows higher probability between -1 and +1 standard deviation than in the Gaussian.

The PDFs for the North Pacific (Figures 1.20 and 1.21 a,b,c) are not Gaussian for PC2 and PC3 but have very close to Gaussian values for PC1 in both periods.

Therefore we could conclude the the standardized PCs for the regions of study are Gaussian outside +1 and -1 standard deviation but in general they show higher probability within those values than a Gaussian curve.

2.4 Conclusions

We investigated the statistical characteristics of atmospheric weather noise from the point of view of the total surface heat flux variability, as quantity is important for forcing SST variability, and compared the properties in a CGCM simulation with those in AGCM simulations forced by the CGCM SST. The first three EOF modes of the CGCM and AGCM THF weather noise, calculated globally and over several distinct regions, correspond closely to each other in terms of spatial patterns. They are associated with synoptic-scale SLP patterns. The dominant noise SLP patterns in CGCM and AGCM also corresponded closely, but had much larger spatial scales that those associated with the THF. The PCs of the THF noise are temporally not distinguishable from white noise at timescales longer than approximately a year. The PDF's of the THF noise did not show a strong response to the changing external forcing between 1871-1901 and 1951-1998. However, the PDF's were not those of random noise, having higher probability than a Gaussian distribution for small amplitudes.

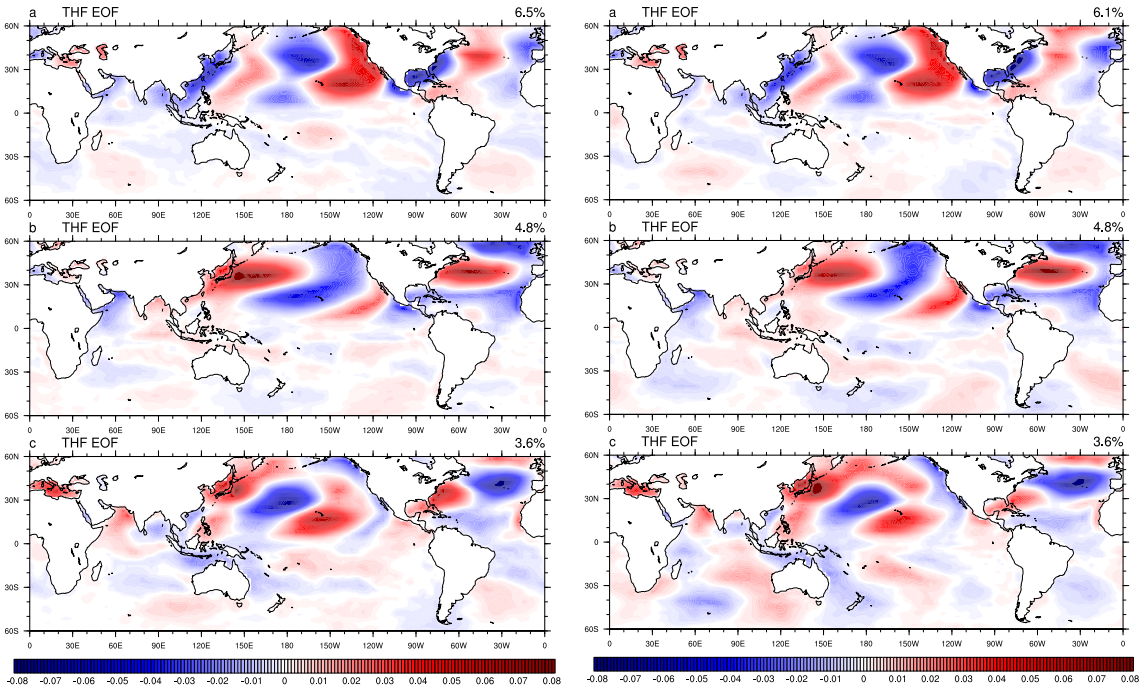

Figure 2.1 Noise EOFs for CGCM (left) and AGCM (right); EOF1 (a and d respectively); EOF2 (b and e respectively) and EOF3 (c and f respectively)

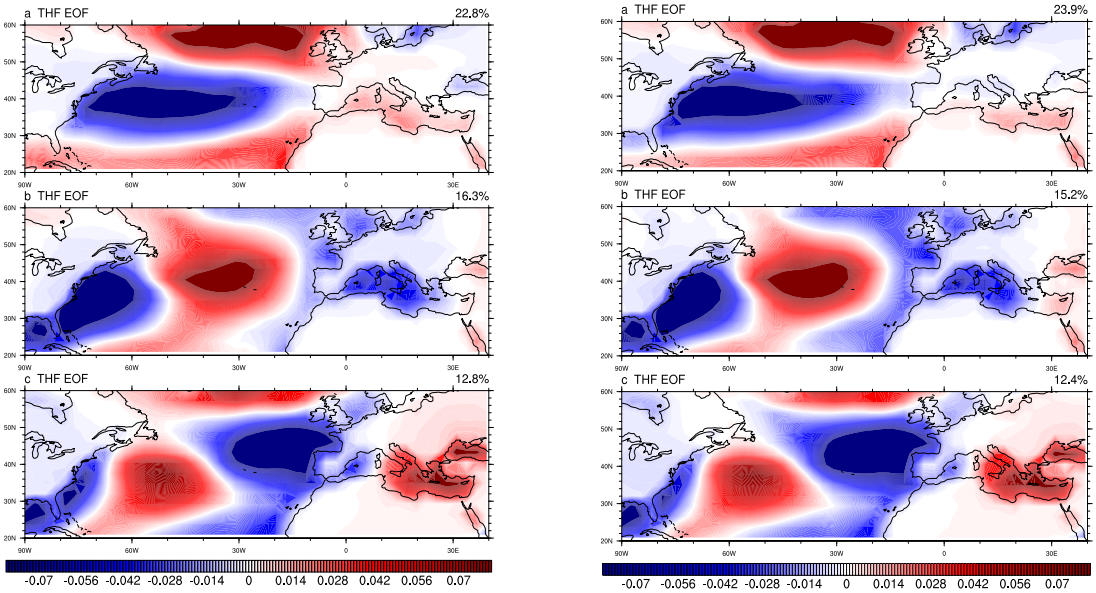

Figure 2.2 Atlantic CGCM THF noise EOF1 (a), EOF2 (b),EOF3 (c) and AGCM THF EOF1 (d), EOF2 (e) and EOF3 (f).

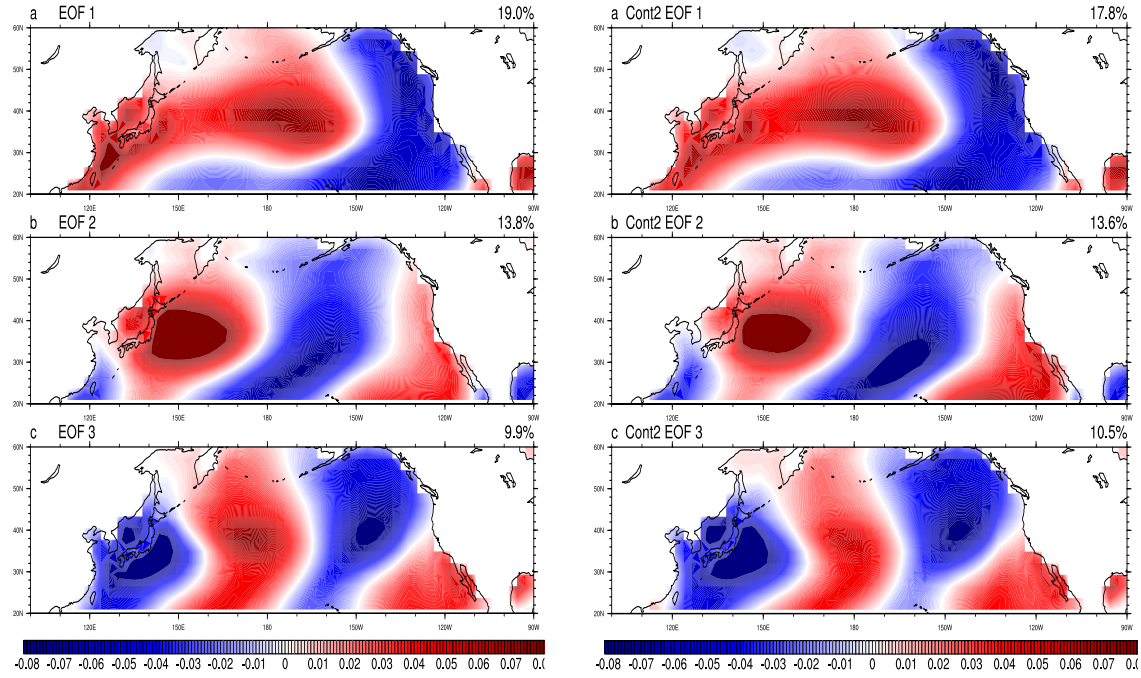

Figure 2.3 North Pacific CGCM THF noise EOF1 (a), EOF2 (b),EOF3 (c) and AGCM THF EOF1 (d), EOF2 (e) and EOF3 (f).

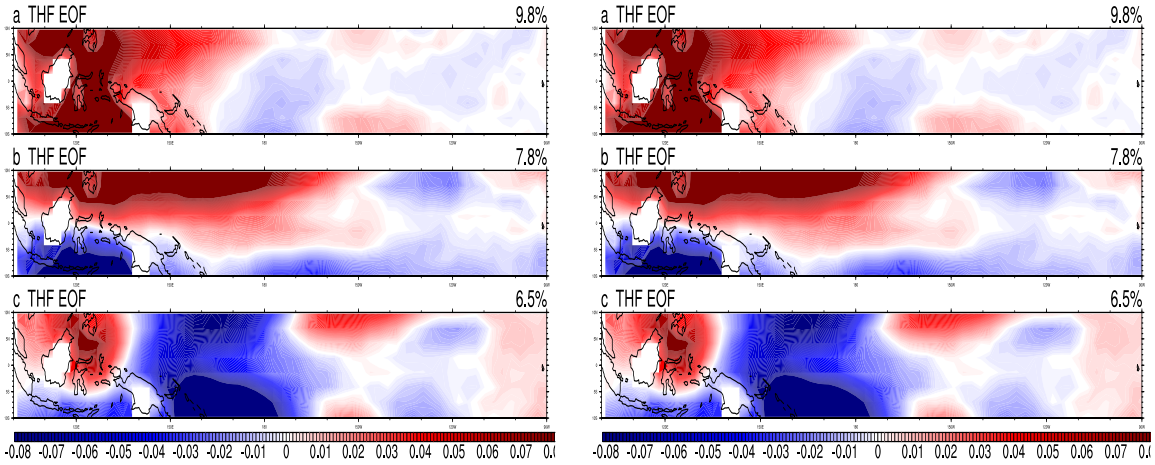

Figure 2.4 Same as in Fig 2.4 but for ENSO region

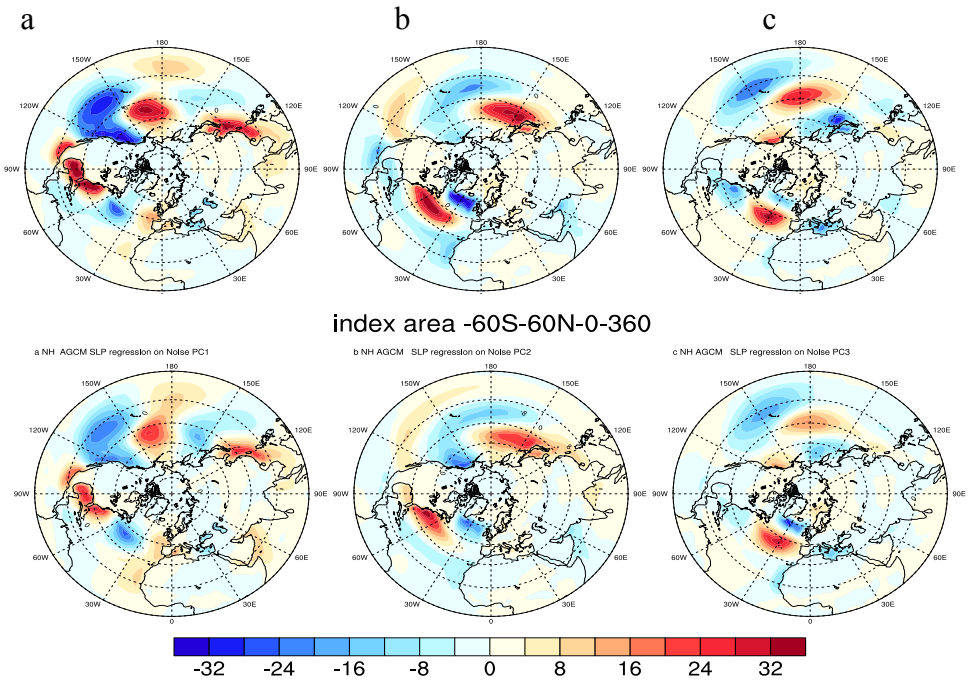

Figure 2.5 Regressions of Noise SLP onto Global Noise THF (-60S-60N and 0-360) PC1 (column 1), PC2 (column2) and PC3 (column3) for CGCM first row and AGCM second row.

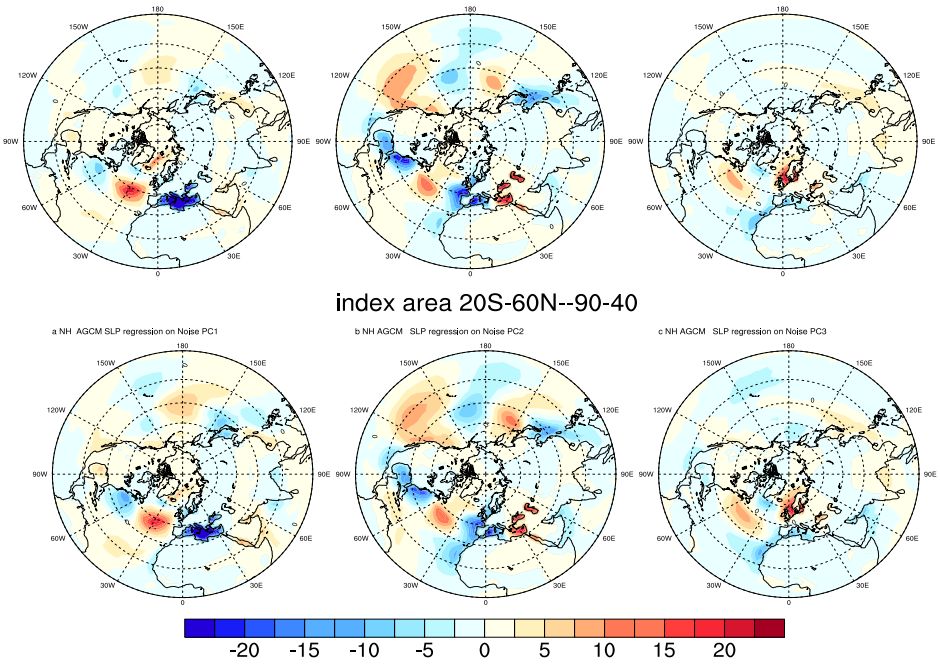

Figure 2.6 Regressions of Noise SLP onto Noise THF (-20S-60N and 90W-40E) PC1 (column 1), PC2 (column2) and PC3 (column3) for CGCM first row and AGCM second row.

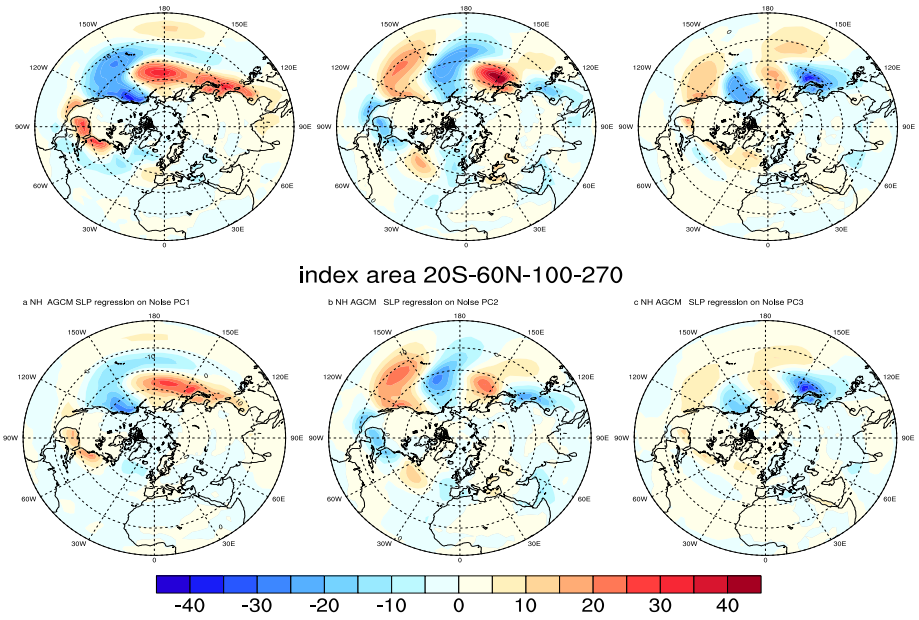

Figure 2.7 Regressions of Noise SLP onto Noise THF (-20S-60N and 100W-270W) PC1 (column 1),PC2 (column2) and PC3(column3) for CGCM first row and AGCM second row.

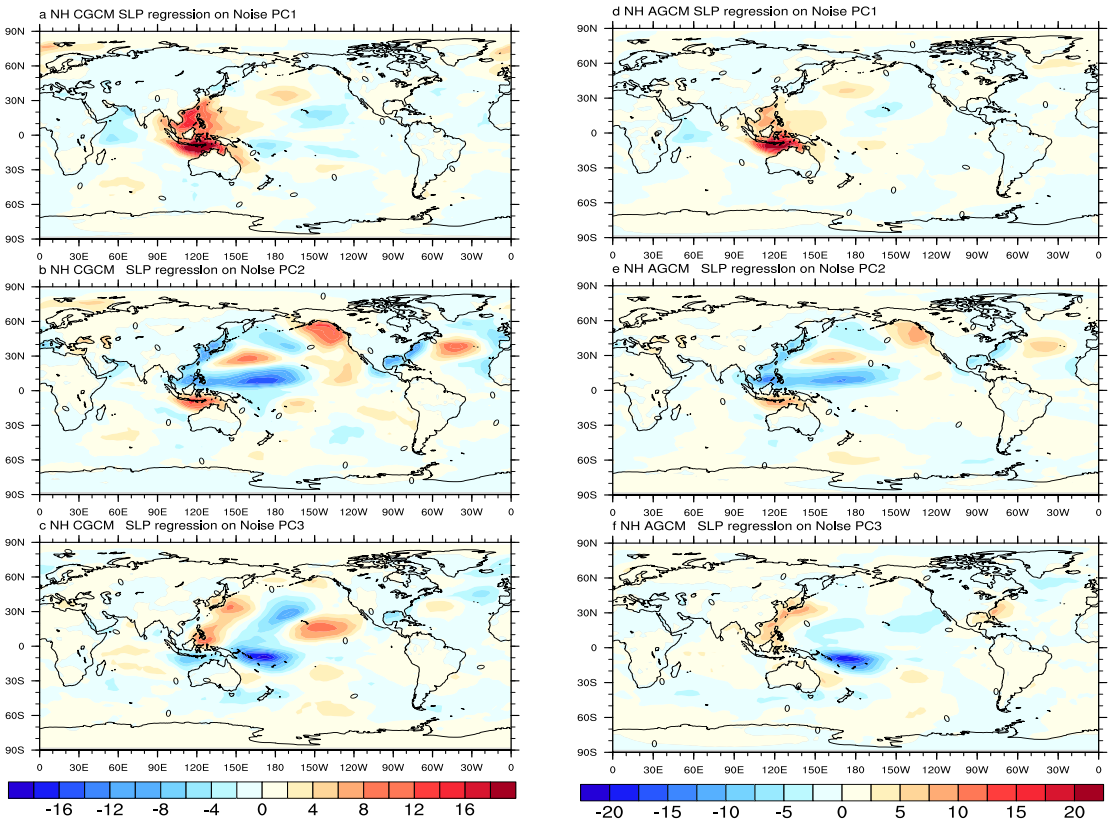

Figure 2.8 Regressions of Noise SLP onto Noise THF (-20S-60N and 100W-270W) for CGCM PC1 (a), PC2 (b) and PC3 (c) and for AGCM , PC1 (d), PC2(e) and PC3 (f).

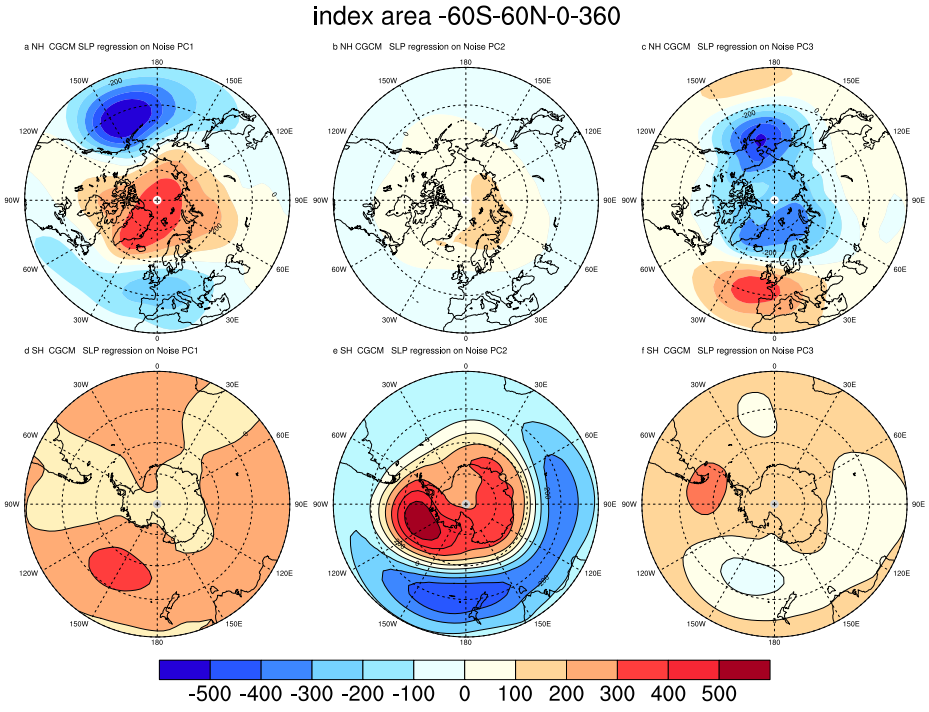

Figure 2.9 Regressions of CGCM Noise SLP onto Global Noise PC1 (a), PC2 (b) and PC3 (c)

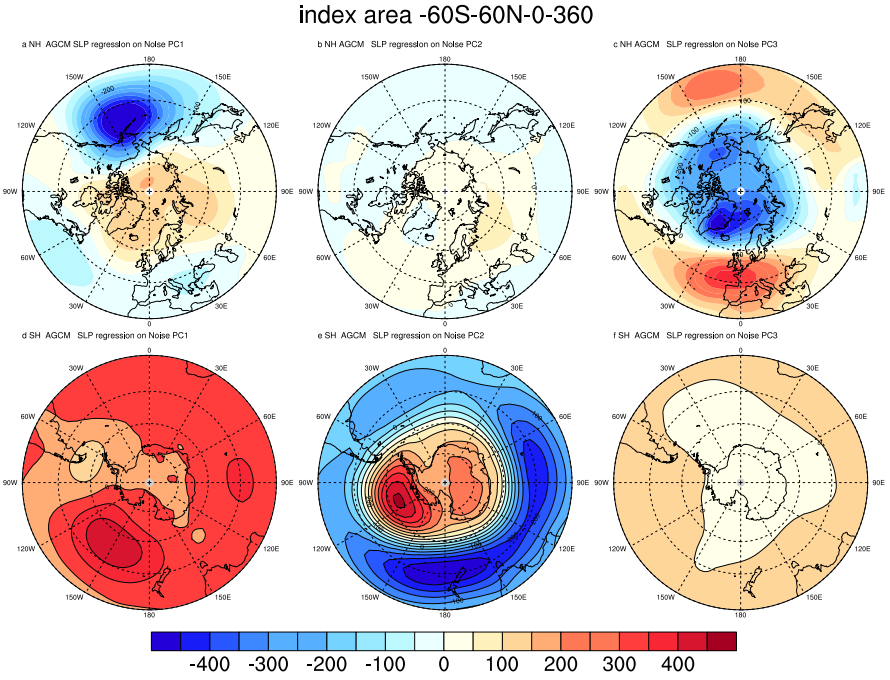

Figure 2.10 Regressions of AGCM Noise SLP onto Global Noise PC1 (a), PC2 (b) and PC3 (c)

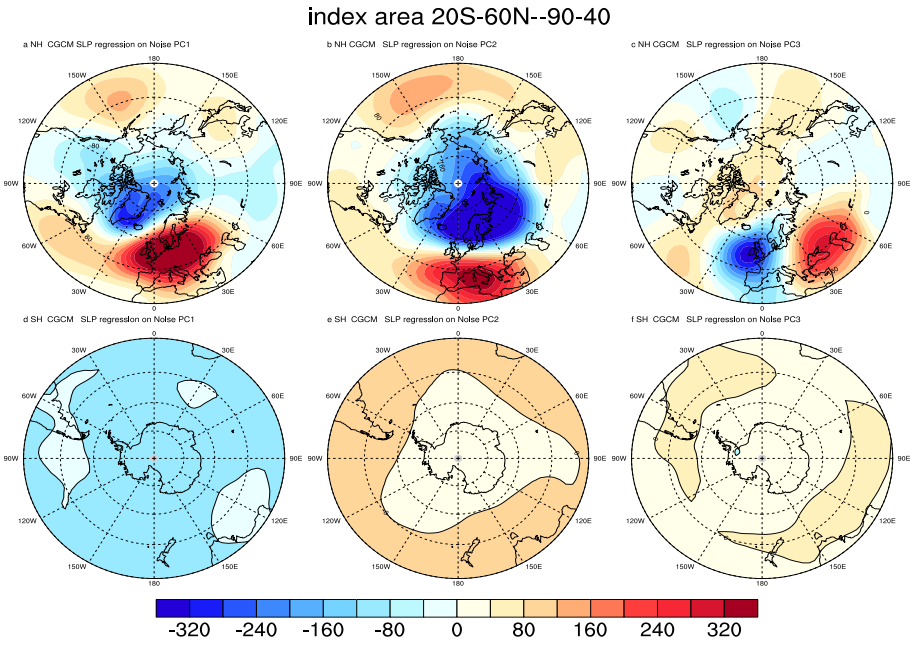

Figure 2.11. Same as Figure2 1.6 but for Atlantic Region, CGCM

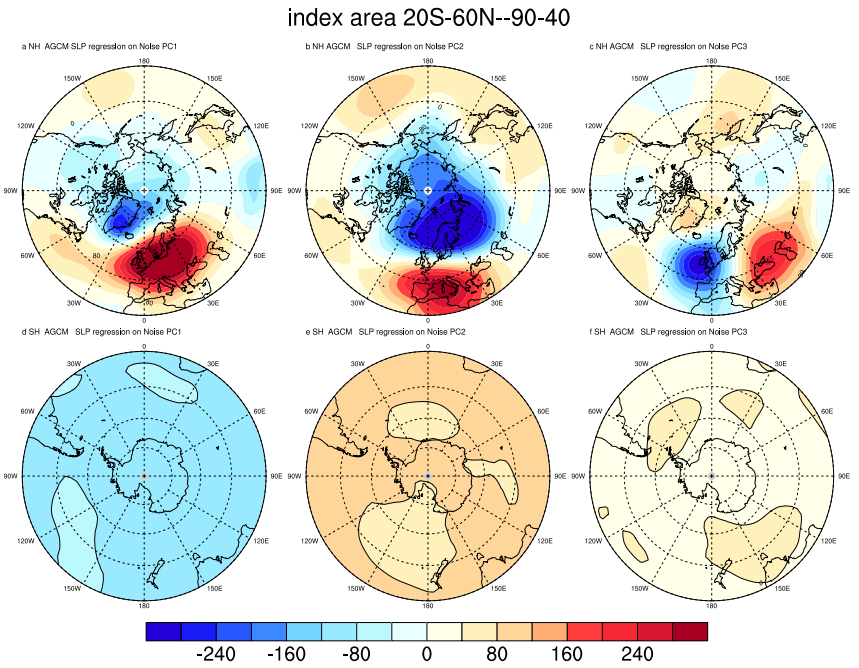

Figure 2.12 Same as 1.7 but for Atlantic region,AGCM.

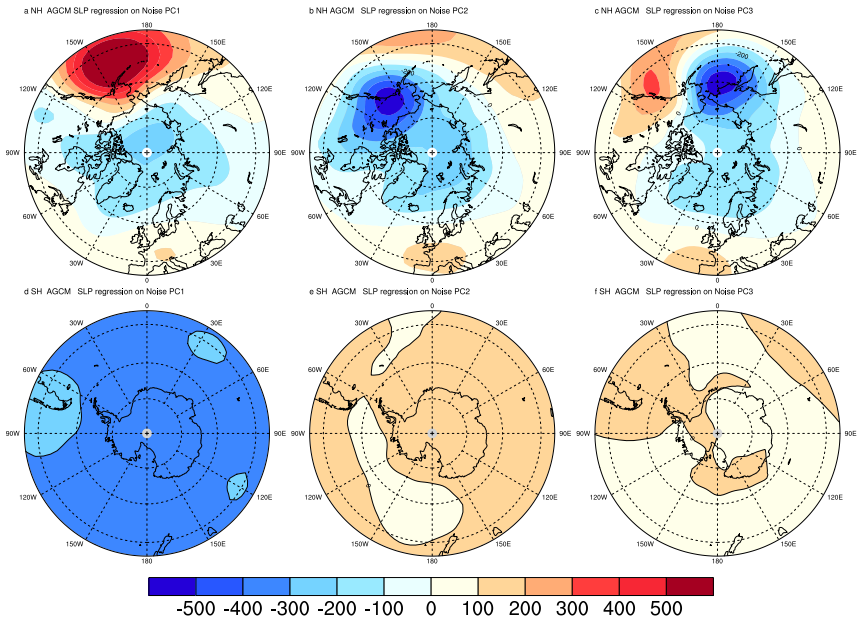

Figure 2.13 Same as in Fig.2.6 but for North Pacific

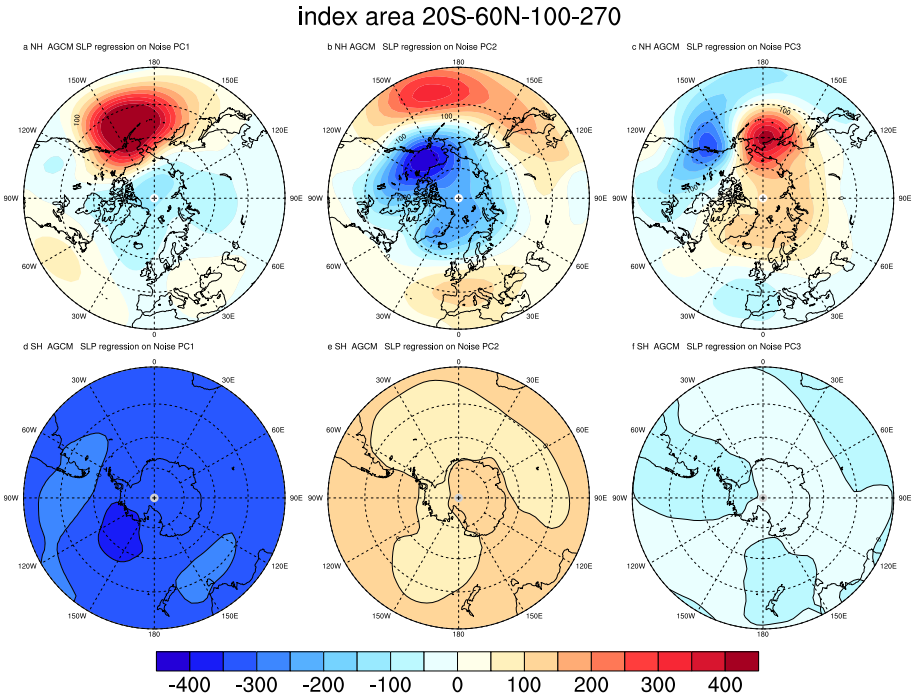

Figure 2.14 Same as in 1.7 but for North Pacific

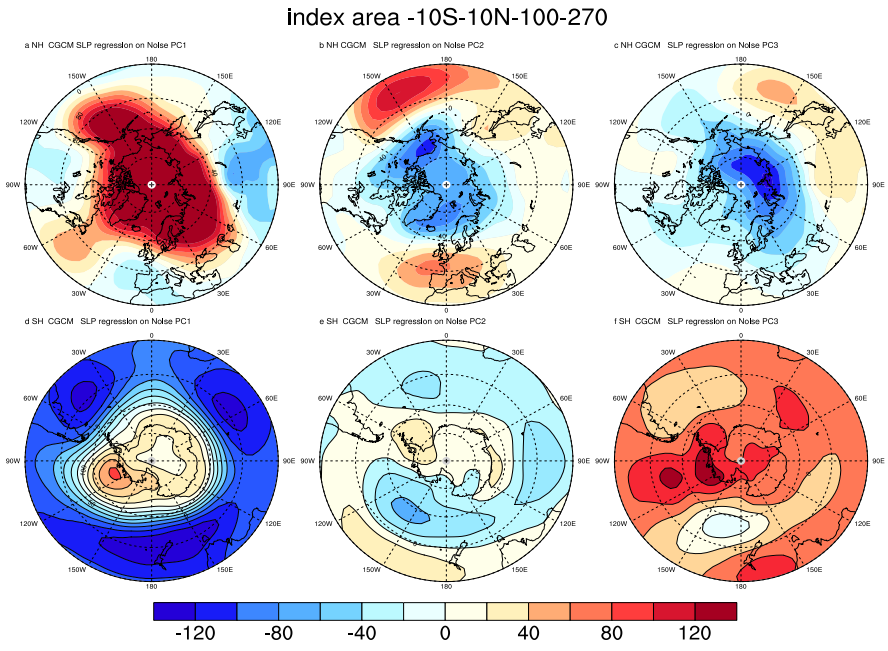

Figure 2.15 Same as in 1.6 but for ENSO region index

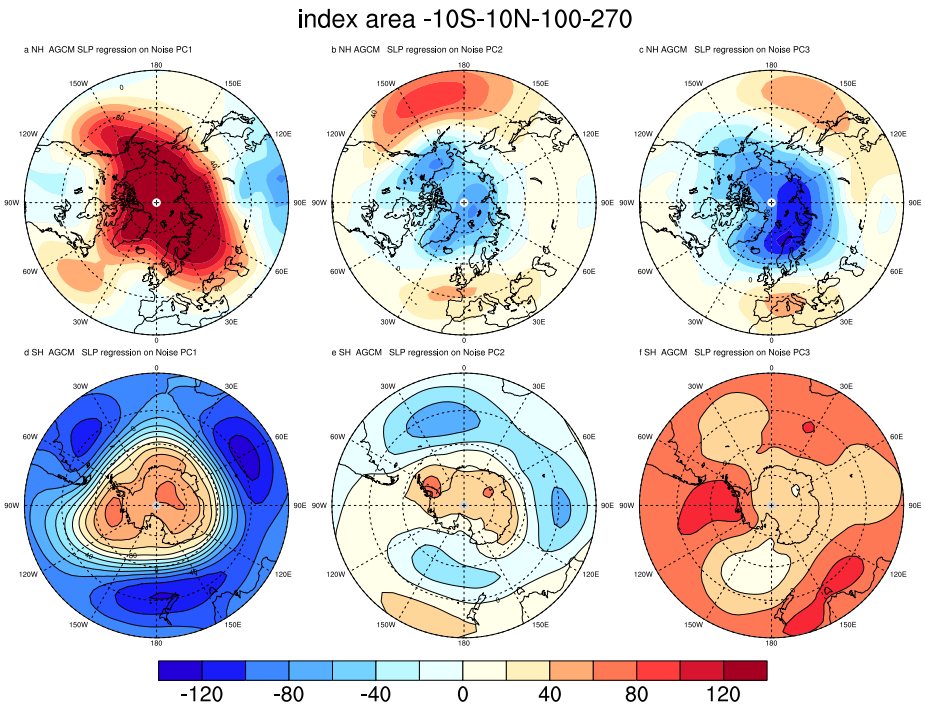

Figure 2.16 Same as in 1.7 but for ENSO index

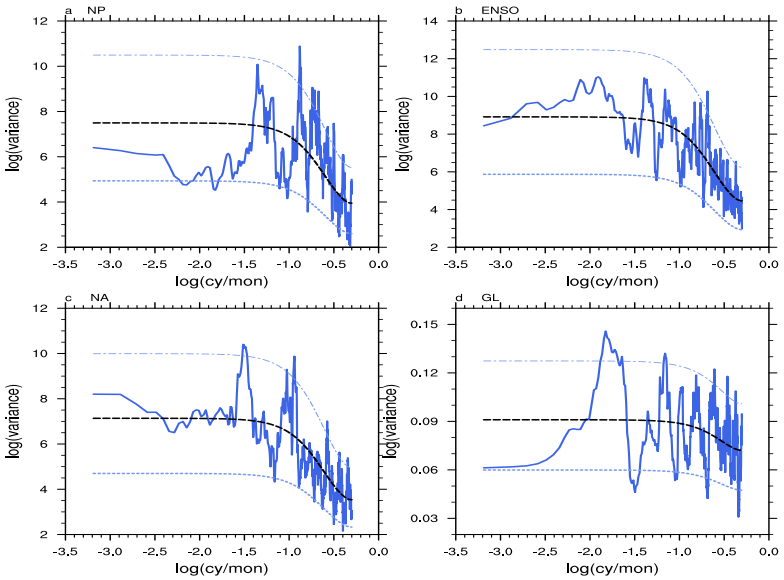

Figure 2.17 Spectrum of PC1 for NP(a), ENSO(b),NA(c) and GL(d) in the AGCM. The blue dotted curves represent 5(lower) and 95% white noise confidence intervals and the black curve the AR (1) white noise fitted model.

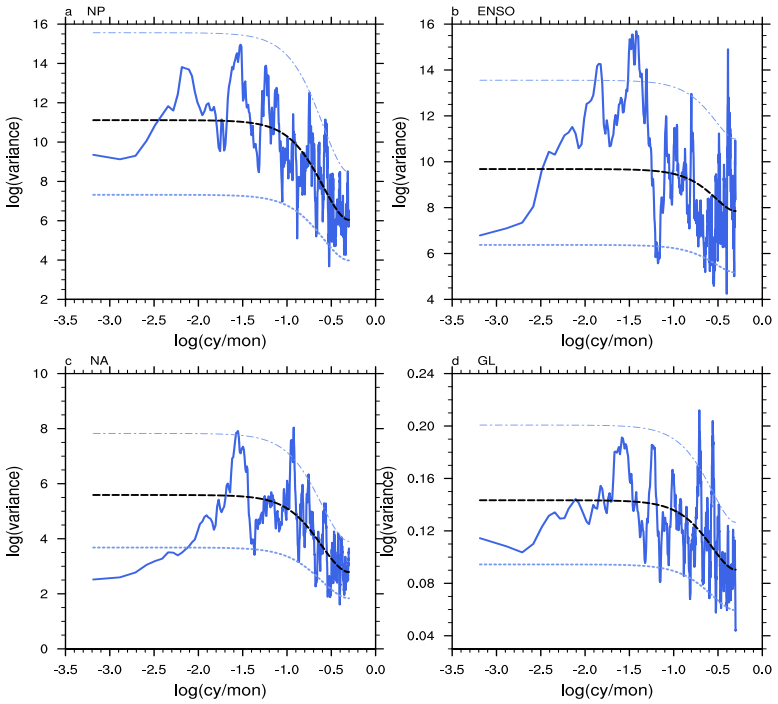

Figure 2.18 Spectrum of PC1 for NP(a), ENSO(b),NA(c) and GL(d) in the CGCM. The blue dotted curves represent 5(lower) and 95% white noise confidence intervals and the black curve the AR (1) white noise fitted model.

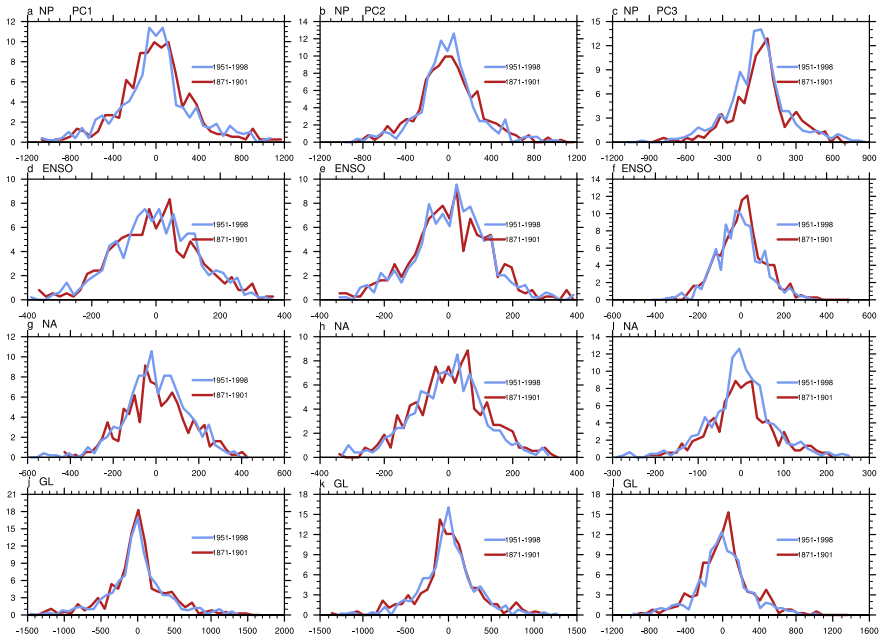

Figure 2.19 Probability Density Functions for CGCM PC1(column 1), PC2 (column 2) and PC3 (column3) for

NP(a,b,c),ENSO (d,e,f),NA(g,h,i) and Global(j,k,l). Red curve PDF for 1871-1901 and blue 1951-1998.

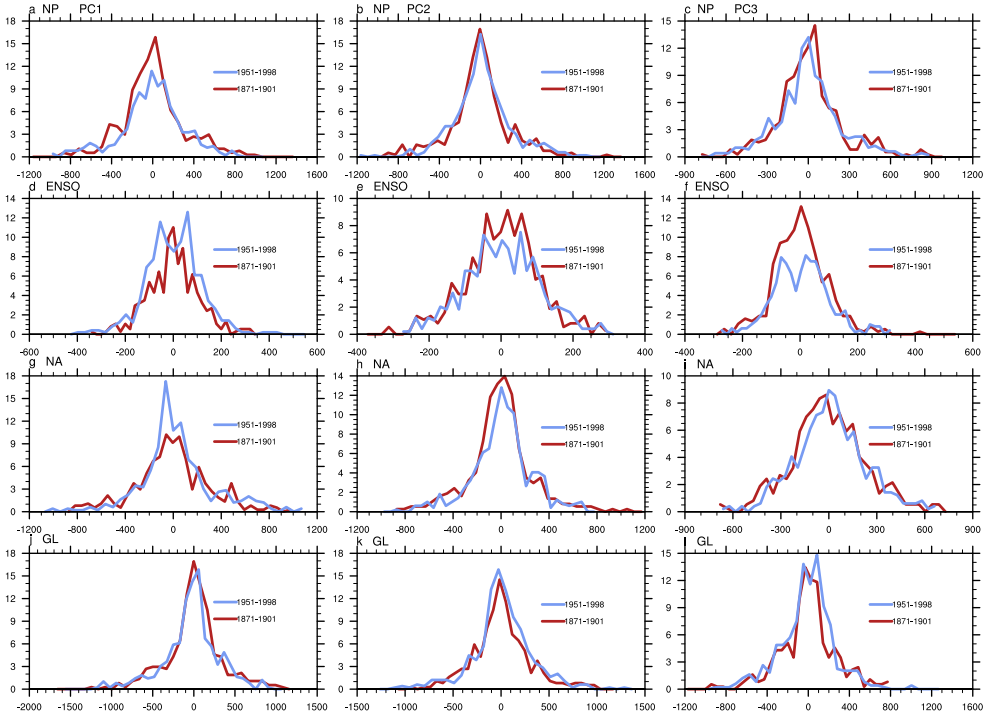

Figure 2.20 Probability Density Functions for AGCM PC1(column 1), PC2 (column 2) and PC3 (column3) for NP(a,b,c),ENSO (d,e,f),NA(g,h,i) and Global(j,k,l). Red curve PDF for 1871-1901 and blue 1951-1998

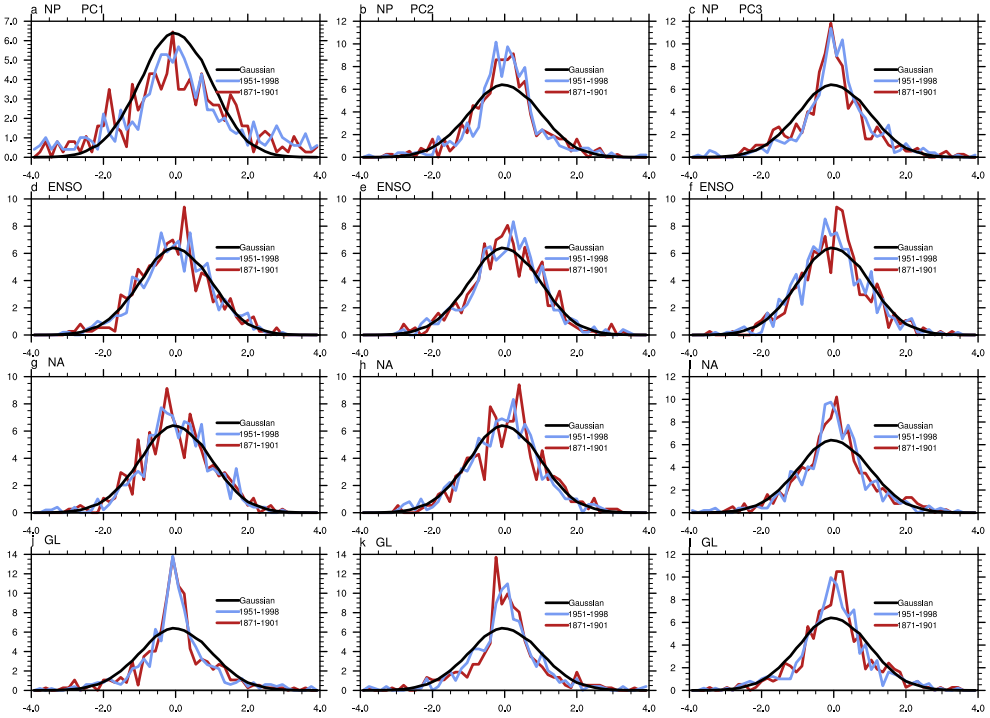

Figure 2.21 CGCM PDFs of THF PC1 for NP(a),ENSO(b),NA(c) and Global(d)

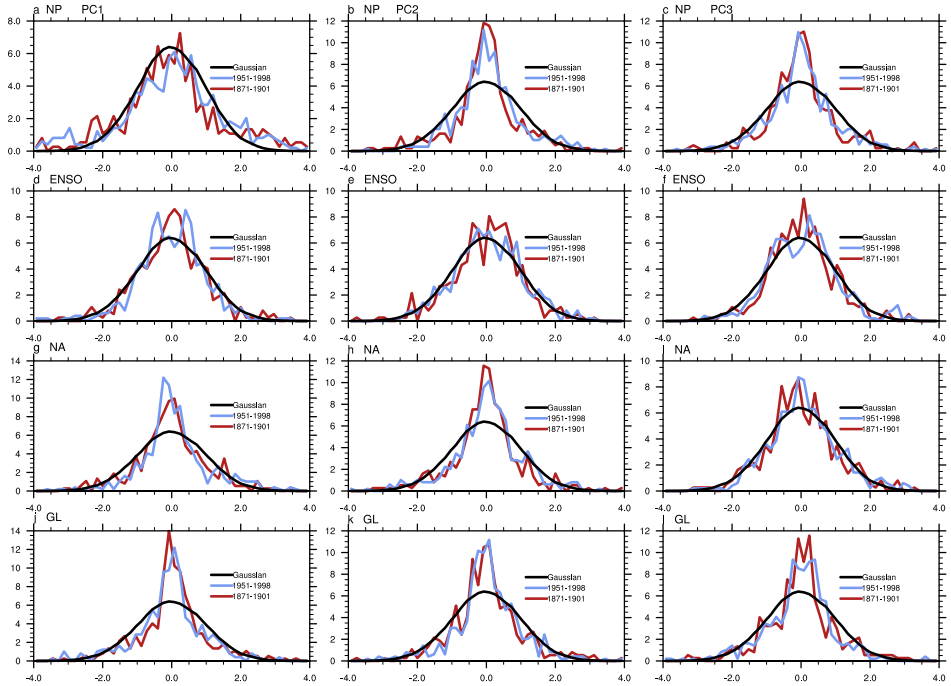

Figure 2.22 Same as in 1.16 but for AGCM

CHAPTER 3 ATTRIBUTION OF ATLANTIC MULTIDECADAL VARIABILITY TO EXTERNAL FORCING, INTERNAL VARIABILITY AND WEATHER NOISE

3.1 Introduction

Separating the SST variability forced by atmospheric weather noise from that due to other natural and external sources is a challenging problem. Hasselman (1976) suggested that the low frequency variability of sea surface temperature could be forced by atmospheric weather noise fluxes. Hasselmann's ideas suggested the following null hypothesis: surface temperature climate variability is forced by weather noise (Schneider and Fan 2007). While Hasselmann's work was a first step in the direction of attributing the causes of SST variability to noise vs. more deterministic sources, other studies using both simple and more complex and realistic models followed, including Frankignoul and Hasselmann (1977), Barsugli and Battisti 1998 , Bretherton and Battisti 2000, Marshall et al. 2001, Kirtman et. al. 2009,,Kirtman et al. 2011, Fan and Schneider 2012, Schneider and Fan 2012, and Chen (2013). SF2007 introduced a new model-based method that separates the weather noise from other internal sources of climate variability. This method uses a generalization of the Interactive Ensemble introduced by Kirtman and Shukla (2002) to isolate the role of the atmospheric weather noise for the low frequency variability of SST and tests the null hypothesis for a coupled general circulation model

(CGCM) . A schematic description of the noise extracting procedure is shown in Fig. 3.1.

The findings of SF2007, Kirtman et al. (2009), and Chen (2013) suggest that the null hypothesis is true in current climate CGCM (coupled general circulation model) control simulations (i.e. with constant external forcing on interannual and longer time scales) regionally over much of the world including much of the North Atlantic. However, these studies also identify important regions where the null hypothesis fails, including the equatorial Pacific, and some regions in the high latitude oceans. The results are consistent with an important role for unstable coupled atmosphere ocean dynamics in the equatorial Pacific related to ENSO (Kirtman et al 2002), and an significant influence of noise originating from internal ocean dynamics (oceanic noise) in high latitudes (Wu et al. 2004) of these models.

This study extends previous work to isolate the role of the atmospheric weather noise forcing in the climate variability of a CGCM (coupled general circulation model) forced by an estimate of the 20^{th} century external forcing. A decomposition of the origins of the simulated SST/climate variability for 1870-1999 of individual CGCM simulations into externally and internally generated components, and attribution of the internally generated variability to forcing by atmospheric noise and other causes is performed with the aid of an ensemble of externally forced CGCM simulations and interactive ensemble CGCM diagnoses. The focus of the investigation is attribution of the low-frequency variability in the North Atlantic of the CGCM to external forcing, atmospheric noise forcing, and other causes.

The underlying issue that we are addressing is attribution of the climate variability

in the observed system. However, attribution inevitably involves the use of CGCM simulations, usually as analogues of the observed system, and always as spatial and temporal interpolators of the observed data for quantitative analysis. It follows that a thorough understanding of model-simulated climate variability, where data and model are "perfect", is therefore reduced to a mathematical problem, and is a prerequisite to addressing the much more complex issues encountered in understanding the real system. Our techniques combine the ideas and framework for understanding provided by the simple models with the detailed representation of the physical laws and empirical relationships provided by the complex CGCMs. The use of the interactive ensemble allows the role of noise to be addressed deterministically rather than statistically, and produces a detailed representation of the internal variability amenable to a process-level decomposition.

In the North Atlantic, two main modes of low frequency climate variability of SST have been documented during the period of instrumental observations: a biennial and a decadal time scale SST variability. The decadal one, now called Atlantic Multidecadal Variability (AMV) (Bjerknes 1964, Deser and Blackmon 1993, Kushnir 1994, Schlesinger, and Ramankutty 1994, Mann and Park 1996, Delworth et al. 2007), has a period of oscillation in the range of 30 to 70 years and a spatial pattern characterized by basin-wide fluctuations over in the North Atlantic SST with a single-signed SST structure (Fig. 3.2). Beginning with the study of Folland, Palmer and Parker (1986), it has been understood that changes of the ocean sea surface temperature in the Atlantic might have a crucial role in producing 20th century Sahel droughts; other studies, such as Giannini et.

al 2003, Held et. al 2005 and Zhang et. al 2006, Enfield 2001 have made a strong case for the importance of the oceanic sea surface variability on the African climate variability, in particular on the precipitation at decadal and multidecadal timescales. These studies link AMV with land processes such over Africa, North America or Europe and with Atlantic hurricane activity.

The role of internally versus externally forcing of AMV has been previously documented by many studies (Franckcobe 2009, 2008; Farnetti and Wallis 2009; Fan and Schneider 2012). The results show that although external forcing might have been contributed to the observed multidecaldal variations in SST over the Atlantic, the AMV seems to be a manifestation of internal climate variability. Studies find an important contribution of Atlantic Meridional Overturning Circulation (AMOC) on AMV modulation. Delworth and Greatbatch (2000) conclude that the AMV in their model was produced by a damped mode of the AMOC forced by the atmospheric weather noise, with both heat and salt transport playing a role. However other studies (e.g. Ottera et.al. 2010) show that external forcing as solar forcing and the volcano activity might also be an important modulator of AMV.

Thus, different models and different approaches highlight different mechanisms. It it is has not been settled how much of the observed AMV variability is externally forced, how much is internal, or the roles played by the various dynamical mechanisms (weather noise forcing, coupled atmosphere-ocean modes, ocean dynamics including AMOC, Rossby waves, and gyre circulations) and their interrelationships.

Our study addressed the following specific questions:

- What are the roles of internally generated vs. externally forced variability in the AMV and AMOC time scale, mechanism and fluctuations in the 20th century model world of a specific CGCM.
- What is the effect of the weather noise and external forcing interaction (if any) on AMV, AMV-AMOC ?
- To what extent are the AMV and AMOC fluctuations generated internal in the North Atlantic, Subtropical Atlantic, or forced from other parts of the globe?
- What are the potential biases that the models and procedures introduce into the diagnosis?

Also the present work will advance the conceptual understanding of the SF2007 method of extracting the atmospheric noise and apply it in a new, a state-of-the-art coupled global climate model with a 20th century forcing.

In section 1.2 the models and experiments are described, the results are presented in section 1.3, while section 1.4 contains the summary and discussion.

3.2 Models, Experiments and Methodology

Diagnostic experiments are performed using the Interactive Ensemble (IE) based on CCSM3 (Chen 2013). All the experiments are carried out in "the model world" i.e the diagnostic models are perfect, in the sense that they have the same dynamics and physics as the CGCM used for the target simulations, and the data is perfect in that the model output data is known without error.

3.2.1 Models

3.2.1.1 The CGCM and AGCM

The base model used is Community Climate System Model 3 (CCSM3, Collins et al., 2006a) and its atmospheric component, the Community Atmosphere Model (CAM3) (Collins et al., 2006b). Both are the same models as used in Chapter 1 and 2.
The model resolution, for both the coupled and atmospheric component, was T42 spectral resolution in the horizontal and 26 levels for the atmosphere, and 1º by 1º degree horizontal, 40 levels for the ocean (the T42gx1v3 resolution).

3.2.1.2 The Interactive Ensemble CGCM

The IE used here is based on the CCSM3 AGCM and includes identical physics and dynamical representations as in CCSM3. The resolutions of the component models are the same as described above. The only difference is in the coupling between the atmosphere and the other components. The IE (first applied by Kirtman and Shukla 2002) consists of the CCSM3 ocean, land, and sea ice models coupled to the ensemble mean of an ensemble of CAM3 atmospheric models (Fig. 3.3). The single CAM3 AGCM that is coupled to the other components is replaced by the ensemble mean of six CAM3 models, and the ensemble mean atmosphere forces and responds to the other components. The capability specified surface flux forcing of the ocean is also included, in order to force the ocean with atmospheric noise data. The data includes the observed estimates of the 1870-1998 time evolving natural and anthropogenic forcing – greenhouse gases, volcanic effects (Amman et. al. 2003), ozone (Meehl et. al 2004), and solar activity (Lean et. al. 1995). All AGCMs have the same boundary conditions; the SST from the OGCM is updated daily, as well as the same land and sea ice, but different initial conditions. The

atmospheric feedback fluxes, i.e. the response of the atmospheric surface fluxes to the SST are determined as the mean of the AGCM ensemble. The atmospheric weather noise surface fluxes obtained from CGCM simulations are used to force the IE-CGCM in a series of controlled experiments designed to isolate the sources of the decadal variability of the targeted simulation and regionally. Chen (2013) applied this version of the IE with constant current-climate external forcing.

The rationale behind the IE is that the noise in one of the AGCM simulations is uncorrelated with that in each of the others, but the SST and externally forced part of the solution in each is the same, since each AGCM is started with different initial conditions, but each is forced by the same SST , land, and sea ice conditions. The ensemble mean of the AGCMs then approximates the atmosphere's response by the boundary conditions only, as the noise is filtered out., assuming that each atmospheric ensemble member is statistically identical. When the ocean component is forced by the atmospheric feedback fluxes only, atmospheric noise due to the chaotic internal atmospheric dynamics is filtered out (Fig. 3.3), and climate variability due to atmospheric noise is eliminated. Forcing the IE with specified noise then reinserts the atmospheric noise back into the system, but in a controlled and deterministic manner.

The current implementation of the IE is incomplete in that the atmosphere/land and atmosphere/sea ice components is inaccurate – the fluxes are computed from the ensemble mean atmosphere prognostic variables, whereas they should be computed separately for each of the atmospheric ensemble members and then averaged, and there is noise forcing only over ocean, not land or sea ice.

3.2.2 Experiments

The main purpose of these experiments is to study what are the roles of internally generated vs. externally forced variability in the fluctuations of Atlantic SST, in particular on AMV and AMOC at decadal and time scales, in the 20th century model world of a specific CGCM. The experimental design contains three parts. The first is an ensemble of CCSM3 simulations of the 1870-1999 climate, started from preindustrial initial conditions. The simulations are the same as the ones used in Colfescu et al. 2013, plus an additional ensemble member. An ensemble of climate of the 20th century produced with CCSM3 similar to the ones used here, but with different atmospheric resolution (T85) is used in Kirtman et al. (2011). The overall experimental design of Kirtman et al. 2011 is the same as the one used here with the main exception that the IE-CGCM in Kirtman et.al is not forced by the weather noise. Therefore our experimental design is an extension of the one in Kirtman et al. (2011). The second part is a set of experiments carried out in order to define the weather noise surface fluxes for specific members of the CCSM3 ensemble. The third is a set of diagnostic simulations carried out to isolate the roles of external forcing and weather noise on the AMV and AMOC. of the target CGCM simulations.

3.2.2.1. CGCM Simulations

The CGCM_ens simulations (Table 3.1) will be used both as analogues of the observed climate system and to separate these "observations" into externally forced and internally generated variability. A set of 6 CCSM3 simulations of the 20th Century is performed. The period covered is 1870-1999. Each member of CGCM_ens is forced by

the standard "IPCC" forcing used in CCSM3 in the CMIP3 atmospheric model intercomparison project (the SRES A1B scenario, IPCC AR4). The initial conditions of the coupled ensemble members (both atmosphere and ocean) were obtained by choosing arbitrarily January 1 restart files from a 500 year pre-industrial control run with external forcing fixed at 1870 levels (archived as run b30.043 as part of the Community Earth System Model database at the National Center for Atmospheric Research).

The first member and second members of the ensemble, Cont1 and Cont2, will represent the "observations" of the climate of the 20th century in the model world, and will be subject to diagnoses using the IE. Daily data for SST, surface foxes, wind and fresh water are saved for Cont1 and Cont2 and used for calculating the weather noise surface fluxes for each run.

Table 3.1 SET 1 of experiments: CGCM Simulations. All simulations are from 1870-1998.

Experiment Name	Model	Ensemble members	External Forcing
CGCM_ens	CCSM3	Cont1 Cont2 Cont3 Cont4 Cont5 Cont6	20th century

3.2.2.2 AGCM Simulations

The AGCM ensembles are used in the calculation of the weather noise surface fluxes, which, will be used to force IE –CGCM simulations. Two ensembles of 1870-1998 AGCM simulations were carried out (Table 3.2). Each ensemble has six-members

with different initial conditions, but the same SST for each ensemble member. All of the AGCM simulations use the same, 20th century, external forcing as in the CGCM ensemble. The ensemble members of AGCM_ens_Cont1 and AGCM_ens_Cont2 are forced by the time evolving daily SST from Cont1 and Cont2, respectively.

As described in Chapters 1 and 2, the ensemble mean of the results from the AGCM ensemble members estimates the response of the atmospheric model to the applied SST and external forcing (the "forced response"). That is, the ensemble mean from AGCM_ens_Cont1 provides an estimate of the atmospheric response to the external forcing and SST in Cont1, and AGCM_ens_Cont2 estimates the forced response in Cont2. The weather noise for a field in Cont1 is then estimated by subtracting the AGCM_ens_Cont1 forced response from the Cont1 results for that field, and in Cont2 by subtracting the AGCM_ens_Cont2 forced response from the Cont2 results. Due to an oversight, the weather noise heat flux did not include the latent heat contribution from melting of snowfall.

Table 3.2 SET 2 of experiments: AGCM Ensemble Simulations. All simulations are from 1870-1998.

Experiment Name	Model	Ensemble members	External Forcing	SST Forcing
ACGM_ens_Cont1	CAM3	ACGM1_Cont1 AGCM2_Cont1 ACGM3_Cont1 AGCM4_Cont1 ACGM5_Cont1 AGCM6_Cont1	20th century	Cont1
AGCM_ens_Cont2	CAM3	ACGM1_Cont2 AGCM2_Cont2 ACGM3_Cont2 AGCM4_Cont2 ACGM5_Cont2 AGCM6_Cont2	20th century	Cont2

3.2.2.3 IE Simulations

The IE experiments are listed in Table 3.3 and described below. The noise forcing data is from Cont1 and AGCM_ens_Cont1, and ocean initial conditions are the same as in Cont1, except for IEAllCont2, where they are from Cont2/AGCM_ens_Cont2.

3.2.2.3.1 No weather noise - IEnn

IEnn is an IE-CGCM simulation with 20th century external forcing and no specified noise forcing. It corresponds to the IE simulation described in Kirtman et al. (2011). In this experiment, variability forced by atmospheric weather noise is suppressed, and all climate variability is due to external forcing, coupling between the forced solution of the atmosphere and the ocean, land, and/or ice, and internal variability of the ocean, land, and ice components. If the atmospheric noise and external forcing are the dominant sources of SST variability, then IEnn will simulate the externally forced variability.

3.2.2.3.2 Global weather noise – IEAll

IEAll is forced by prescribed 20th Century historical forcing and the Cont1 atmospheric noise forcing over the ice-free parts of the oceans (heat flux, wind stress, and fresh water flux). If all climate variability in Cont1 is forced by atmospheric weather noise, then the SST variability in IEAll will reproduce that in Cont1.

3.2.2.3.3 Weather Noise restricted to Atlantic regions - IE030,IE3060

To study the response of the SST to regional Cont1 weather noise forcing, two simulations were performed. In The first one –IE030- the SST is forced with weather noise surface fluxes restricted to the Atlantic ocean region from 0 to 30N. Outside of this region, no weather noise forcing is applied. In the second, IE3060, the noise forcing is

applied only in a more northern part of the Atlantic ocean basin, from 30N to 60N. Both simulations include 20th century external forcing. The simulations are designed to show to what extent the Atlantic SST variability is forced directly by local weather noise, as opposed to originating in other regions and transmitted by dynamical teleconnections. Moreover, since the forcing is local, the separation between the Northern and Southern parts of the basins will show the role from the noise forcing in the adjacent region.

3.2.2.3.5 No 20th century forcing - IENoIpcc

IENoIpcc is a simulation forced with Cont1 atmospheric noise forcing over the global ice-free ocean in the absence of the external 20th Century forcing, IENoIpcc is used to isolate the role of noise forcing in the SST variability. This simulation is also used to evaluate secular drift in the IE.

3.2.2.3.6 Global weather noise – IEAllCont2

IEAllCont2 is the equivalent of IEAll, but the weather noise forcing used to forced the ocean model is obtained from Cont2 and AGCM_Ens_2, and Cont2 ocean initial conditions are used for the ocean.

Table 3.3 SET 3 of experiments: IE Simulations. All simulations are from 1870-1998.

Experiment Name	Model	External Forcing	Other forcing
IEnn	CCSM3 Interactive Ensemble	20th century	No noise forcing
IEAll	CCSM3 Interactive Ensemble	20th century	Noise evaluated from Cont1 applied over the global ocean
IE030	CCSM3 Interactive Ensemble	20th century	Noise evaluated from Cont1 applied only in the 0-30N box over the Atlantic
IE3060	CCSM3 Interactive Ensemble	20th century	Noise evaluated from Cont1 applied only in the 30-60N box over the Atlantic
IENoIpcc	CCSM3 Interactive Ensemble	Preindustrial control	Noise evaluated from Cont1 applied over the global ocean
IEAllCont2	CCSM3 Interactive Ensemble	20th century	Noise evaluated from Cont2 applied over the global ocean

3.1.2 Methodology

In this section we describe the methods used in separating and quantifying the SST variability, into weather noise forced, externally forced and other sources. An evaluation of the differences between the IE and CGCM simulations is presented in Section 3.1.2.3. We note unrealistic features in both the CGCM and the IE simulations. AMV and AMOC indices are defined that are appropriate for analysis of the externally forced and internal variability.

3.1.2.1 Decomposition of CGCM Simulations

The decomposition of the solution for any variable from a CGCM simulation is the same as described in Chapter 1, Eqs. (1.1-1.6), but for variability on all time scales – not just the trends. The externally generated component is taken to be the ensemble mean from a CGCM ensemble with all members having the same external forcing. The internally generated component is then the CGCM solution minus the externally forced

component.

The SST and externally generated component of an atmospheric variable is the ensemble mean of an AGCM ensemble, with each member forced by the external forcing and SST of the CGCM. The atmospheric noise in the CGCM is then the CGCM solution minus the SST and externally forced component.

3.1.2.2 Decomposition of IE simulations

Similarly to the decomposition of a CGCM simulation, a given variable in an interactive ensemble simulation, V_{IE}, can be decomposed into an externally forced, V_{IE}^{Ext}, and an internally generated variability component, V_{IE}^{Noise}:

$$V_{IE} = V_{IE}^{Ext} + V_{IE}^{Int}$$

Equation 3.1

The internal variability of a single IE simulation made with the IE configuration used here (AGCM_ens Cont1, AGCM_ens_Cont2 ensemble coupled to single instances of the other component models) includes that due to process involving coupling between the atmosphere and the other component models, $V_{IE}^{Int\ coupled}$, that due to internal variability of the ocean, land, and, or sea ice components not involving the atmosphere, $V_{IE}^{Int\ noise\ other}$, and variability due to forcing by specified atmospheric noise, $V_{IE}^{Int\ noise\ atm}$

$$V_{IE}^{Int} = V_{IE}^{Int\ coupled} + V_{IE}^{Int\ noise\ other} + V_{IE}^{Int\ noise\ atm}$$

Equation 3.2

A single simulation of the IE without atmospheric noise forcing includes externally forced variability and internal variability represented by Eq. 3.2. This is the case with simulation IEnn:

$$V_{IEnn} = V_{IEnn}^{Ext} + V_{IEnn}^{Int\ coupled} + V_{IEnn}^{Int\ noise\ other}$$

Equation 3.3

The internal variability in the IE due to the atmospheric noise forcing is then found by

$$V_{IE}^{Int\ noise\ atm} = V_{IE} - V_{IEnn} - \left(V_{IE}^{Int\ coupled} - V_{IEnn}^{Int\ coupled}\right) - \left(V_{IE}^{Int\ noise\ other} - V_{IEnn}^{Int\ noise\ other}\right)$$

Equation 3.4

The externally forced component is removed completely in Eq. 3.4. The internal variability due to coupled process is uncorrelated between two IE simulations, but should be otherwise be statistically the same. The same is true of the internal variability due to noise in the other components. Therefore, the variances of these components will be reduced by half compared to their variances in the original IE simulations in the computation of the response of the IE to the atmospheric noise.

The coupled and other noise variability cannot be removed from the IE simulations without conducting ensembles of IE runs for each choice of external or atmospheric noise forcing. Because of the filtering effect of taking the difference between two simulations described above, we use

$$V_{IE}^{Int\ noise\ atm} = V_{IE} - V_{IEnn}$$

Equation 3.5

as an estimate of the IE response to the atmospheric noise forcing, but it should be remembered in interpreting the results that this estimate is accurate only as far as other sources of internal variability are unimportant in the IE. All variability in IENoIpcc is internal, as there is not external forcing.

3.1.2.3 Climatologies of CGCM and IE simulations

The 1871-1998 difference between the CGCM_ens climatology and the one in IEAll, normalized by the pooled standard deviation, is shown in Fig. 3.4. This difference is calculated as : the difference between the SST in IEAll minus the one in Cont1 divided by the pooled variance :

$$\sigma_p^2 = \frac{(N_1 - 1) * \sigma_1^2 + (N_2 - 1) * \sigma_2^2}{N_1 + N_2 - 2}$$

Equation 3.6

where N1 is number of moments of times in IEAll , N2 number of moments of time in Cont1, σ_1 standard deviation in IEAll and σ_2 standard deviation in Cont1.

Thus the pooled variance (Equation 3.1) is obtained from the IEAll and Cont1 SSTs with long term mean for 1871-1998 removed (similar to Kirtman et al. 2011).

The normalized surface temperature differences are highest over ice and land but also the North Atlantic and North Pacific. Over the ocean, the large differences over the North Eastern Pacific and North Atlantic occur in the same regions as in Kirtman et. al (2011), and that study suggests that these differences might be to the fact that in these regions the SST variability is dominated by localized mixed-layer processes.

Figure 3.5 shows that the CGCM_ens experiments substantially overestimate the ice extent compared to the observed (Fig. 3.6) system in the North Atlantic.. The ice extent in Cont1 is the largest in the entire CGCM_ens. On the other hand, the IE (purple curve) also has issues although the ice extent is smaller in comparison to Cont1 and

closer to real one . The atmosphere/land and atmosphere/ice coupling are crude in the IE and are a potentially large source of bias compared to the CGCM. Additionally there are no noise fluxes applied over the ice and land in the IE. Then over regions with extended ice in CGCM_ens the CGCM results may not apply to the real climate system, and the IE is not useful for diagnosing the behavior the CGCM there. These considerations will influence the definition of the AMV index, described below.

3.1.2.4 The AMV index

In analyzing observations, some assumptions are necessary to separate externally forced and internal climate variability. Firstly, the 20th century external forcing is not well known, for example for solar variability and volcanic aerosols. Secondly, the calculation of the influence of this external forcing on the climate system must of necessity involve a model or simplifying assumptions about the behavior of the climate system. Some previous studies, including Schlesinger et al. (1994), Enfield et al. (2001), Sutton and Hodson (2005), Trenberth and Shea (2006), and Knight et al. (2006) , calculate the AMV index as the annual SST average between 0-60N and 0-80W with the linear trend removed and then low-pass filtered (Fig. 3.2). The interpretation of this AMV index as representing internal variability in the North Atlantic is based on the assumption that that the linear trend is a good approximation to the response to the 20th century external forcing, and that trends due to internal variability are unimportant. Another method of calculating the AMV index is to use the global mean SST as a representation of the externally forced signal (Trenberth and Shea 2006; Mann and Emanuel 2006) and then subtract it from the North Atlantic SST in order to remove the forced signal.

Ting et al. (2009) use regressions of the SST onto the globally averaged SST to obtain an estimate of the internal component of AMV as the local difference between the total field and the regression. DelSole et al. (2011) shows that there is a global pattern of internal multidecadal variability, separable from the anthropogenic signal, centered in the Atlantic. This pattern is shown to contribute significantly to the global warming trend of the recent decades -1977–2008- suggesting thus clearly the necessity to separate accurately between the forced and internal SST patterns of variability in the North Atlantic. Thus there are assumptions, first that the global mean SST variability is predominantly due to external forcing, and second that internal AMV variability has no correlation with the global mean SST. The assumptions made in the above examples avoid the necessity for either knowing the external forcing or modeling the climate system.

At the other extreme, in the model world it is possible to determine the externally forced and internally generated signals without making any assumptions, as the ensemble mean of an ensemble of climate model simulations, all with the same external forcing (e.g. Deser et al. 2011). The ensemble can consist of one member for simple models, while for CGCMs, multiple ensemble members are necessary because of the chaotic behavior of weather disturbances. This is the approach we take.

Here the total AMV is calculated as the annual SST average between 0-60N and 0-80W with any grid point containing ice in Cont1 during the entire simulation masked out. This definition allows meaningful comparison of CGCM and IE AMV simulations, as the Cont1 ice mask covers all ice covered regions for all of the other simulations, but is

not the same as the ones commonly used. As in previous studies, the total index is then divided into internal and external components. However, our representation of the internal component doesn't use the direct removing of a linear trend but is done according to the division in Section 3.1.2.1 and Section 3.1.2.2, for the CGCM and IE respectively. Namely, the external AMV component in the CGCM experiments is CGCM_ens AMV ensemble mean and is taken to be the AMV in IEnn for the IE experiments. As noted above, this definition of AMV includes some internal variability as well as the externally forced signal, but can be considered a first approximation subject to later examination. The internal AMV for a member of CGCM_ens is the difference between that particular member and the external component. For the IE experiments the internal component of a particular IE experiment will be taken to be the difference between that IE simulation and IEnn. Again, there is some contamination due to the presence of internal variability in IEnn.

3.1.2.5 The AMOC index

For the period 1871-1998, an EOF analysis of the annual mean stream function, $\psi(z, lat) = \int_z^0 \int_{\lambda_E}^{\lambda_W} V cos(lat)\, dxdz$, is performed for both IE simulations and CGCM_ens. The first PCs are considered the Atlantic Meridional Overturning Circulation index. For the Cont_ens the AMOC reconstructed from the first EOF and associated PC explains 42%-50% of the AMOC variance. For the IE simulations, the first EOF and associated PC explains 58% to 67%.The structure of the EOFs varies only slightly between all the simulations; therefore, the first PC is a reasonable index for

comparison. The AMOC index is also divided into an externally forced and a noise component in the same manner as for the AMV.

3.3 Results

The externally forced IE simulates the CGCM externally forced global SST well whether noise forcing is included or not, so most global mean SST variability is externally forced, in agreement with Kirtman et al 2011. The internal component of the CGCM is simulated reasonably well by noise forced IE but the correlation between internal components is weaker than the total one. Therefore, the atmospheric noise is forces an important part of the internal global mean SST variability in particular in higher latitudes, in agreement with Chen 2013.

The total global SST variability is also similar (well correlated) among the IE simulations due mainly to the presence of the same external forcing; however the internal components are not similar among the IE simulations. The total SST variability in the IE reconstructs the one in the Cont1 with better accuracy in the higher latitudes than near the equator.

3.3.1 Control – IE Global SST Average Comparison

The time series of anomalies of global mean SST for CGCM_ens, IEAll and IEAllCont2 are shown in Fig. 3.7. The global mean surface temperature for CGCM_Ens and IEAll (a) shows a positive trend starting in 1900s with a steeper slope for the period

1940–1998 in both the IE and Control1. The major volcanic eruptions - Krakatau around 1890, Santa Maria 1910, Agung 1970, El Chichon 1982 and Pinatubo 1991 - are associated with sudden decrease in temperature for both the IE and Control as well as for the ensemble envelope. The spread of the ensemble envelope as well as the IE stays mostly within values of ±0.5 K. The noise forced IE is a good reconstruction of Cont1 - the two runs global average SST show a correlation of 0.91.Similarly the correlation between Cont2 and IEAllCont2 it is 0.90 and shows positive temperature trends (b). The external components for Control_ens and IE, i.e the Control_ens ensemble mean and IEnn (c) show a correlation of 0.92. The IE values are above the ones in Control_ens for the period before 1940s and below after it. Thus considering the high correlation between the external components of IE and Control_ens simulations which is comparable/higher to the correlation between the total SST component we can conclude that the externally forced IE simulates externally forced CGCM well whether noise forcing is included or not, thus most global mean SST variability is externally forced.

The internal components of the global temperature for IEAll and Cont1 are shown in Fig. 3.8a. The correlation between the two is 0.52 and the IEAll values stay mostly within the envelope of the CGCM_ens1. The difference between the two time series come mostly from the period between 1930 – 1950, the period when sea ice is much more extensive in Cont1 than in IEAll. The correlation between internal component in Cont2 and IEAllCont2 (Fig. 3.8 b) is 0.55 slightly larger than in Cont1-IEAll. Thus, for two different noise realization the internal component in the respective Cont runs is correlated with the internal component in the IE with about 0.52-0.55.

Therefore, the internal component of the CGCM is simulated reasonably well by noise forced IE but agreement is weaker than for the trend-dominated external component.

Annual mean SST anomalies averaged globally for IEAll, IEnn, IENoIpcc, IEAtl030, IEAtl3060 and IEAll2 (Fig. 3.9 a) show a positive trend in all simulations except for IENoIpcc. The IENoIpcc trend represents a cooling drift in the IE model when it is started from pre-industrial initial conditions. As the CGCM preindustrial control is equilibrated with the pre-industrial forcing, the IE drift can be considered to be a model bias relative to the CGCM simulations. Comparison of the CGCM and IE global means indicates that this drift is present in all IE simulations.

The overall increasing temperature can then be attributed to the 20th century external forcing. The correlation between IEAll and IEnn of 0.81 and the similarity of the magnitude of the trends shows that the external component dominates the global mean SST variability in IE. The correlations of the IEAll simulations with the other IE simulations are high due to the presence of the same external forcing. However, the correlation decreases between the internal components of IEAll, IE030, IE3060 and IEAll2 (Fig. 3.9b) . The correlations of the IE indexes shown in Fig. 3.9b have a maxima of 0.38 which occurs between IE030 and IE3060 and is about zero between IENoIpcc and IEAll.

There are several potential sources for the differences between the CGCM and IE external or internal variability. These include different internal coupled (i.e. ENSO), as well as different unconstrained ocean, land surface, and sea ice variability, and errors in the noise filtering due to using small AGCM ensembles in the AMIP-

type and IE simulations. Differences among IE simulations also reflect the impact of noise forcing in different regions on the global mean SST.

3.3.2 Control-IE regional comparisons

The time series of total, internal and external anomalies of North Atlantic(a,b,c), North Pacific(d,e,f) and Equatorial Pacific (g,h,i) are shown in Fig. 3.10 for Cont1, IEAll and the ensemble of CGCM_ens envelope. The spread of the control ensemble members as well as the variability of IEAll are similar to the variability in the Cont1. As in the case of the global SST the regional total components (a,d,g) shows a positive trend in both the Control_ens simulations and IEAll. For the North Atlantic and North Pacific the correlation between the IEAll and Cont1 total components is 0.72 and 0.78 respectively. Comparisons of the North Atlantic and North Pacific total and external components between CGCM and IE show evidence of the IE systematic cooling drift revealed in IENoIPCC.

The equatorial Pacific (g) has a lower correlation between IEAll and Cont1, 0.54. This can be explained by the fact that in the equatorial Pacific the main mode of variability is ENSO, which is a coupled variability mode somewhat independent of the atmospheric noise. Thus the influence of both external forcing and atmospheric weather noise is smaller there.

The external components for all three regions show a positive trend with similar variance in the North Atlantic (c) and North Pacific (f) and with a higher variance in the IEnn than Cont_ens for Equatorial Pacific. The higher variance in IEnn is due to similar ENSO

variance in IEnn as in the individual CGCM runs. CGCM_ens filters out this variance (reduces it by 5/6), as the ENSO variability is not correlated between the individual ensemble members, but it is not reduced in IEnn. The unfiltered ENSO variance has a noticeable projection on the IEnn global mean temperature in Fig. 3.7c. This emphasizes that IEnn filters out only internal variability due to atmospheric noise – other sources still remain. The correlation of the external components between the two Control_ens and IEnn is 0.55 for North Pacific, 0.44 for equatorial Pacific and 0.50 for North Atlantic. Therefore the correlation of the external components of SST average regionally, between IEnn and Control_ens average is comparable to that of the total components of these two. The correlations of the internal components of IEnn and Cont1 SST for North Pacific (e) , Equatorial Pacific (h) and North Atlantic (b) is 0.47, 0.20 and 0.44 respectively. This suggests that the total SST variability in the IE reconstructs the one in the Cont1 regionally with better accuracy in the higher latitudes than in the equator. Also, regionally, the externally forced component is the one that is most responsible for the similarity between the Control_ens and IE simulations while the internal components are less well correlated. Similar results are found for the case of IEAll2 and Cont2 (not shown).

The SST monthly anomalies correlation values between the Cont1 and IEnn (Fig. 3.11 a) have a maximum of about 0.5 over the Western Equatorial the Pacific, Indian Ocean as well as subtropical and equatorial Atlantic in the Southern hemisphere. The high and mid-latitudes as well as the equatorial Pacific, show little correlation between the two simulations. Only a small fraction of the SST variance in Cont1 is captured by

the IEnn (Figure 3.11 b) and most of regions show STD ratios of under 0.5, with a minima of 0.2 occurring in the North Atlantic. The areas where the correlations are high – values of around 0.4-0.5 in the Eastern Pacific, Indian Ocean and South Atlantic are inferred to be regions where external forcing is locally detectible for the SST variability, since internal variability should be uncorrelated between the CGCM and IE. The regions where the external forcing is locally detectible are also regions where the variance in IEnn is relatively strong compared with that forced by the weather noise (Figure 3.11b a, b), although the converse is not true because of the internal ENSO variability in IEnn.

The inclusion of atmospheric weather noise forcing over the global oceans in IEAll improves the agreement between Cont1 and the IE simulation dramatically. The correlation coefficients between Cont1 and IEAll (Fig. 3.11b) are high all over the globe, except the equatorial Pacific, northern North Atlantic and polar regions. Furthermore, the regions of high correlation correspond to regions where the variance ratio between the Cont1 and IEAll (not shown) is close to one (Figure 3.11b a). Since the externally and weather noise forced IEAll reproduces most of SST variability in Cont1, while the external forcing without the weather noise has much less resemblance, we can conclude that the local SST variability over most of the oceans is forced primarily by a combination of external forcing and weather noise. The regions of low correlation in Fig. 3.11b indicate that the SST variability there is produced by processes other than external forcing or atmospheric weather noise: namely (local or remote) coupled processes (e.g. ENSO) or intrinsic ocean-only variability (e.g. as found in the extratropical North Atlantic by Wu et al. 2004, tropical instability waves, shear instability of mean currents,

etc.).The differences in the northern North Atlantic are associated with large ice cover in the Cont1 in comparison to the IE. However, the values of the correlation between Cont2 and IE2 (Fig. 3.11c) are very similar to Cont1-IEAll, and, the sea ice bias of IEAll_Cont2 compared to Cont2 is much smaller than for Cont1, so it can be tentatively inferred that the low correlation cannot be attributed to the IE treatment of sea ice.

The values of the correlations between Cont1 and IENoIpcc (Fig. 3.11 d) shows that that in the absence of external forcing, the patterns and correlation magnitudes are similar to the ones in Fig. 3.11b, but weaker. This is consistent with the role of external forcing of the SST. The areas where the correlation coefficients are high correspond to areas of standard deviation (SD) close to one, indicating that in those regions the SST variability is primarily forced by noise while areas where the correlation coefficients are lower than in Cont1-IE1 represent areas where the 20th century external forcing is contributing to the SST variability.

The correlations between Cont1 and the IE experiments with regional noise forcing in the upper and lower North Atlantic Basin are shown in Figs. 3.11e,f. The Cont1-IEAtl030 and Cont1-IEAtl3060 correlations are very similar to those in IEnn (Fig. 3.11a), except over the respective forcing regions, where they are much larger.

The SST monthly anomalies correlation values between the internal and external components of Cont_ens and the IE simulations are shown in Fig. 3.12. The correlation of the external components of Cont_ens and IEnn (Fig. 3.12a) is similar in distribution to the Cont1-IEnn correlation in Fig. 3.11a, but with substantially larger values. This is consistent with IEnn being dominated by the forced component in the

regions of high correlation. The systematically higher correlations in Fig. 3.12a than in Fig. 3.11a result from the reduced noise variance in the Control_ens ensemble mean compared to Cont1, while the externally forced component is the same in both. The regions of low correlation in Fig. 3.12a indicate that the origin of the variability there is not primarily external forcing. The low correlations over the tropical Pacific are due to the fact that ENSO is an internal but noise influenced coupled mode in the model, and thus is not forced by external forcing but rather air-sea interactions and ocean dynamics, which can be different between IE and Cont_ens, runs. The influence of the weather noise forcing is demonstrated by the increased correlations in the Tropical Pacific between the internal components Cont1-IEAll (Fig.3.12b) and Cont2-IEAll_Cont2 (Fig. 3.12c) compared to Fig. 3.12a. When weather noise forcing is included, the correlation also increases over the North Atlantic region and polar regions as well as North Pacific in both the Cont1-IEAll and Cont2-IEAll_Cont2 compared to ContEns-IEnn. The correlation between internal component of Cont1 and IENoIpcc shows similar values as for the previous cases but with a higher correlation over the ENSO region. The correlation between the internal component in the regional noise forcing IE experiments and internal component of Cont1 shows values between 0.5-0.7 in the region where the forcing is applied in the case of IEAtl030. In the case of the forcing applied to the 30N-60N region values of 0.3-0.5 are also localized within the forcing region.

3.3.3 Atlantic Multidecadal Variability

3.3.3.1 Total index

The total AMV index, calculated as the annual SST average between 0-60N and 0-80W , with any grid point containing ice at any time in any of the CGCM_ens members masked, shows a correlation of 0.82 between IEAll and Cont1 and 0.81 between IEAll_Cont2 and Cont2 (Fig. 3.13 a and b). All the indices show a positive trend that becomes larger starting in 1940-1950. The external components of AMV in the Control_ens and IE, IEnn (Fig. 3.13c) have correlation 0.78 demonstrating an important role of the 20th century forcing in the total AMV variability.

The internal AMV indexes are shown in Fig 3.14 a for Cont1 and and the associated IE run IEAll,, and in 3.13b for Cont2 and IEAllCont2. The correlation between IEAll and Cont1 is 0.51, and 0.52 between IEAllCont2 and Cont2. The variance of the internal AMV for the CGCM and the associated IE runs is similar, and the IE internal AMV stays mostly within the values of the Control_ens envelope. Throughout most of the period but especially after the 1940s, the internal IEAll AMV index is higher than in Cont1. This can probably be linked to the different ice cover representation and evolution between the IE and Control_ens.

The total AMV index for the IE simulations (Fig. 3.15,a) shows that in the case of no external forcing, IENoIpcc, the AMV index has a decreasing trend, while the AMV in all of the other IE simulations has increasing trends. This supports the result in Fig. 3.13c that the AMV trend is externally forced. The decreasing trend in IENoIpcc indicates that the difference between the IEnn and Cont_ens estimates of the external AMV, positive before 1900 and negative after 1940, is probably due to the drift in the IE simulations.

The correlations between internal AMV indexes of Cont1 and the various IE runs forced

by the noise from Cont1 are given in Table 3.2. The highest correlation with Cont1 is with the IEAll AMV index. The correlations with Cont1 are lower for the cases when the weather noise is applied locally only in the Atlantic, IE030, IE3060, as well for IENoIPCC, the run with the same global noise forcing as IEAll, but no external forcing. The lower correlation with IENoIPCC than with IEAll is probably due to the drift bias shown in Fig. 3.15a. As the internal response of SST to the noise forcing appears to be localized to the forcing region (Fig. 3.12), the higher correlation with IEAll is probably due to applying the noise forcing over the whole AMV region, rather than due to teleconnections from noise-forced SST in other oceans. From the Cont1/IE030 and Cont1/IE3060 correlations, the roles of noise forcing in the AMV region poleward and equatorward of 30N are roughly comparable.

The correlation of the IEAll internal AMV with the regionally forced internal AMV indexes is again roughly comparable for noise forcing poleward or equatorward of 30N. The noise forcing in the two regions is not completely independent, as shown by the positive correlation between the IE030 and IE3060 AMV indexes.

Table 3.4. Correlation of internal AMV among IEAll and IEnn,IE030,IE3060 and Control.

Model	IEAll				
IEAll	1	IENoIpcc			
IENoIpcc	0.53	1	IE030		
IE030	0.60	0.33	1	IE3060	
IE3060	0.61	0.39	0.22	1	Cont1
Cont1	0.53	0.35	0.31	0.35	1

The SST regression patterns of the SST on the AMV index, for each of the CGCM_ens members for the internal, total, and external components are shown in Fig. 3.16. The regression patterns for the internal component (Fig. 3.16 a to f) are similar for all the six CGCM_ens simulations. The structure has negative values in the high latitudes, north of from 50N, a band of strong positive values near 40N, and positive values extending southward from this band in the eastern Atlantic to cover the subtropics and tropics. In the mid-latitude western Atlantic, the regressions pattern is weak. The pattern is similar to that obtained from a long constant 1990 external forcing control simulation with the same model (Chen and Schneider 2014). The patterns associated with the internal AMV in the CGCM_ens simulations have some similarity with the one obtained from observations in Trenenberth and Shea (2006), but with the exception of the negative values at high latitudes. The externally forced AMV pattern (Fig. 3.16h) has a single-signed blander pattern throughout the AMV region with some intensification near 40N as in the total pattern. The total AMV regression patterns (Fig. 3.16g-l) resemble the internal patterns, but with negative regressions replaced by weak regressions of both signs at high latitudes, and weak positive regressions in the western mid-latitude Atlantic. The more positive regressions at high latitudes and in the western mid-latitudes are due to the influence of the external component.

The SST regression patterns of the IE SST on the respective IE experiment AMV indexes,(Fig. 3.17) show an internal AMV pattern in IEAll with negative values in the western Atlantic Basin and a structure similar to the Cont1 pattern but weaker. Thus,

excepting the small differences in the Eastern Atlantic and the weaker negative above 50N the pattern reproduces well the one in Cont1. With noise forcing but not external forcing (Fig. 3.17b) the AMV internal component pattern has similar structure to IEAll but with positive sign throughout the AMV region. When the noise forcing is applied only over 0-30N (Fig. 3.17c) the pattern obtained is similar to the IEAll pattern, but emphasizes the lower latitude part. Applying the noise over the higher latitude AMV region in IE3060 (Fig. 3.17d) produces the IEAll pattern, but with the high latitude part emphasized. Thus must be is a dynamical connection between the internal AMV variability forced in the lower and the higher latitudes.

Lag regressions of the internal SST against the internal AMV index are shown for Cont1 in Fig. 3.18 and for IEAll in Fig. 3.19. It is difficult to identify any coherent low frequency behavior in either the CGCM or the IE. The AMV pattern appears to pop up out of background SST noise on a time scale of less than five years, and disappear then into the background noise on a similar time scale. A similar view is obtained from lag regressions of the internal AMV onto itself for the members of Cont_ens and the noise forced IE runs (Fig. 3.21). On the other hand, the external AMV has strong persistence due to the large trend.

The envelope of the power spectra of the AMV indexes for the CGCM_ens runs and the average of the spectra of the CGCM_ens members is shown in Fig. 3.20a. The significance of the spectrum is evaluated in each case using a Markov red noise confidence spectrum with upper and lower confidence curves of 5% and 95% respectively. The average of the spectra shows no significant peak at 95% red noise

confidence level.The power of the spectral components for each individual CGCM as well as for the total average stays mostly under -0.8. The spectra of the externally forced part of the AMV, Fig. 3.20b, show that IEnn (red) and the Cont_ens (red) are very coherent but neither is significantly different from red noise at the 95% level. The power spectra of the internal AMV variability for IEAll and Cont1 also show strong coherence and no significant difference from red noise at the 95% level (Fig. 3.20c). The same result is obtained form the spectra of the internal components in Cont2 and IEAllCont2 (Fig. 3.20d). The power spectra are consistent with the conclusions that the externally forced AMV variability in Cont_ens is reproduced by IEnn, that the internal AMV variability is indistinguishable from red noise, and that the internal AMV variability is forced by atmospheric noise.

The lead-lag regressions of the AMV (internal component) onto itself for the CGCM_ens members (Fig. 3.21a) shows an abrupt drop from year 0 to ~year 2 after which all the correlation components are under 0.2-0.3. This, together with the results shown by the spectrum analysis, shows that the internal AMV component has no preferred time scale and is a random/white noise time series after one or at most 2 years.

3.3.4 Atlantic Meridional Overturning Circulation

The first EOFs of the annual mean Atlantic meridional overturning (AMOC) stream function were calculated for each simulation (Fig. 3.22a-k), and for the Cont_ens ensemble mean (Fig. 3.22l). They have similar structures and magnitudes. Each EOF1 shows a cell with the maximum value centered at around 1.5-2 km at 30N-40N in the

Control_ens ensembles and 40N-50N in the IE. The PCs associated with these patterns are taken to be the AMOC indices for the total and external components.

For the Control_ens runs (Fig. 3.22a-f) the structure explains 40%-50% of the total variance and for the IE experiments the variance explained is higher, with the maximum, 66%, in the case of IE030 (Fig. 3.22i). The Cont_ens EOF1 has two different cells: the main AMOC cell that is centered around 1.5 km, a shallow opposite sign cell at 60N and approximately 0.2 kilometers depth. The pattern explains 40%-50% of the total variance, depending on ensemble member. The two separate centers of opposite signs appear in the external component of the AMOC (Fig. 3.22k). The secondary high latitude cell does not appear in IE EOF1 (Fig. 3.22g-k). The patterns explain 58-68% of the AMOC IE variance when external forcing is included and 53% for IENoIpcc, where no external forcing is included.

The PCs associated with the total and external AMOC EOF1 (Fig. 3.23) show a negative trend, for both Control_ens and IE experiments. The decreasing trend represents the external signal (Fig. 3.23l) and its physical meaning is a decrease in the AMOC strength. As expected, in the absence of external forcing (Fig. 3.23k) the negative trend is weaker. The reduction in MOC strength associated with increasing greenhouse gases is well known and represents a negative feedback for the warming in and around the North Atlantic. That is, through reducing the transport of heat from low to high latitudes, SSTs are cooler than they would otherwise be if the MOC was unchanged. The external component PCs, Cont_ens and IEnn (Fig. 3.23l and h) are closely related with correlation 0.71, so the externally forced AMOC behavior in the CGCM is well simulated by the IE.

The internal components of the AMOC are calculated by removing the external components of the streamfunction (before EOF decomposition) from the total. The PCs of the first EOF of the internal AMOC is then used as the internal AMOC index. The structures of the internal EOF1 are shown in Fig. 3.24, and are very similar to those of the total AMOC. While the IE and Cont_ens internal AMOC components have similar variance, the noise forced IE does *not* produce a good simulation of the Cont_ens internal AMOC. The internal AMOC indexes in Cont1and IEAll (Fig. 3.25a) have a negative correlation of -0.16. The correlation of internal AMOC in Cont2 and IEAll_cont2 (Fig. 3.25b) is small, 0.08. Therefore, the internal AMOC variability in Cont_ens is *not* forced by atmospheric noise. On the other hand, there are high correlations between IE simulations forced by the Cont1 noise (Table 3.5), especially when the forcing region includes the high latitude North Atlantic (e.g. between IEAll and IENoIpcc, or between IEAll and IE3060). This indicates that the Cont1 internal AMOC in the IE *is* noise forced primarily in the high latitude North Atlantic. The internal AMOC variability in Cont1 or Cont2 that is not noise forced can then be estimated by removing the internal noise forced component given by the IEAll. We have not yet done this.

Table 3.5 Correlation between internal AMOC indexes.

Model	IEAll			
IEAll	1	IENoIpcc		
IENoIpcc	0.74	1	IE030	
IE030	0.24	0.19	1	IE3060

IE3060	0.63	0.65	0.31	1	Cont1
Cont1	-0.15	-0.21	-0.12	-0.05	1

The internal SST regression onto the internal Cont_ens AMOC indexes (Fig. 3.26a-f) has a similar pattern for Cont2-6, with negative values above 45N and strong positive values in a narrow zonal band near 42N, which will be called the Gulf Stream Extension or GSE. For Cont1 the SST regression pattern the negative values in the north are much weaker, and the GSE feature is not strong anymore. Thus, a qualitatively different projection of the AMOC onto the SST internal component is found in Cont1, in comparison to the other CGCM simulations. The total SST regressions against the total AMOC indices for Cont_ens members (Fig. 3.26g-i) have a number of different structures but they are predominantly negative above 50N and under 20S and positive along the GSE in three of the models (Cont3,Cont4 and Cont5). The regression of the Cont_ens external SST against the external AMOC index is negative, except for some small positive regions in the western high latitude North Atlantic, consistent with decreasing AMOC associated with increasing AMV index.

The regression of the IE internal SST onto the internal AMOC for the various simulations (Fig. 3.27a-3) has positive values in the GSE region surrounded by negative values. There is also a region of positive or weak negative values to the southwest of Spain. The Atl3060 internal regression (Fig. 3.27d) differs from the other in having positive regressions equatorwards of 30N. However the Atl030 internal regression has similar structure to Atl3060 north of 30N. The external IE regression is negative everywhere, and

stronger in high relative to low latitudes, basically the same sign, but contrasting in structure somewhat with the Cont_ens external regression

The lag regression of the Int Cont1 SST onto its Int AMOC index mode is shown in Fig. 3.28. It is difficult to identify coherent features in this sequence. Rather it appears to consist of maps of uncorrelated noise.

The lead-lag regressions of the AMOC internal component onto itself for every CGCM_ens components (Fig. 3.29a) shows, as in the AMV internal component case (Fig. 3.20) an abrupt drop from year 0 to ~year 2 after which all the correlation components are very low and close to 0. This shows that, similarly to the AMV internal component, the AMOC internal component behaves like a random/white noise time series after one or at most 2 years.

The correlations of AMOC with itself for External AMOC in Control_ens (green curve in panel b), IEnn (red) as well as internal components of IEAll (orange) and IEAllCont2 (dark red) are shown in Fig. 3.29 b. The internal AMOC indexes in the IE behave in a similar manner to the internal components in Cont_ens showing an abrupt drop from 1 to 0 in the first 2-4 years and then oscillation around 0 suggesting a random time series. The external component of IE (red) maintains a substantial positive values for all lags, as does the external component of Cont_ens, reflecting the long term trends of the externally forced AMOC component in both cases (a linear trend would have lag regression equal to one for all lags).

The relationship between the internal AMOC and AMV indices in Cont_ens (Fig. 3.30 a) shows that for five of the simulations (Cont2, Cont3, Cont5, Cont4, Cont6) lagging AMO is associated with positive AMOC values from lag -10 up to 0. At the simultaneous regression the AMV index is associated with positive AMOC. When AMV leads the AMOC, the regression decreases and after about 2 years positive AMV is associated with negative AMOC values. A correlations significance test was done for the AMV-AMOC relationship (not shown) and at 95% significance levels the correlations for AMV-AMOC when AMV leads were significant for lags 0 to 2 and for AMV lagging the correlations were significant for lags 0-6 and from 11 to 15.

The case for Cont1 is different – at - 5 years positive AMV is associated with negative AMOC values. In the both of the global noise and externally forced IE runs (Fig. 3.25b) for 2 IE cases positive AMOC leads positive AMV when AMOC leads by 1-10, simultaneous correlations are small, and positive AMV leads negative (reduced) AMOC when AMV leads by 1-7 years. The noise forced internal AMOC therefore follows the expected sequence of strong AMOC transporting more heat poleward, leading to warming of AMV SST, leading to reduced upper ocean density and reduced AMOC.

3.4 Conclusions and Summary

The roles of weather noise forced versus externally forced variability in the AMV and AMOC were studied in a series of externally forced 20th century CCSM3 simulations. The present work is based on, and advanced the conceptual understanding of the SF2007

method of extracting the atmospheric noise by applying it in a new, a state-of-the-art coupled global climate model with a 20th century forcing.

Few technical aspects in which our analysis is new are :

- It employed the IE-CGCM to isolate the variability due to atmospheric weather noise from other sources of climate variability (namely ocean internal variability, intrinsic coupled variability, and external forcing) and from the one due to external forcing. Also, the analysis is improved in comparison to models used in previous studies on this topic.
- Used a perfect model/perfect data framework
- The simulations were made in the context of the "Climate of the 20th century"
- The variability modes studied are the AMV and AMOC both of which have not been documented previously using this method

Our main findings show that:

- Most SST variability is forced by atmospheric noise after externally forced signal is removed.
- AMV variability is predominantly noise forced.
- Noise forcing 0-30 and 30-60 both produce similar AMV patterns 0-60
- Internal AMV is noise (no preferred time scale)
- Internal AMOC is noise (no preferred time scale)
- Internal AMOC is not predominantly noise forced
- The part of the internal AMOC that is noise forced acts to amplify and then terminate AMV events

- The internal AMV and AMOC relationships show a positive AMOC leads positive AMV.
- The IE represents the response to external forcing well. In the global mean, this response dominates the internal variability. However, on a regional scales the internal variability dominates the external response.

SUMMARY

This thesis addressed several problems in the attribution of climate variability.

Figure 1 shows how the total Sea Surface Temperature (SST) variability can be divided into externally forced and internally generated parts, and the internally generated part can be divided into atmospheric weather noise, ocean weather noise and coupled variability.

The first question studied was why the AGCM ensemble forced by observed SST does not simulate the observed 20th century sea level trends in the Indian Ocean. Our findings show that the AGCM and CGCM ensembles are consistent with each other, and suggest that the failure to simulate the observed trends is due to model bias rather than coupling.

Our preliminary investigation of the spatial and temporal properties of the weather noise shows that the temporal structure of the noise is consistent with white noise for annual and longer periods, although the probability density functions (PDF) are not Gaussian. No change is detected between the statistical properties of the noise in the early and late

20th century, so that changes in extreme events can be attributed primarily to changes in the mean rather than the noise.

The AMV is shown to have a strong contribution from the external 20th century forcing. The internal AMV variability is primary forced by the weather noise, but other sources of internal variability are also important. An important contribution to the internal AMV is associated with the internal variability of the oceanic Atlantic Meridional Overturning Circulation, and this contribution is distinct from the weather noise forced component.

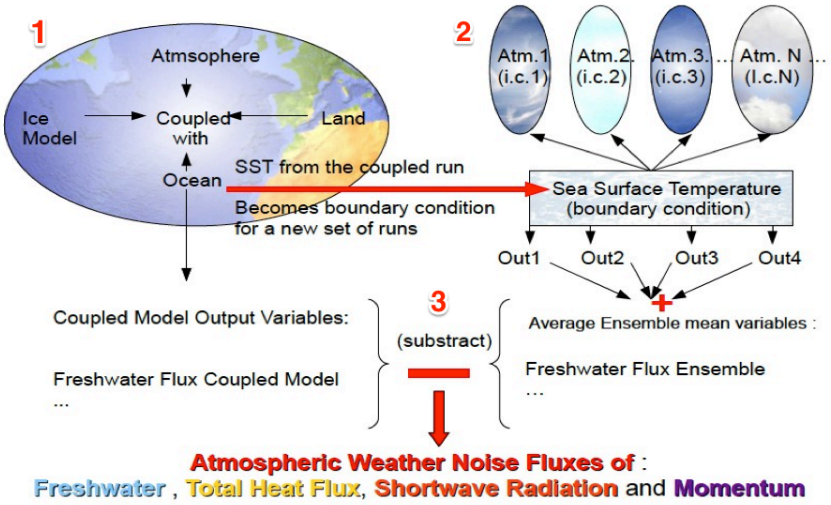

Figure 3.1 Noise Extracting Procedure. The SST from Cont1 (1) represents the boundary conditions for the ensemble of AGCMs (2). (3) The difference between the output of the Coupled Model (Cont1) minus the output from the SST forced ensemble of AGCMs represents the weather noise.

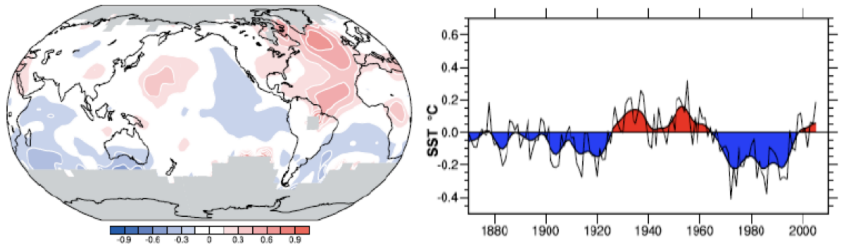

Figure 3.2 Correlation of the annual values AMV index with global surface air temperatures for 1900 to 2004. Values in the North Atlantic are considered significant (Fig.4 in Trenberth and Shea,2006). (Right) 1870-2005 annual SST anomalies, relative to 1901 to 1970, averaged over the North Atlantic (0° to 60°N, 0° to 80°W) (°C) with global mean SST removed. The heavy line with fill from the low-pass filter shows the AMV (Fig.3 in Trenberth and Shea 2006).

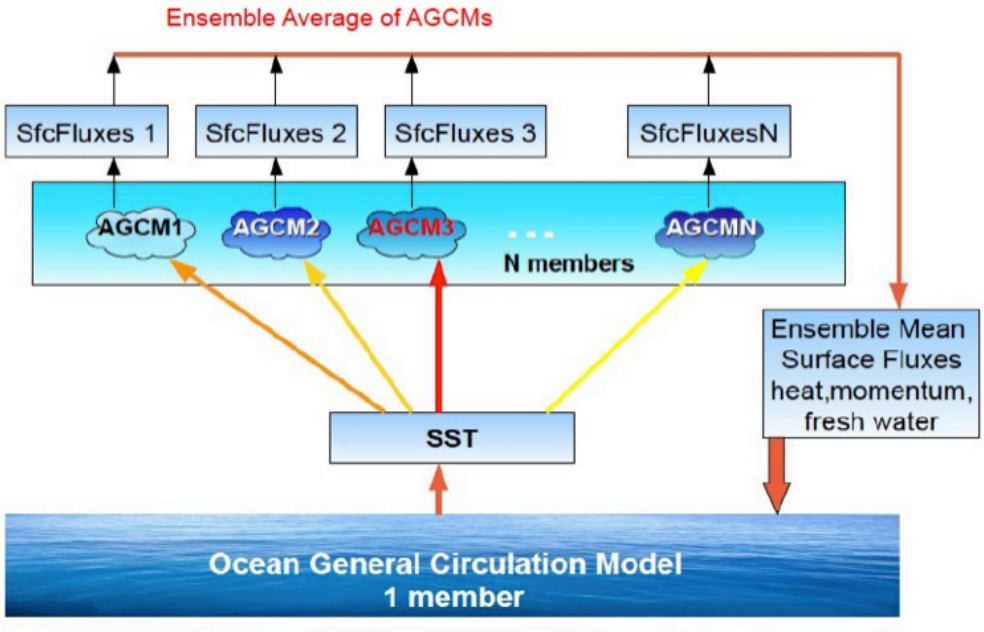

Figure 3.3 The Interactive Ensemble – One ocean model coupled with an ensemble of 'N' atmospheric models. The output of the ensemble of atmospheric models is averaged among all the AGCM ensembles, thus the atmospheric noise forcing is filtered, and the filtered quantities are passed as input to the ocean model.

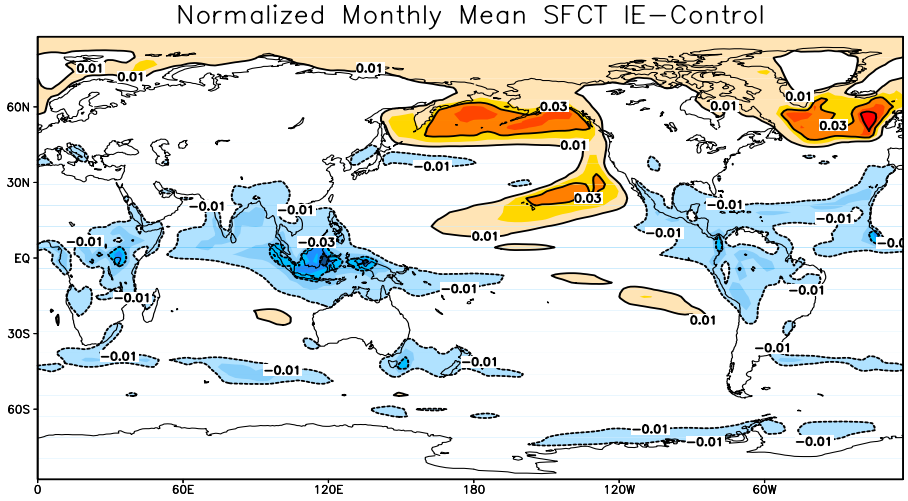

Figure 3.4 Annual mean surface temperature difference between IE and Control, normalized by the pooled standard deviation from the two simulations. The units are °C/σ^2.

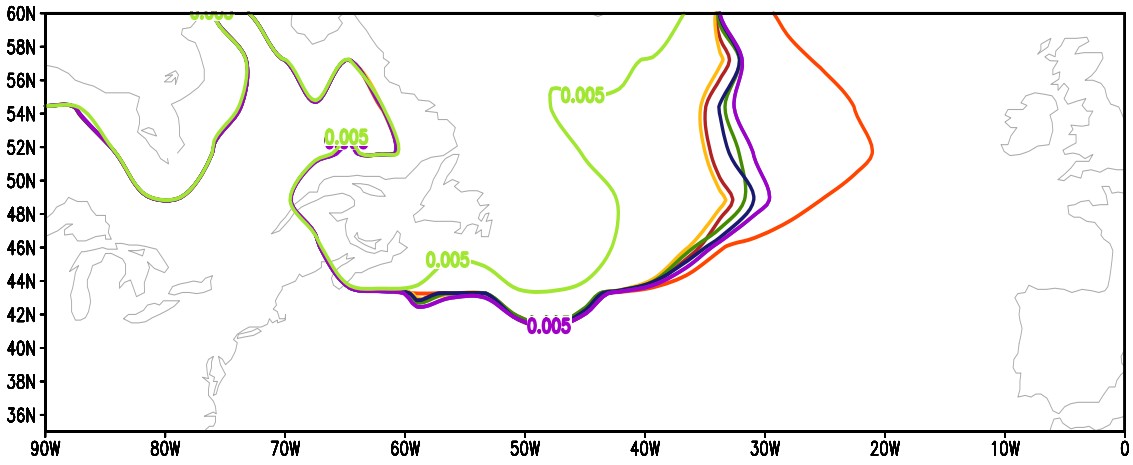

Figure 3.5 Ice cover in CGCM_ens experiments for: Cont1(red), Cont5 (blue),Cont3 (dark blue), Cont6(green), Cont4(red) and Cont (yellow) and IEAll (purple).

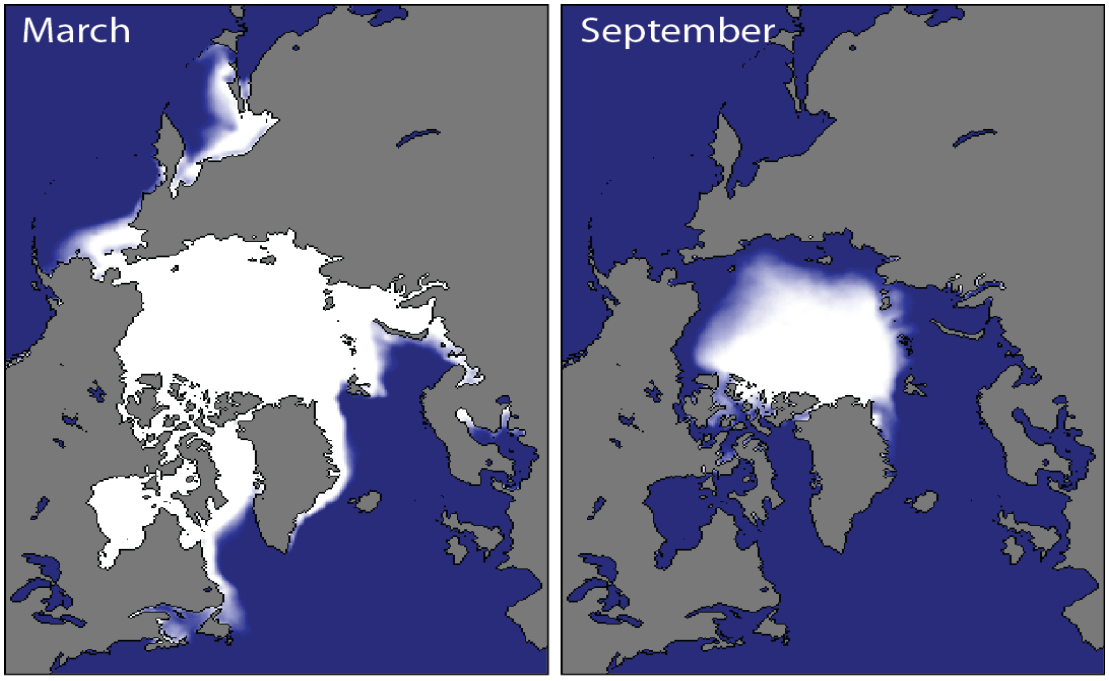

Figure 3.6 Sea ice climatology: Arctic sea ice concentration climatology from 1981-2010, at the approximate seasonal maximum and minimum levels based on microwave satellite data. Data provided by National Snow and Ice Data Center, University of Colorado, Boulder.

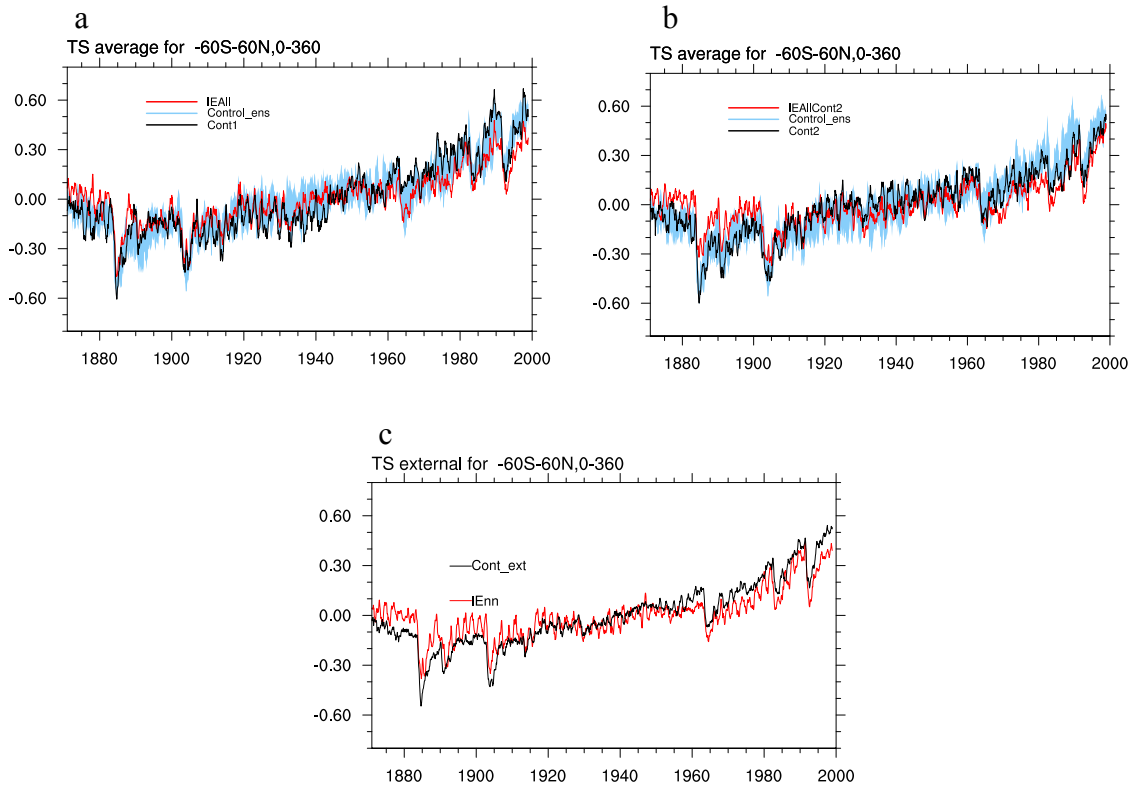

Figure 3.7 Annual SST anomalies averaged globally for (a) Cont1 (black), IEAll (red) and Control_ens envelope (blue) (b) Cont2 (black), IEAllCont2(red) and Control_ens Envelope (blue) (c) Cont_ens external (black), IEnn external(red).Units degC.

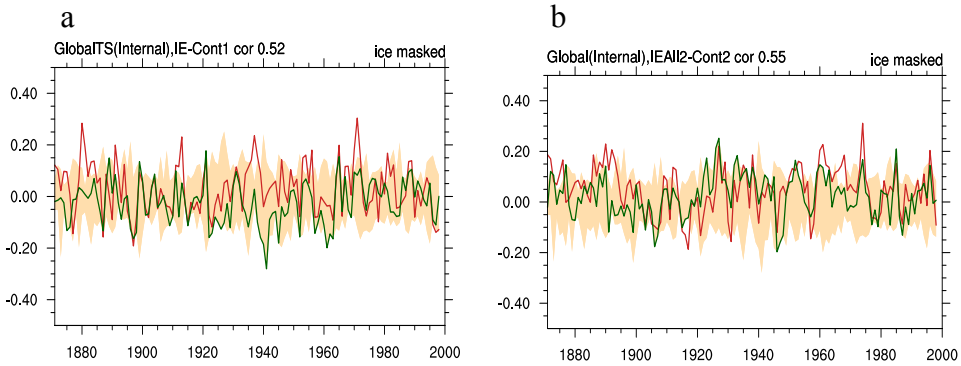

Figure 3.8 Annual Internal SST anomalies averaged globally, for Control (green),IE(red) and Control Envelope (beige) in Cont1 and IEAll(a) and Cont2 and IEAll2(b). Units degC.

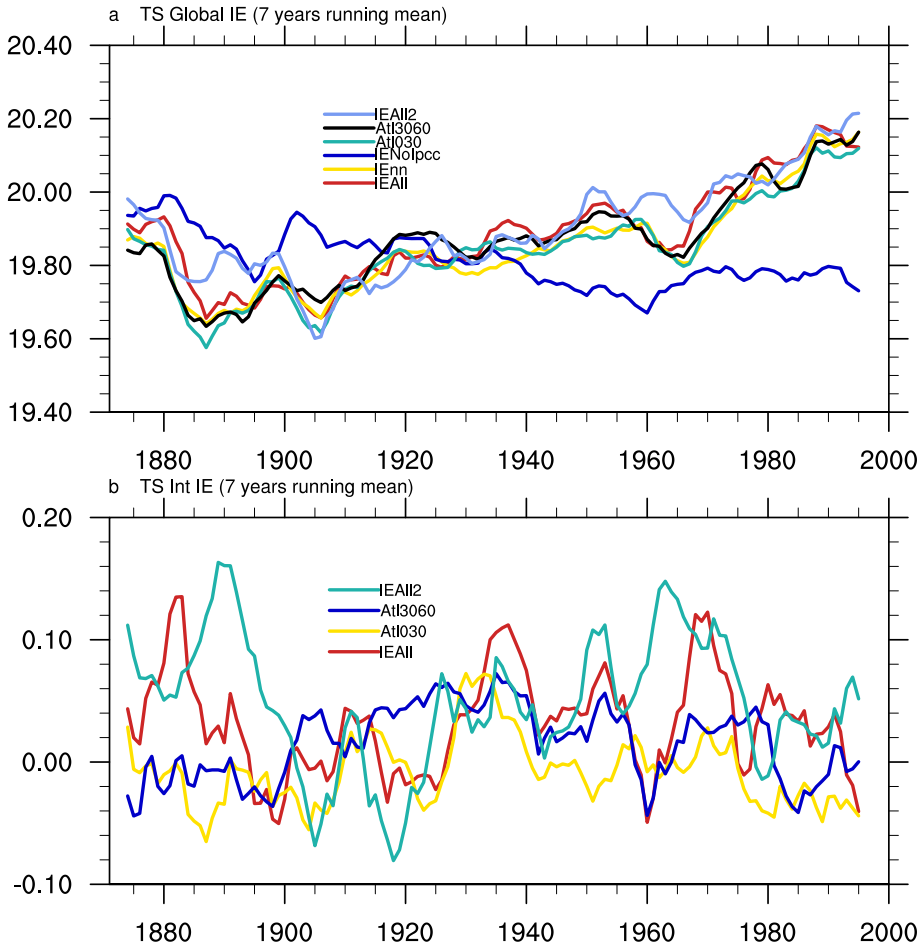

Figure 3.9 SST global 7 years running mean for (a) total IEAll (red), IEnn(yellow), IENoIpcc (dark blue), Atl030(green), Atl3060 (black) and IEAll2(light blue) and (b) Internal component for IEAll (red), Atl030(yellow), Atl3060(blue) and IEAllCont2 (green). Units degC.

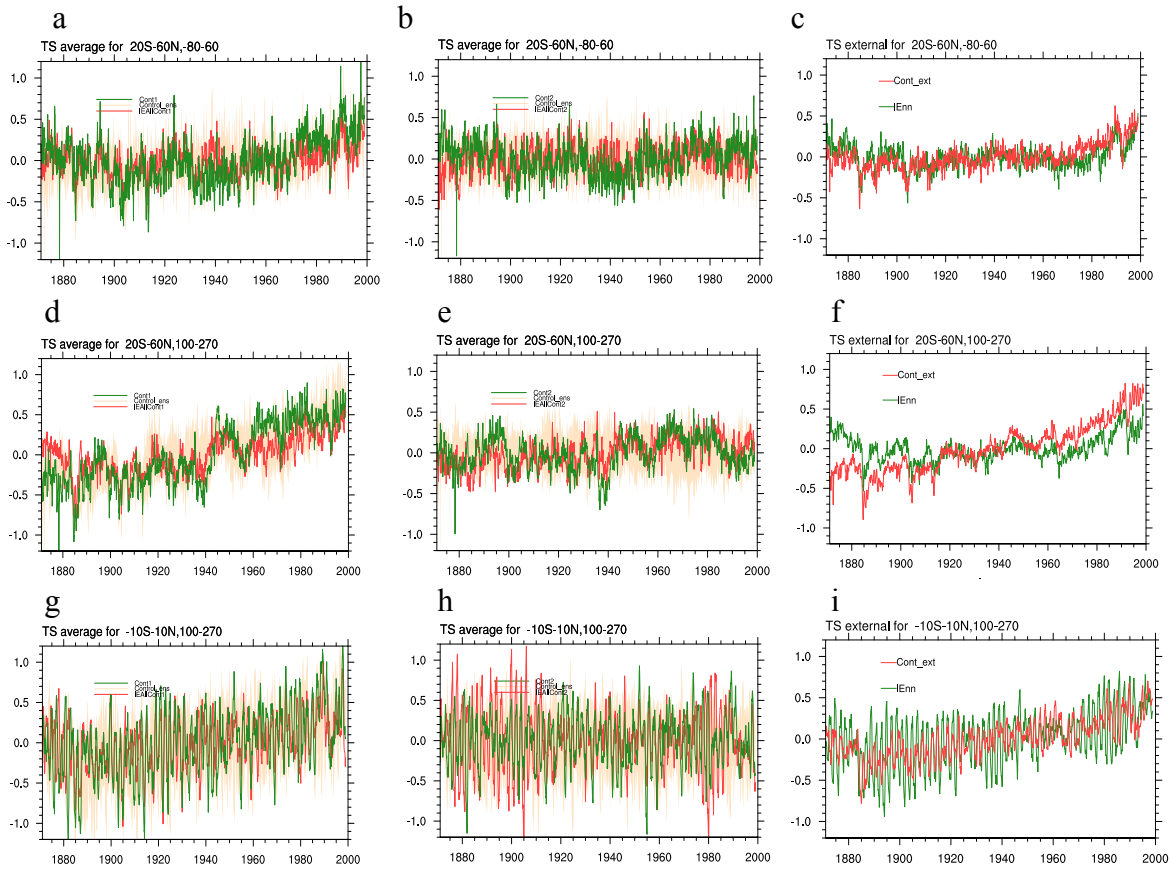

Figure 3.10 Annual SST anomalies for), total in left column, internal in middle column and external in right column, averaged over the North Atlantic (0° to 20N-60°N, 0° to 80°W-60E)- top row, North Pacific 20S-60N and 270W-100W – middle row and Equatorial Pacific ,10N-10S and 270W-100W bottom row for the period 1871-1998 for Cont1 (green),IEall (red) and CGCM Envelope (beige). Units degC.

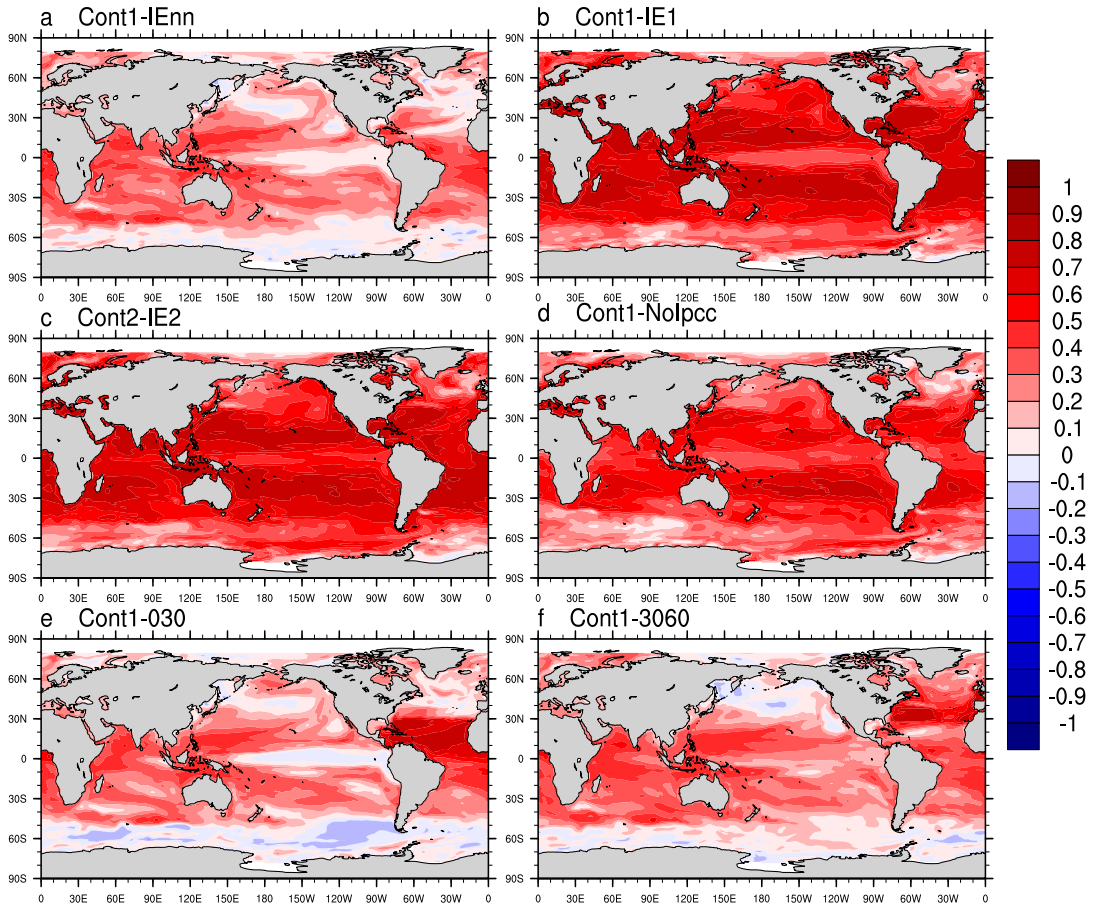

Figure 3.11 Point by point correlations of monthly SST in (a) Cont1-IEnn,(b)Cont1-IE1,(c)Cont2-IE2,(d)Cont1-NoIpcc,(e)Cont1-030,(f)Cont1-IE3060.

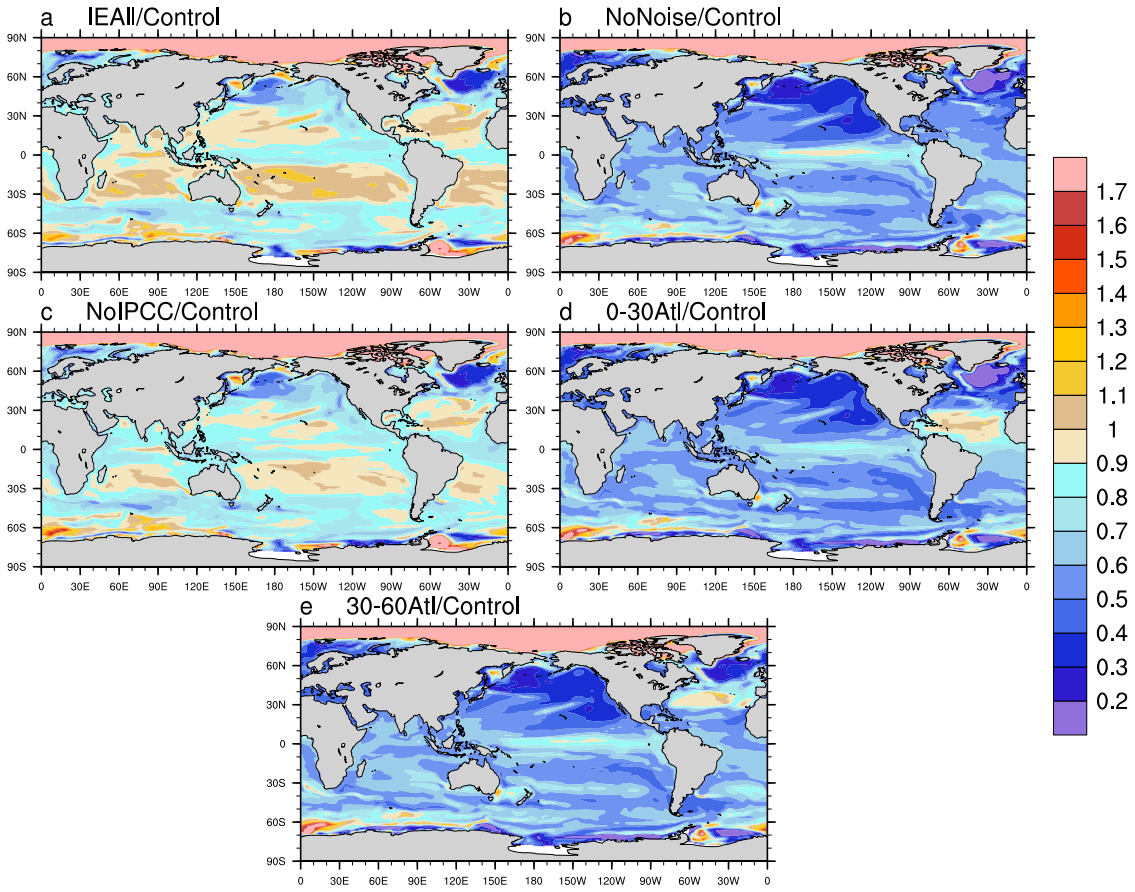

Figure 3.11 b Point by point standard deviation ratios between monthly SST in (a) IEAll, (b) IEnn, (c) IENoIpcc, (d) IEAtl030, (f) IEAtl3060 and Control.

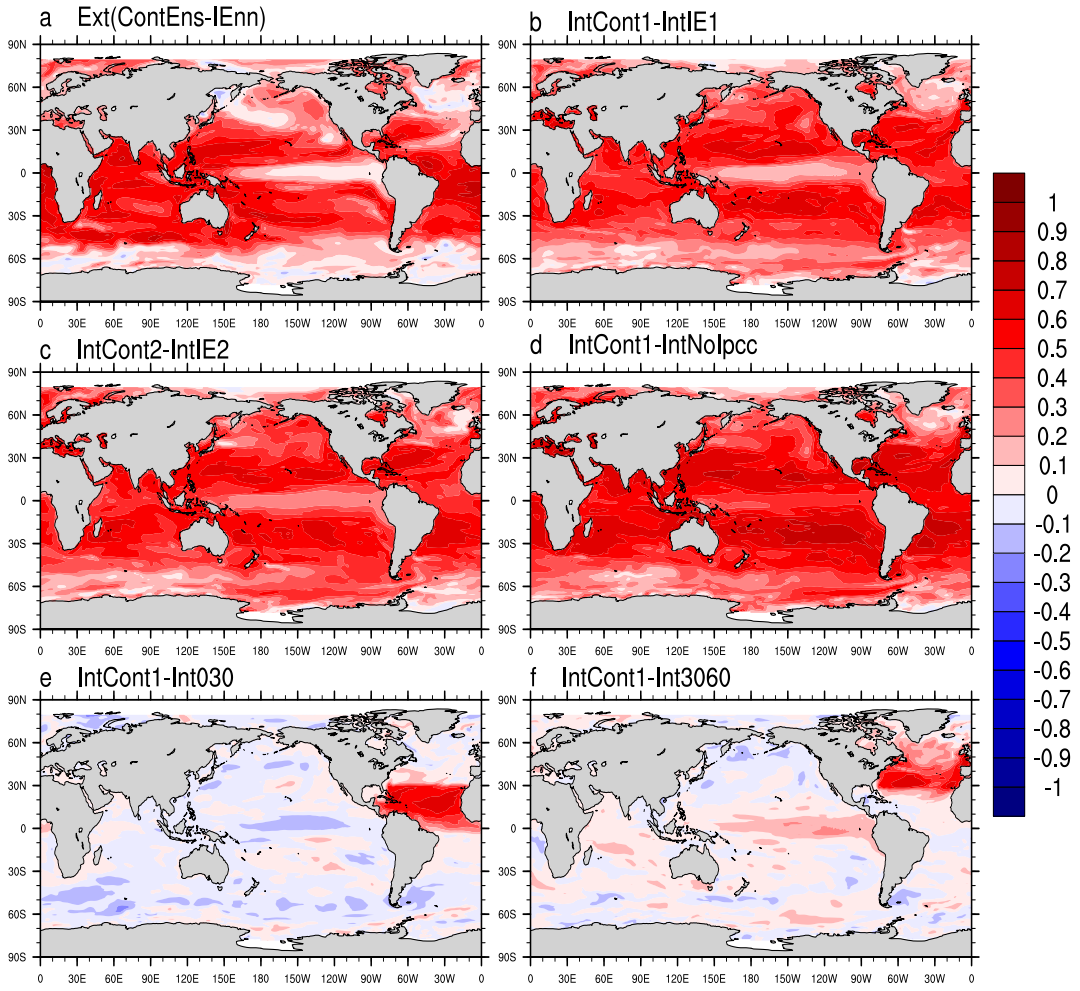

Figure 3.12 Point by point correlations of monthly SST in (a) ExtCont-Enn, (b)IntCont1-IntIE1,(c)IntCont2-IntIE2,(d)IntCont1-IntNoIpcc,(e)IntCont1-Int030,(f)IntCont1-IntIE3060

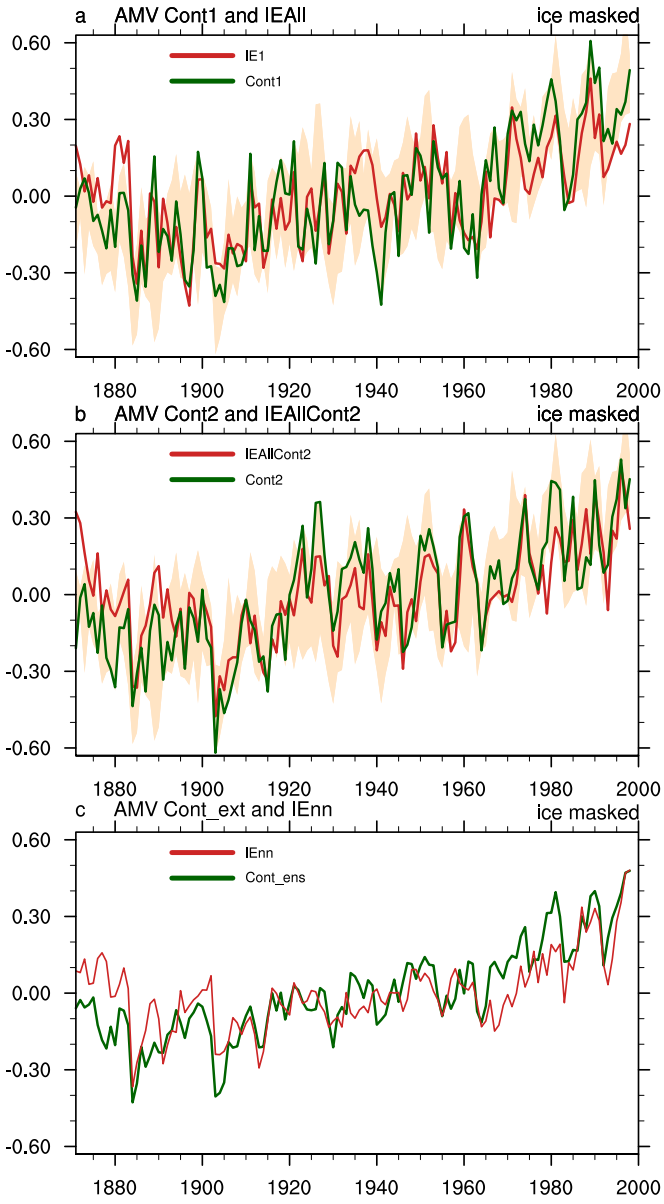

Figure 3.13 AMV Index total for (a) IEAll1(red), Cont1 (green) and Cont_ens envelope (beige); (b) IEAllCont2(red) and Cont2(green) and Cont_ens envelope (beige);(c) External components for Cont_ens (green) and IEnn (red). Units degC.

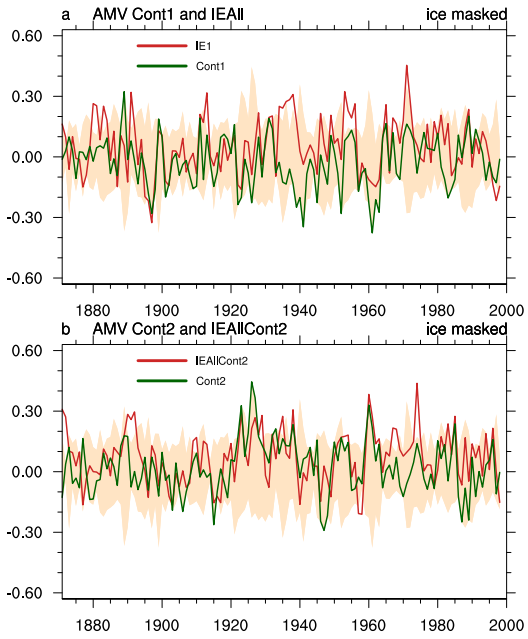

Figure 3.14 AMV Index internal component for (a) IEAll1(red), Cont1 (green) and Cont_ens envelope (beige); (b) IEAllCont2(red) and Cont2(green) Cont_ens envelope (beige). Units degC.

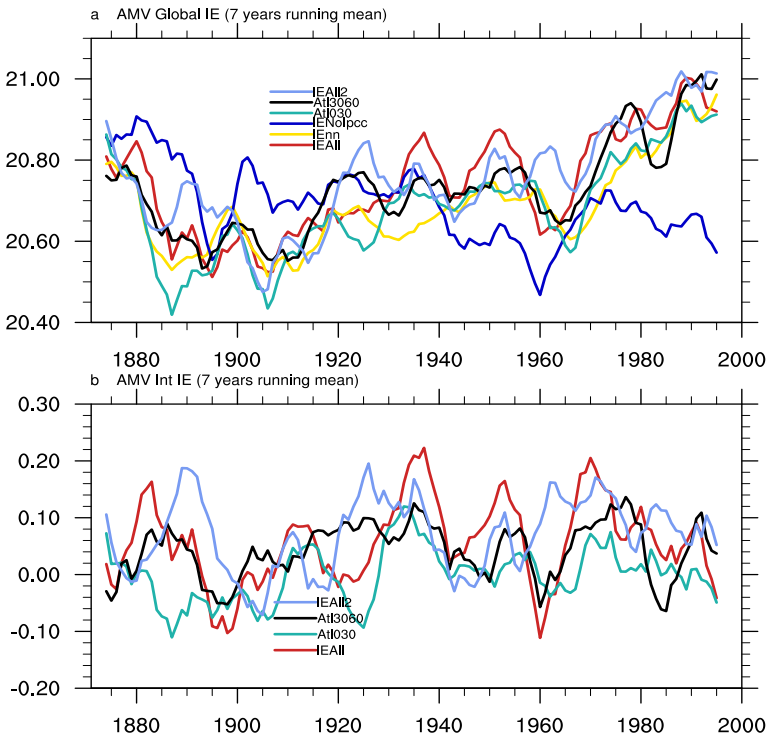

Figure 3.15 AMV total and Internal (a) total IEAll (red), IEnn (yellow), IENoIpcc (dark blue), Atl030(green), Atl3060(black) and IEAll2(light blue) and (b) internal component for IEAll (red), Atl030(green),Atl3060(black) and IEALl2(blue). Units degC.

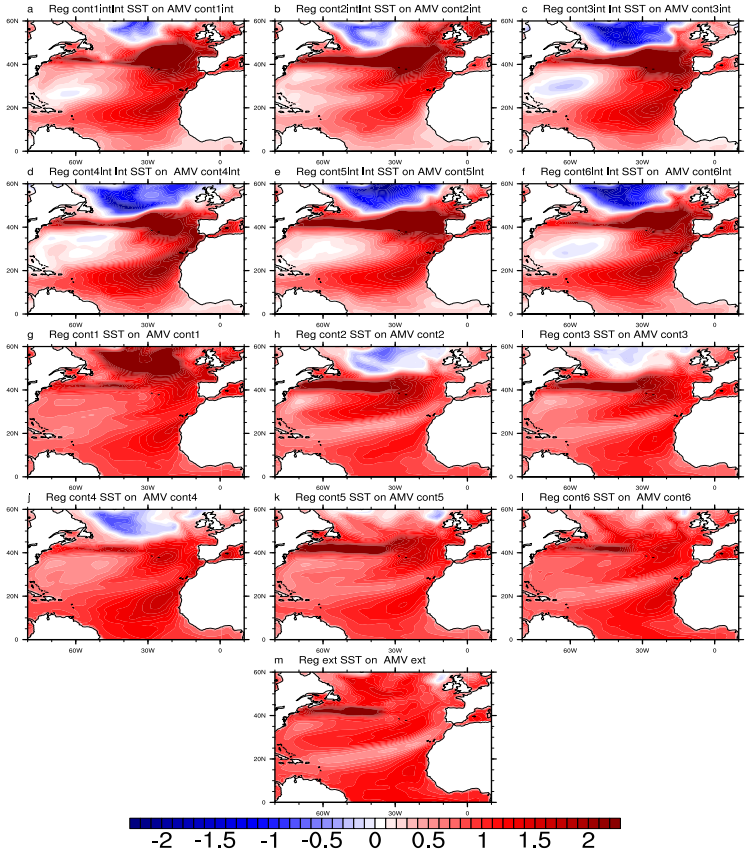

Figure 3.16 Regressions of Internal SST in (a) Cont1,(b)Cont2,(c)Cont3,(d) Cont4, (e) Cont5 and (f) Cont6 onto its respective internal AMV index. Regressions of SST in (g) Cont1,(h)Cont2,(i)Cont3,(j) Cont4, (k) Cont5 and (l) Cont6 and (m) External_ens onto its respective AMV index. Units degC/degC.

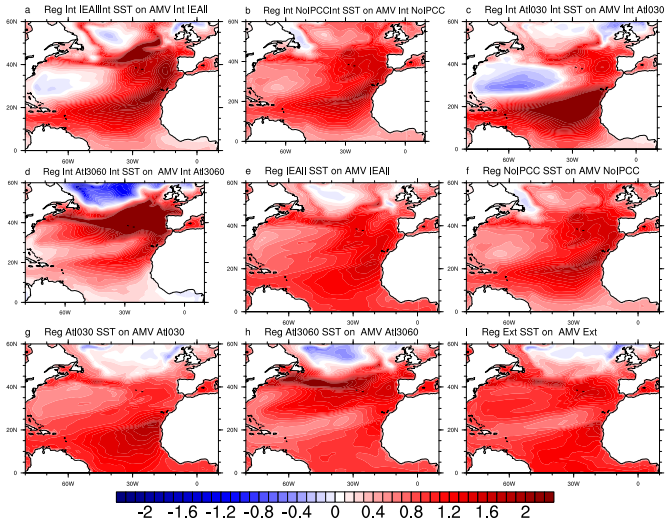

Figure 3.17 Regressions of SST Internal in (a) IEAll,(b) IENoIpcc ,(c)IE030 (d) IE3060 onto its respective AMV index. Regressions of SST Total in (e) IEAll,(f) IENoIpcc ,(g)IE030 (h) IE3060 onto its respective AMV index and (i) SST external (IEnn) onto IEnn AMV index. Units degC/degC.

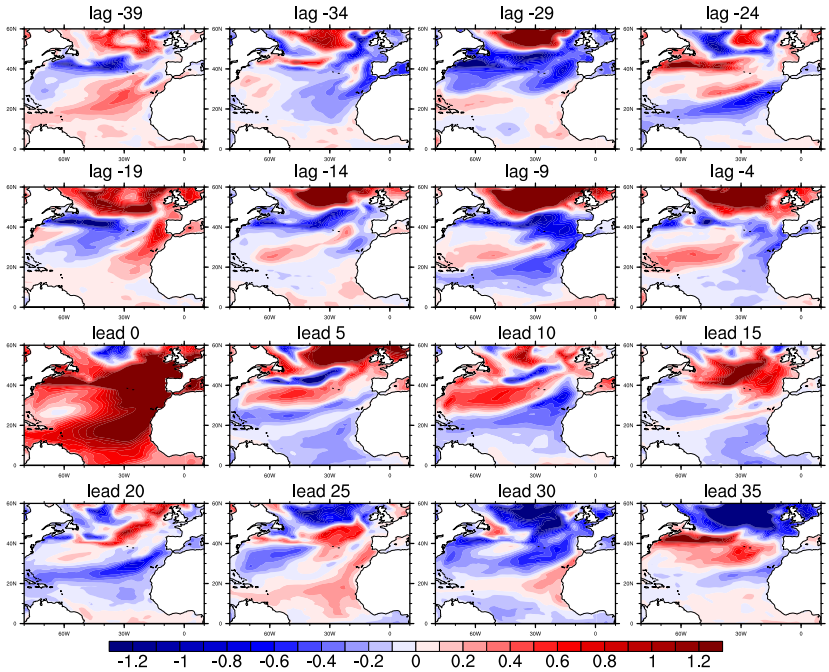

Figure 3.18 Lag regressions of internal SST in Cont1 onto the Cont1 internal AMV index. Lag in years is given. The AMV index is leading for positive values and lagging for negative ones. Units degC/degC.

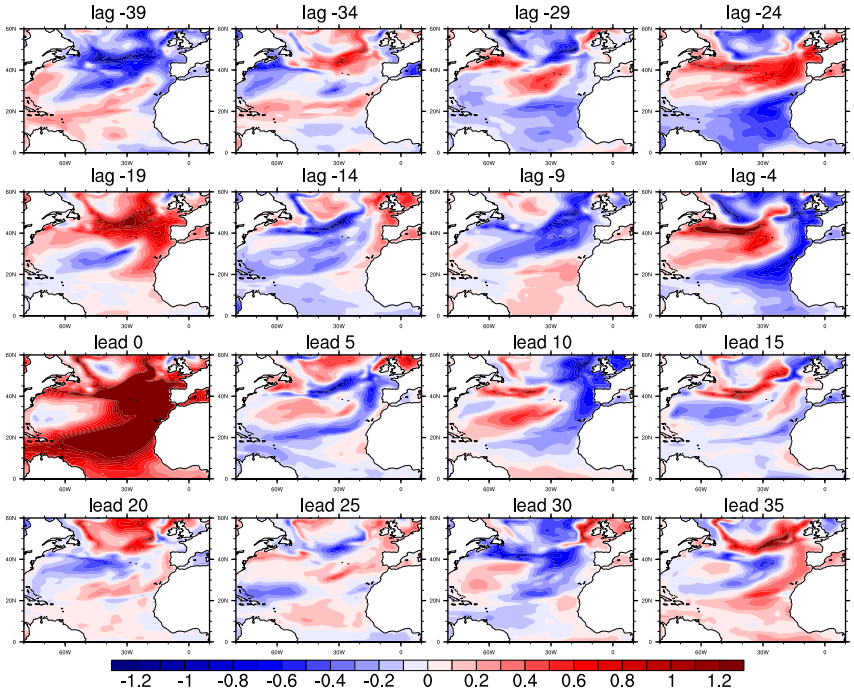

Figure 3.19 Lag regressions of Internal SST in IEAll onto the AMV index in IEAll. Starting with lag 0 (years). The AMV mode is leading for positive values and lagging for negative ones. Units degC/degC.

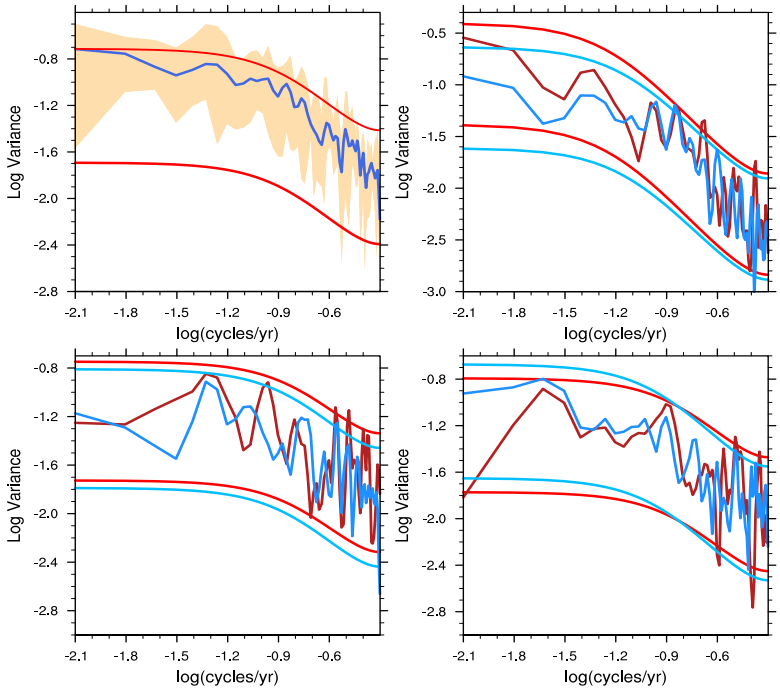

Figure 3.20 AMV Spectrum for (a) the Cont_ens runs, average of the raw spectra and the spread.
(b) spectrum of the externally forced AMV in Cont_ens and spectrum of IEnn (blue) (c) Spectra of internal for Cont1 and for IEAll (red) ; (d) Spectra of internal for Cont2 and for IEAll2 (red)

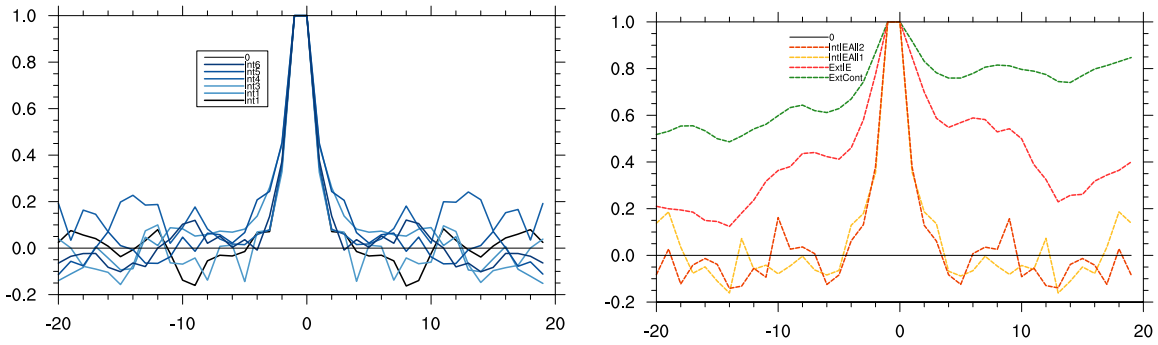

Figure 3.21 (left) Lag regressions of internal AMV onto itself in Cont1 (black) and the other Cont_ens members in blue; (right) Lead-Lag regressions of internal AMV onto itself for IntIEAllCont2(orange), IntIEAll(yellow),and external AMV onto itself for,ExtIE (IEnn,red) and ExtControl (green). Units degC/degC.

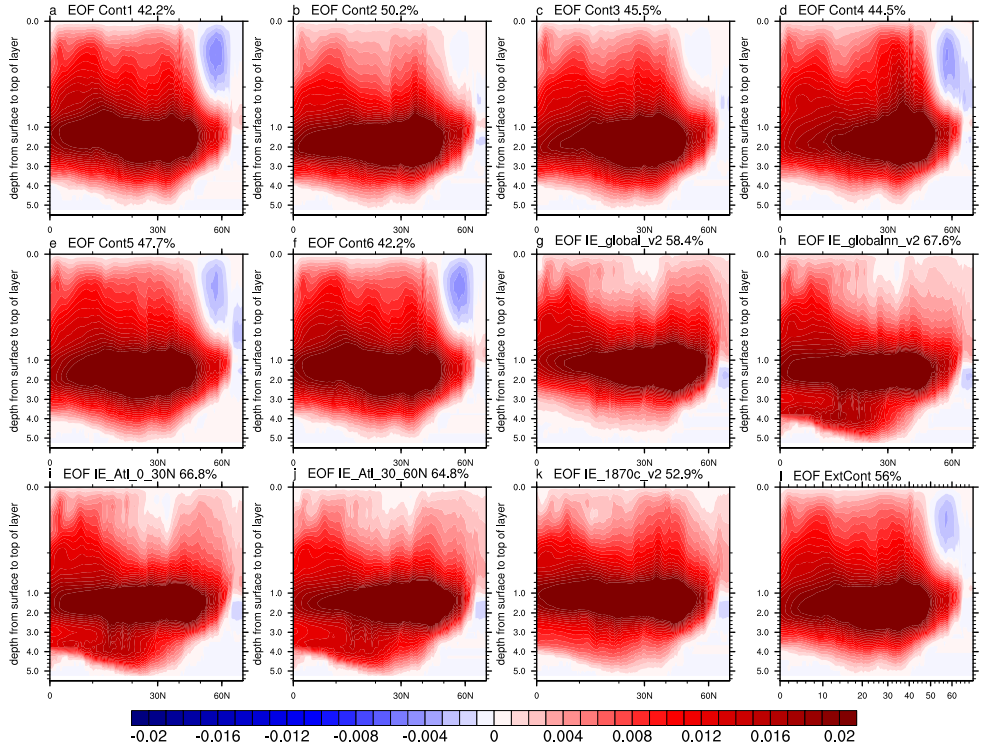

Figure 3.22 First EOF of the Atlantic meridional overturning stream function for (a) Control 1, (b) Control2, (c) Control 3, (d) Control 4, (e) Control 5, (f) Control 6, (g) IEAll, (h) IEnn,(i) IE030,(j) IE3060, (k) IENoIpcc and (l) Ensemble mean of Cont_ens.

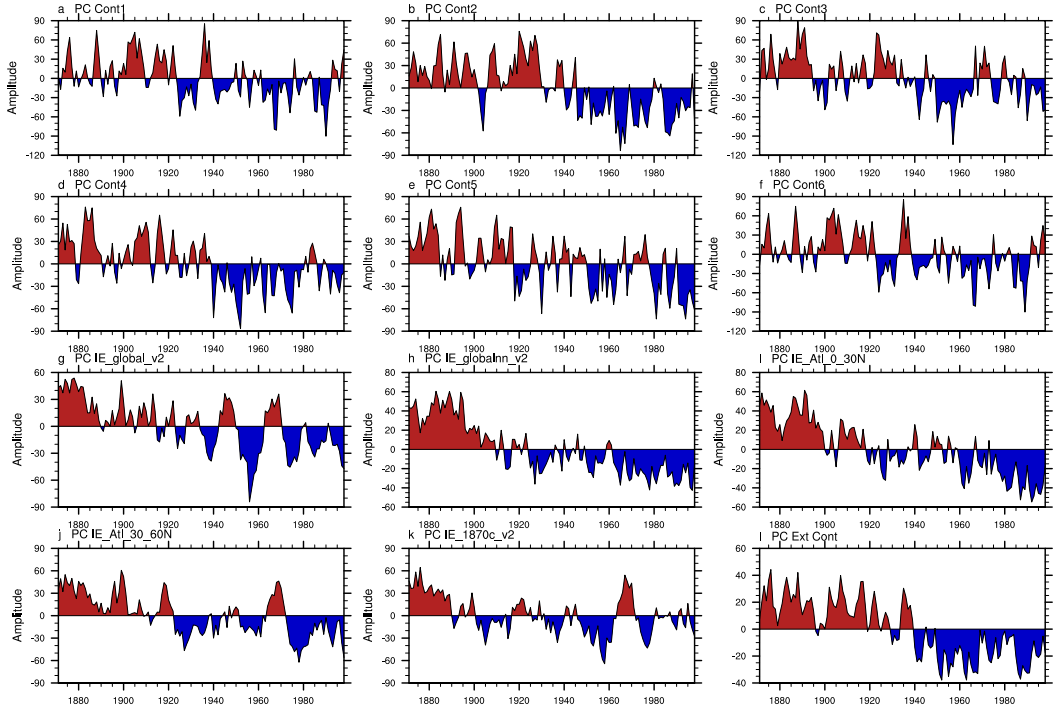

Figure 3.23 First PC associated with the EOFs in Figure 0.17, for (a) Control 1, (b) Control2, (c) Control 3, (d) Control 4, (e) Control 5, (f) Control 6, (g) IEAll, (h) IEnn,(i) IE030,(j) IE3060 and (k) IENoIpcc and (l) Ensemble mean of Cont_ens. Units Sverdrups.

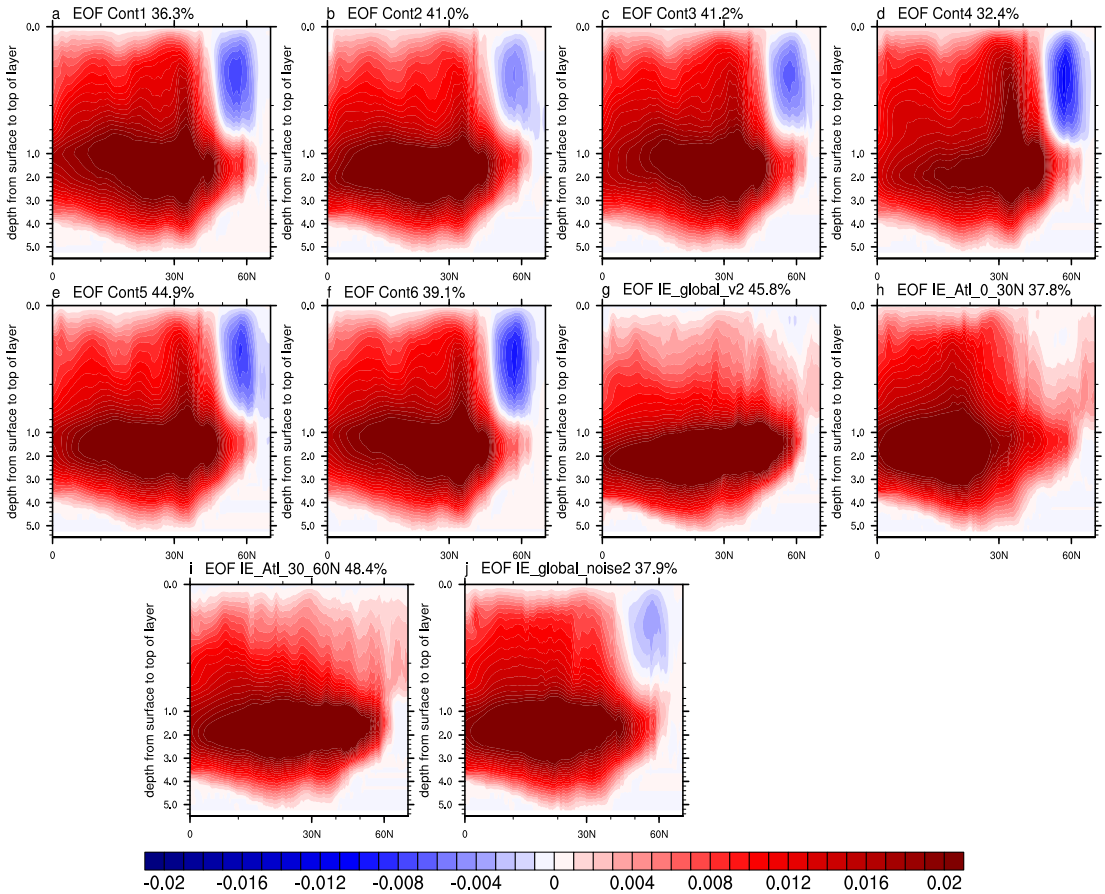

Figure 3.24 First EOF of the Atlantic meridional overturning stream function for (a) Cont11, (b) Cont2, (c) Cont 3, (d) Control 4, (e) Control 5, (f) Control 6, (g) IEAll, (h) IE030,(i) IE3060, (j) IEAll_Cont2.

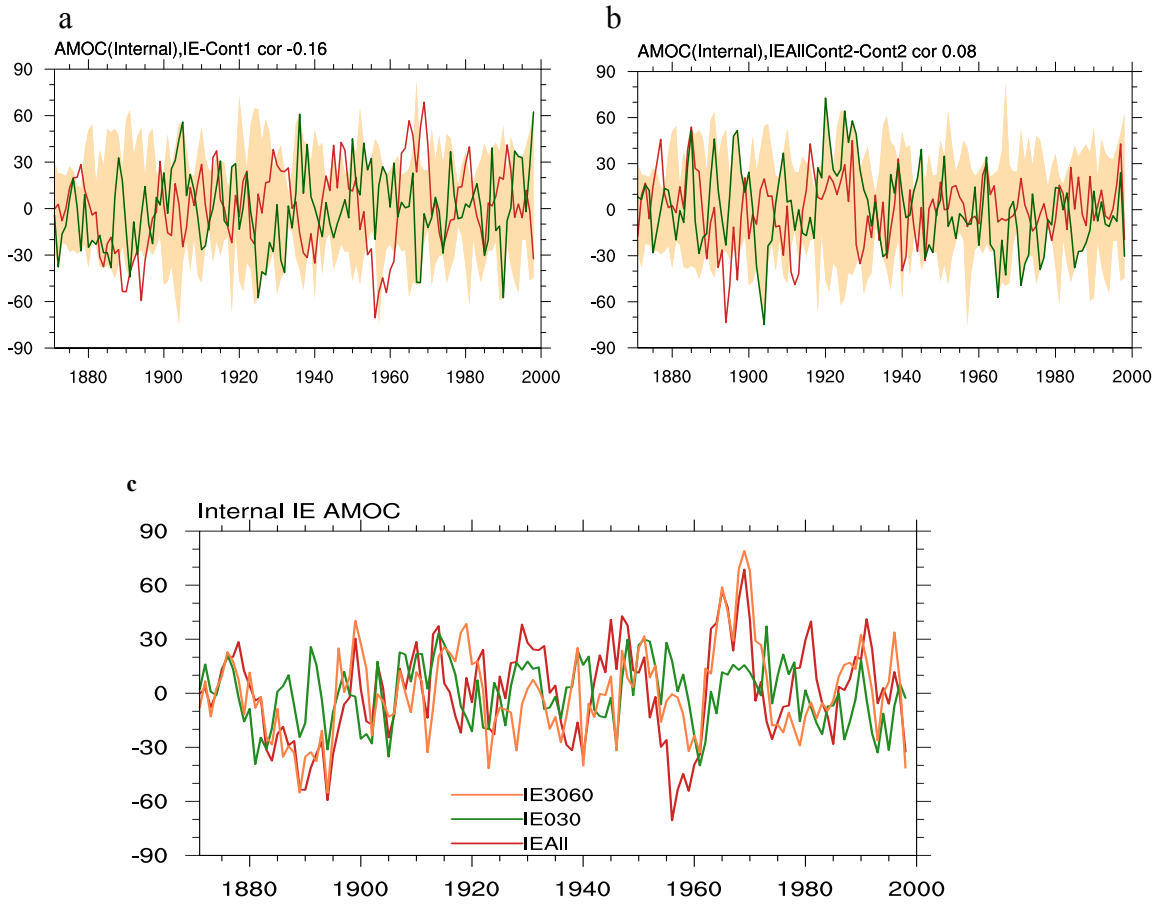

Figure 3.25 Internal AMOC index for (a) Cont_ens Envelope (beige), IEAll (red) and Cont1 (green) (b) same thing as in a) but for Cont2 and IEAllCont2; (c) IE runs with IEAll (red), IE030(green) and IE3060(orange).Units degC/degC.

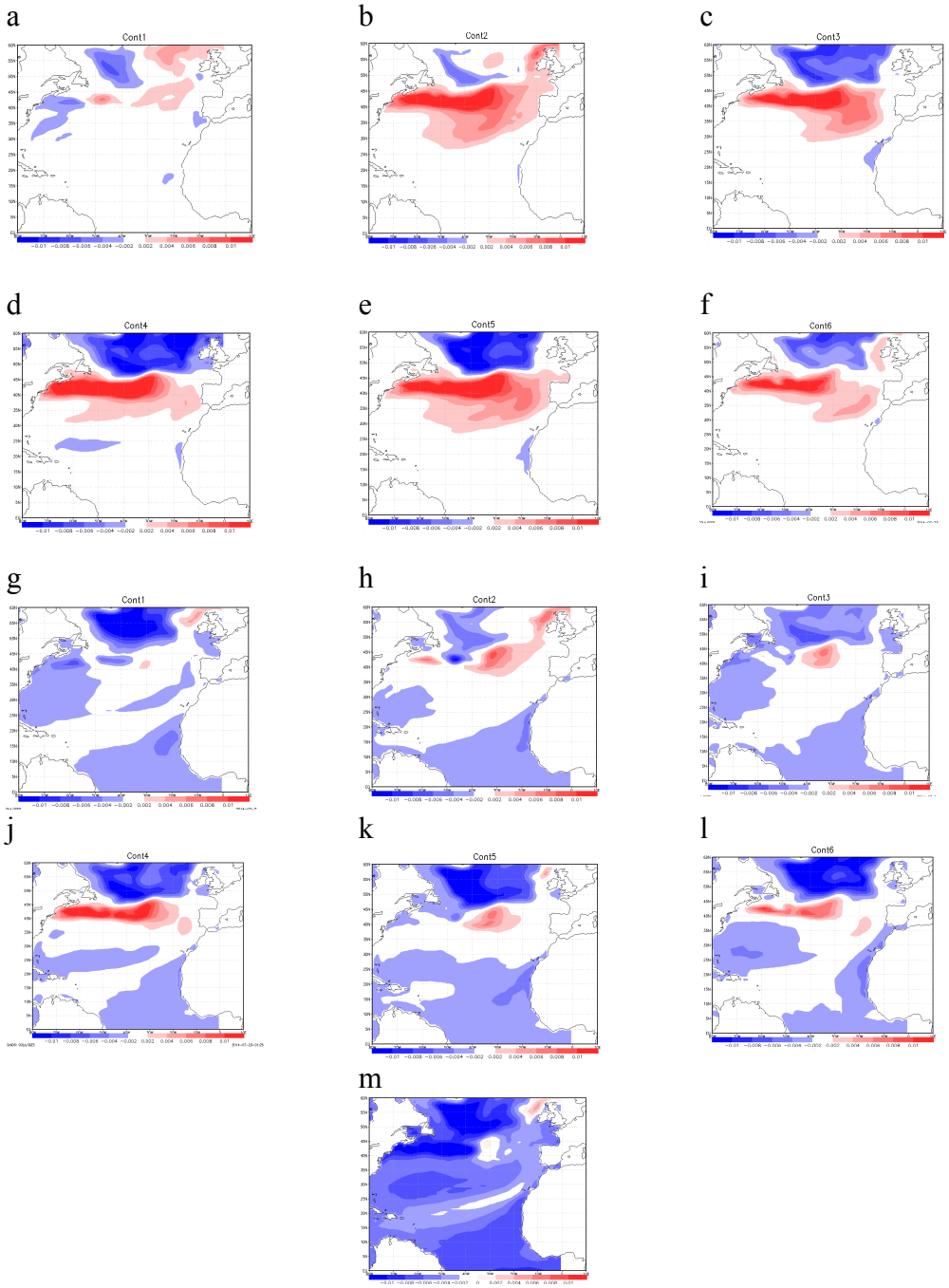

Figure 3.26 Regressions of Internal SST in (a) Cont1,(b) Cont2,(c) Cont3,(d) Cont4, (e) Cont5 and (f) Cont6 onto its respective internal AMOC index. Regressions of total SST in (g) Cont1,(h) Cont2,(i) Cont3,(j) Cont4, (k) Cont5 and (l) Cont6 and (m) External Control_ens onto the AMOC external index. Units degC/Sv.

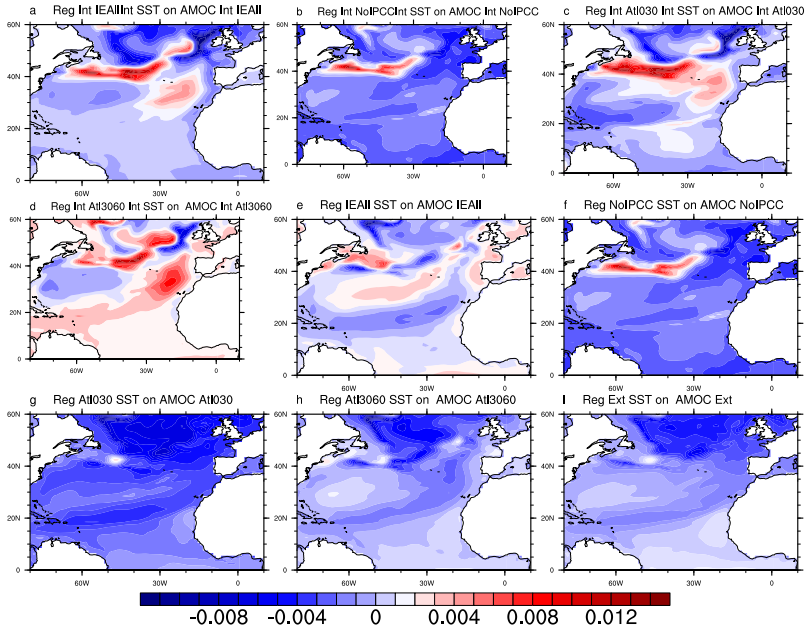

Figure 3.27 Regressions of internal SST in (a) IEAll, (b) IENoIpcc ,(c)IE030 (d) IE3060 onto its respective AMOC index. Regressions of total SST in (e) IEAll,(f) IENoIpcc ,(g)IE030 (h) IE3060 and (i) External IE (IEnn) onto its respective AMOC index. Units degC/Sv.

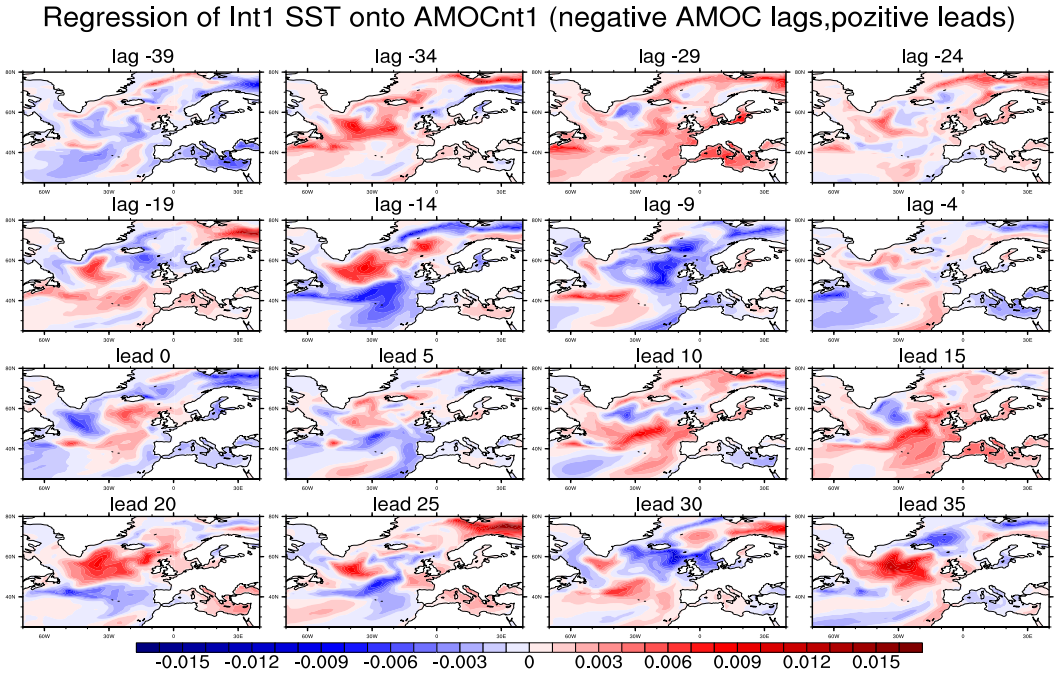

Figure 3.28 Lead-Lag regressions of Internal SST in Cont1 onto the AMOC index in Cont1. Starting with lag 0 (years). The AMOC mode is leading for positive values and lagging for negative. Units degC/Sv.

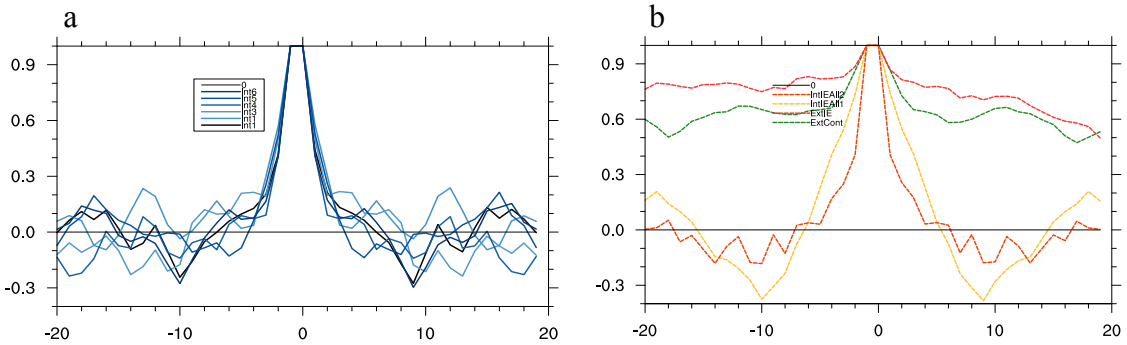

Figure 3.29 (a) Lead-Lag regressions of internal AMOC onto itself in Control (balck) and each Control Ensemble member in blue and (b) Lead-Lag regressions of AMOC onto itself ExtCont1 (green), ExtIE (red), IntIEAll (yellow) and IntIEAll2 (orange). Units Sv/Sv.

a

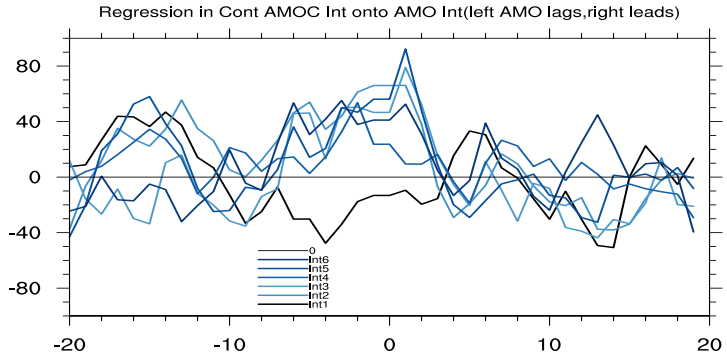

b

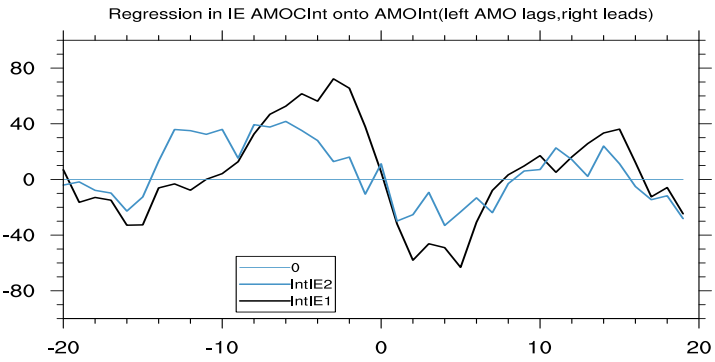

Figure 3.30 Lead-Lag regressions of internal AMV onto AMOC in (a) Control (black) and each Control Ensemble member in blue and (b) IEAll and IEAll_Cont2 black and blue respectively. The AMOC is leading to the left and lagging to the right. Units degC/Sv.

References

Barsugli, J.J. and D.S. Battisti, 1998: The basic effects of atmosphere-ocean thermal coupling on midlatitude variability. *J. Atmos. Sci.* , **55**, 477-93.

Battisti, D. S. and A. C. Hirst, 1989: Interannual variability in the tropical atmosphere/ocean system: Influence of the basic state, ocean geometry and non-linearity. *J. Atmos. Sci*., **46**, 1687-1712.

Bjerknes, J., 1964: Atlantic air-sea interaction. *Advanc. Geophys*., H. E. *Landsberg and J.V. Mieghem, Eds., Academic Press*, **10**, 1-82.

Bretherton, C. S. and D. S. Battisti, 2000: An interpretation of the results from atmospheric general circulation models forced by the time history of the observed sea surface temperature distribution. *Geophys. Res. Lett.*, **27**, p. 767-770.

Cahalan RF, Wharton LE, Wu M-L (1996) Empirical orthogonal functions of monthly precipitation and temperature over the United States and homogenous stochastic models. *J Geo-phys Res* 101(D21):26309–2631

Carton, J.A., and B. Huang, 1994: Warm events in the tropical Atlantic. *J. Phys. Oceanogr.*, **24**, 888-903.

Cessi, P., 2000: Thermal feedback on wind stress as a contributing cause of climate variability. *J. Climate*, **13**, 232-244.

Chen, H., E. K. Schneider, B. P. Kirtman, and I. Colfescu, 2013: Evaluation of weather noise and its role in climate model simulations. *J. Climate*, **26**, 3766-3784, DOI: 10.1175/JCLI-D-12-00292.1.

Colfescu, I., E. K. Schneider, and H. Chen, 2013: Consistency of 20th century sea level pressure trends as simulated by a coupled and uncoupled GCM. *Geophys. Res. Lett.,* 40, 3276–3280, doi:10.1002/grl.50545

Collins, W. D., C. M. Bitz, M. L. Blackmon, G. B. Bonan, C. S. Bretherton, J. A. Carton, P. Chang, S. C. Doney, J. J. Hack, T. B. Henderson, J. T. Kiehl, W. G. Large, D. S. McKenna, B. D. Santer, and R. D. Smith (2006a), The Community Climate System Model version 3 (CCSM3), *J. Clim,* 19, 2122-2143, doi: http://dx.doi.org/10.1175/JCLI3760.1.

Collins, W. D., P. J. Rasch, B. A. Boville, J. J. Hack, J. R. McCaa, D. L. Williamson, and B. P. Briegleb (2006b), The formulation and atmospheric simulation of the Community Atmosphere Model version 3 (CAM3), *J. Clim*, 19, 2144-2161

Copsey, D., R. Sutton, and J. Knight (2006), Recent trends in sea level pressure in the Indian Ocean region, *Geophys. Res. Lett*. 33, L19712, doi: 10.1029/2006GL027175.

Czaja, A., and Frankignoul, C., 1999: Influence of North Atlantic SST on the atmospheric circulation. *Geophys. Res. Lett*., **26**, 2969–2972.

Czaja, A, and C. Frankignoul, 2002: Observed impact of Atlantic SST anomalies on the North Atlantic Oscillation. *J. Climate*., **15**, 606–623.

Czaja, A. and J. Marshall, 2000: On the interpretation of AGCMs response to prescribed time-varying SST anomalies. *Geophys. Res. Lett.*, **27**, 1927-1930

Czaja, A. and J. Marshall, 2001: Observations of atmosphere-ocean coupling in the North Atlantic. *Quart. J. Roy. Meteor. Soc*., **127**, 1893-1916.

Czaja, A., and C. Frankignoul, 1999: Influence of the North Atlantic SST on the atmospheric circulation. *Geophys. Res. Letters*, 26, 2969-2972.

DelSole, T., M. K. Tippett, and J. Shukla, 2011: A significant component of unforced multidecadal variability in the recent acceleration of global warming. *J. Clim*., 24, 909–926.

Delworth, T. L., S. Manabe, and R. J. Stouffer, 1993: Interdecadal variations of the thermohaline circulation in a coupled ocean-atmosphere model. *J. Climate*, **6**, 1993-2011.

Delworth, T. L., 1996: North Atlantic variability in a coupled ocean-atmosphere model. *J. Climate*, **9**, 2356-2375.

Delworth, T. L., and R. J. Greatbatch, 2000: Multidecadal thermohaline circulation variability driven by atmospheric surface flux forcing. *J. Climate*, **13**, 1481–1495.

Delworth, T. L. and M. E. Mann, 2000: Observed and simulated multidecadal variability in the Northern Hemisphere. *Climate Dyn*., **16**, 661-676.

Delworth, T. L., R. Zhang, and M. E. Mann, 2007: Decadal to centennial variation of the Atlantic from observations and models. *Ocean Circulation: Mechanisms and Impacts*. *Geophys. Monogr*. **173**, pp. 131-148. DOI 10.1029/173GM10

Deser, C. and M. L. Blackmon, 1993: Surface climate variations over the North Atlantic Ocean during winter: 1900-1989. *J. Climate*, **6**, 1743-1753.

Deser, C., A. Phillips, V. Bourdette, and H. Teng (2012), Uncertainty in climate change projections: the role of internal variability, *Clim. Dyn.,* 38, 527-546, doi:10.1007/s00382-010-0977-x.

Dong, B.-W. and R. T. Sutton, 2002a: Variability in North Atlantic heat content and heat transport in a coupled ocean-atmosphere GCM. *Climate Dyn.*, **19**, 485-497.

Dong, B.-W., and R. T. Sutton, 2002: Adjustment of the coupled ocean–atmosphere system to a sudden change in the Thermohaline Circulation, *Geophys. Res. Lett.*, **29**(15), 1728, 4 pp.

Enfield, D. B., A. M. Mestas-Nuñez, and P. J. Trimble, 2001: The Atlantic Multidecadal Oscillation and its relation to rainfall and river flows in the continental US. *Geophys. Res. Lett.*, **28,** 2077–2080

Fan, M., 2008: Low Frequency North Atlantic SST Variability: Weather Noise Forcing and Coupled Response. *PhD. thesis, George Mason University*. 205 pp.

Fan, M. and E. K. Schneider, 2011: Observed decadal North Atlantic tripole SST variability. Part I: Weather noise forcing and coupled response. *J. Atmos. Sci.*, COLA Technical Report 307 version.

Fan, Meizhu, Edwin K. Schneider, 2012: Observed Decadal North Atlantic Tripole SST Variability. Part I: Weather Noise Forcing and Coupled Response. *J. Atmos. Sci*., 69, 35–50. doi: http://dx.doi.org/10.1175/JAS-D-11-018.1

Farneti,R.,Vallis K. G.,2009 : Mechanisms of interdecadal climate variability and the role of ocean–atmosphere coupling,*Climate Dyn.*, **10**, 485-498

Ferreira, D. and C. Frankignoul, 2005: The transient atmospheric response to midlatitude SST anomalies. *J. Climate*, **18**, 1049-1067.

Ferreira, D., C. Frankignoul, and J. Marshall, 2001: Coupled ocean-atmosphere dynamics in a simple midlatitude climate model. *J. Climate*, **14**, 3704-3723.

Folland, C. K., Palmer, T. N. & Parker, D. E. ,1986 : Sahel rainfall and the worldwide sea temperatures : 1901-85, *Nature* **320,** 602–607.

Frankcombe, L. M., H. A. Dijkstra, and A. von der Heydt, 2009: Noise-Induced Multidecadal Variability in the North Atlantic: Excitation of Normal Modes. *J. Phys. Oceanogr.*, **39**, 220–233.

Frankcombe L.M.,2010: The Atlantic Multidecadal Oscillation in Models and Observations. *Ph.D Dissertation*, University of Utrecht,127 pp.

Frankignoul, C. and K. Hasselmann, 1977: Stochastic climate models. Part II: Application to sea-surface temperature variability and thermocline variability. *Tellus*, **29**, 289-305.

Frankignoul, C., P. Müller, and E. Zorita, 1997: A simple model of the decadal response of the ocean to stochastic wind forcing. *J. Phys. Oceanogr.*, **27**, 1533-1546.

Frankignoul, C., 1999: A cautionary note on the use of statistical atmospheric models in the middle latitudes: Comments on‘‘Decadal variability in the North Pacific as simulated by a hybrid coupled model.’’*J. Climate*,12,1871–1872

Ghil, M., 2002: Natural climate variability, in *Encyclopedia of Global Environmental Change, volume 1*, edited by T. Munn, M. C. MacCracken, and J. S. Perry, Wiley.

Giannini, A., Saravanan, R. & Chang, P., 2003 : Oceanic forcing of Sahel rainfall on interannual to interdecadal time scales, *Science* **302,**102–1030.

Griffies, S. M. and E. Tzipermann, 1995 A linear thermohaline oscillator driven by stochastic atmospheric forcing. *J. Climate*, **8**, 2440-2453.

Grötzner, A., M. Latif, and T. P. Barnett, 1998: A decadal climate cycle in the North Atlantic Ocean as simulated by the ECHO coupled GCM. *J. Climate*, **11**, 831-847.

Häkkinen, S., 2001: Variability in sea surface height: A qualitative measure for the meridional overturning in the North Atlantic, *J. Geophys. Res.*, **106**, 13,837–13,848, doi:10.1029/1999JC000155.

Hasselmann, K., 1976: Stochastic climate models. Part I: Theory. *Tellus*, **28**, 473-485.

Hazeleger W and S. S. Drijfhout SS, 1999: Stochastically forced mode water variability. *J. Phys Oceanogr.*, **29**, 1772-1786.

Held, I. M., T. L. Delworth, J. Lu, K. L. Findell, and T. R. Knutson, 2005: Simulation of Sahel drought in the 20th and 21st centuries. *Proceedings of the National Academy of Sciences*, 102(50), 17891-17896

Hilmer R, M. Harder, and P. Lemke, 1998: Sea ice transport: a highly variable link between Arctic and North Atlantic. *Geophys. Res. Lett.*, **25**, 3359-3362.

Holland, M. M., C. M. Bitz, M. Eby, and A. J. Weaver, 2001: The Role of Ice–Ocean Interactions in the Variability of the North Atlantic Thermohaline Circulation. *J. Climate*, **14**, 656–675.

Horel, J. D., and J. M. Wallace, 1981: Planetary-scale atmospheric phenomena associated with the Southern Oscillation. *Mon.Wea. Rev.,*109,813–829

Hu, Z.-Z., and B. Huang, 2006: Physical processes associated with tropical Atlantic meridional SST gradient. *J. Climate*, **19**, 5500-5518.

Hurrell, J.W., Y. Kushnir, M. Visbeck, and G. Ottersen, 2003: An overview of the North Atlantic Oscillation. *The North Atlantic Oscillation: Climate Significance and Environmental Impact,Eds. Geophys. Monogr.*, **134**, pp. 1-35.

Hurrell, J. W., and Coauthors, 2006: Atlantic Climate Variability and Predictability: A CLIVAR Perspective. *J. Climate*, **19**, 5100–5121. doi: 10.1175/JCLI3902.1

Joyce, T. M., C. Frankignoul, J. Yang, and H. E. Phillips, 2004: Ocean response and feedback to the SST dipole in the tropical Atlantic. *J. Phys. Oceanogr.,* **34,** 2525–2540.

Jungclaus, J.H., H. Haak, M. Latif, and U. Mikolajewicz, Arctic-North Atlantic interactions and multidecadal variability of the Meridional Overturning Circulation, *J. Climate*, **18**, 4013-4031, 2005.

Kaplan, A., M. A. Cane, Y. Kushnir, and A. C. Clement, Analysis of global sea surface temperatures 1856-1991, *J. Geophys. Res.*,103, 18,567-18,589, 1998.

Kirtman, B. P., and J. Shukla, 2002: Interactive coupled ensemble: A new coupling strategy for CGCMs. *Geophys. Res. Lett.*, **29**, 17-20.

Kirtman, B. P., D. M. Straus, D. Min, E. K. Schneider, and L. Siqueira, 2009: Toward linking weather and climate in the interactive ensemble NCAR climate model. *Geophys. Res. Lett*., **36**, L13705, DOI:10.1029/2009GL038389.

Kirtman, B. P., E. K. Schneider, D. M. Straus, D. Min, and R. Burgman, 2011: How weather impacts the forced climate response. *Climate Dyn*., **37**, 2389-2416. DOI 10.1007/s00382-011-1083-3

Knight, J. R., C. K. Folland, and A.A. Scaife, Climatic impacts of the Atlantic Multidecadal Oscillation, *Geophys. Res. Lett*., **33**, L17706.

Kushnir, Y. and I. M. Held, 1996: Equilibrium atmospheric response to North Atlantic SST anomalies. *J. Climate*, **9**, 1208-1220.

Latif, M., 1998: Dynamics of interdecadal variability in coupled ocean-atmosphere models. *J. Climate*, **11**, 602-624.

Latif, M., E. Roeckner, M. Botzet, M. Esch, H. Haak, S. Hagemann, J. Jungclaus, S. Legutke, S. Marsland, U. Mikolajewicz, and J. Mitchell, 2004: Reconstructing, monitoring, and predicting multidecadal-scale changes in the North Atlantic thermohaline circulation with sea surface temperature, *J. Climate*, **17**, 1605-1614.

Leith,C.E. (1973) :The Standard Error of time-average estimates of climatic means, *J.Appl.Meteor*.,1 2,1066-1069

Mann, M. E. and J. Park, 1996: Joint spatiotemporal modes of surface temperature and sea level pressure variability in the northern hemisphere during the last century. *J. Climate*, **9,** 2137-2162

Marshall, J., H. Johnson, and J. Goodman, 2001: A study of the interaction of the North Atlantic oscillation with ocean circulation. *J. Climate*., **14**, 1399–1421.

Marshall, G.J., 2002: Trends in Antarctic geopotential height and temperature: A comparison between radiosonde and NCEP-NCAR reanalysis data. *J. Climate*, 15, 659-674.

Mehta V. M., M. Suarez, J. Manganello, and T. Delworth, 2000: Oceanic influence on the North Atlantic Observation and associated Northern Hemisphere climate variations: 1959-1993. *Geophys. Res. Lett*., **27**, 121-124.

M. B. Menary, M. B., W. Park, K. Lohmann, M. Vellinga, M. D. Palmer, M. Latif, J. H. Jungclaus, 2011: A multimodel comparison of centennial Atlantic meridional overturning

circulation variability, *Climate Dyn.*

Meng, Q, M. Latif, W. Park, N. S. Keenlyside, V. Semenov and M. Thomas M.(2012), Twentieth Century Walker Circulation Change: Data Analysis and Model Experiments, *Clim. Dyn*, 38 . pp. 1757-1773, doi: 10.1007/s00382-011-1047-8.

Minobe S., A. Kuwano-Yoshida, N. Komori, S.-P. Xie (2008), Small Influence of the Gulf Stream on the troposphere, *Nature*, 452, pp. 206‑20

Monahan, A. H., J. Alexander, and A. J. Weaver, 2008: Stochastic models of the meridional overturning circulation: time scales and patterns of variability. *Phil. Trans. R. Soc. A*, **366**, 2527–2544.

Muñoz, E., B. Kirtman, and W. Weijer, 2011: Varied representation of the Atlantic Meridional Overturning across multidecadal ocean reanalyses, *Deep Sea Research Part II* (in press).

Ottera, O. H., Bentsen, M., Drange, H., and Suo, L. L.: External forcing as a metronome for Atlantic multidecadal variability, *Nat. Geosci*., 3, 688–694, doi:10.1038/NGEO955, 2010.

Palmer, T. N. and Z. Sun, 1985: A modelling and observational study of the relationship between sea surface temperature in the north-west Atlantic and the atmospheric general circulation. *Quart. J. Roy. Meteor. Soc.*, **111**, 947-976.

Panofsky H. A., Wolff P., 1956: Spectrum and Cross Spectrum Analysis of Hemispheric Westerly Index. *Tellus*,Vol 9, No2, DOI: 10.1111/j.2153-3490.1957.tb01873.x

Rabe, B., F. A. Schott, and A. Köhl, 2008: Mean Circulation and Variability of the Tropical Atlantic during 1952–2001 in the GECCO Assimilation Fields. *J. Phys. Oceanogr.*, **38**, 177–192.

Rodwell, M. J., D. P. Rowell, and C. K. Folland, 1999: Oceanic forcing of the wintertime North Atlantic Oscillation and European climate. *Nature*, **398**, 320-324.

Sarachik, E. S., M. Winton, and F. L. Yin, 1996: Mechanisms for decadal-to-centennial climate variability, eds. NATO ASI Series, **44**, 158-210.

Saravanan, R. and J. C. McWilliams, 1998: Advective ocean-atmosphere interaction: An analytical stochastic model with implications for decadal variability. *J. Climate*, **11**, 165-188.

Scaife, A. A., D. Copsey, C. Gordon, C. Harris, T. Hinton, S. Keeley, A. O'Neill, M. Roberts, and K. Williams (2011), Improved Atlantic winter blocking in a climate model, *Geophys. Res. Lett.*, 38, L23703, doi:10.1029/2011GL049573.

Schlesinger, M. E. and N. Ramankutty, 1994: An Oscillation in the Global Climate System of Period 65-70 Years. *Nature*, **367**, 723-726.

Schneider, E. K., and M. Fan, 2007: Weather noise forcing of surface climate variability. *J. Atmos. Sci*., **64**, 3265-3280.

Schneider, E. K. and M. Fan, 2011: Observed decadal North Atlantic tripole SST variability. Part II: Diagnosis of mechanisms. *J. Atmos. Sci,*. COLA Technical Report 308 version.

Schneider, E. K., Bengtsson L. and Hu, Z. Z. (2003), Forcing of Northern Hemisphere climate trends, *J. Atmos. Sci*., 60, 1504–1521, doi:10.1175/1520-0469

Schneider, E. K., and M. Fan, (2007): Weather noise forcing of surface climate variability. *J. Atmos. Sci*., 64, 3265-3280.

Seager, R., Y. Kushnir, M. Visbeck, N. Naik, J. Miller, G. Krahmann, and H. Cullen, 2000: Causes of Atlantic Ocean climate variability between 1958 and 1998, *J. Climate,* **13***,* 2845-2862.

Solomon, A., J. P. McCreary, R. Kleeman, and B. A. Klinger, 2003: Interannual and decadal variability in an intermediate coupled model of the Pacific region. *J. Climate*, **16**, 383-405.

Sutton, R. T. and D. L. R. Hodson, 2003: Influence of the ocean on North Atlantic climate variability 1871–1999. *J. Climate*, **16**, 3296–3313

Te Raa, L. A. and H.A. Dijkstra, 2002: Instability of the Thermohaline Ocean Circulation on Interdecadal Timescales. *J. Phys. Oceanogr.*, **32**, 138–160.

Thompson, D. W. J., and J. M. Wallace, 2000: Annular modes in the extratropical circulation. Part I: Month-to-month variability. *J. Climate,* 13, 1000-1016.

Trenberth, K. E., G. W. Branstator, D. Karoly, A. Kumar, N. Lau, and C. Ropelewski, 1998: Progress during TOGA in understanding and modeling global teleconnections associated with tropical sea surface temperatures, *J. Geophys. Res*.,103,14 291–14 324.

Vecchi,G. A., B. J. Soden, A. T. Wittenberg, I. M. Held, A. Leetmaa and M. J. Harrison, (2006), Weakening of tropical Pacific atmospheric circulation due to anthropogenic forcing, *Nature,* 441, 73-76, doi:10.1038/nature04744

Weng, W. and J. D. Neelin, 1998: On the role of ocean-atmosphere interaction in midlatitude interdecadal variability**,** *Geophys. Res. Lett.*, **25**, 167-170.

Wu, L., and Z. Liu, 2002: Is tropical Atlantic variability driven by the North Atlantic Oscillation? *Geophys. Res. Lett.* **29**(13), 1653

Wu, Z., E. K. Schneider, and B. P. Kirtman, 2004: Causes of low frequency North Atlantic SST variability in a coupled GCM. *Geophys. Res. Lett.*, **31**, L09210, doi:10.1029/2004GL019548.

Zhang, Rong, Thomas L. Delworth, 2005: Simulated Tropical Response to a Substantial Weakening of the Atlantic Thermohaline Circulation. *J. Climate*, **18**, 1853–1860.

Zhang, R., and T. L. Delworth, 2006 : Impact of Atlantic multidecadal oscillations on India/Sahel rainfall and Atlantic hurricanes, *Geophys. Res. Lett.*, 33, L177 doi:10.1029/2006GL026267.

Zorita, E. and C. Frankignoul, 1997: Modes of North Atlantic decadal variability in the ECHAM/LSG coupled ocean-atmosphere general circulation model. *J. Climate*, **10**, 183-200.

BIOGRAPHY

I grew up in Bucharest (Romania) but I always spent every summer in the foothills of the Carpathian Mountains in a remote village called Cosminele. The summers spent there are the most beautiful memories of my childhood and the Romanian countryside it's been the first place that thought me to observe nature and weather (I was particularly fascinated by heavy summer and winter storms which I still love so much to this day).

In the elementary school the geography as well as natural sciences were thought as a long series of dull arrays of numbers and names therefore I never saw the link between what I loved about weather and what I was thought in class. However because of love of the subject and admiration for my teacher, I decided in the early years of my primary school that I'll become a teacher/Professor of Mathematics. In 2001 I started my B.Sc at the Faculty of Mathematics of University of Bucharest and graduated in 2006.I started my masters after my graduation from the B.Sc and in 2008 I received my master in Mathematics and Mechanics from the same university.

While participation in a Summer School in ICTP, Trieste Italy I met a group of atmospheric scientists – Professors from the department of Atmospheric Oceanic and Earth Sciences at George Mason University. I thought that applying my knowledge of mathematics to Atmospheric Sciences would be the most exciting and beautiful thing I could do for the next few years and started my PhD at George Mason in 2008. I now look forward in continuing my research in this field and of course, as the initial plan was, one day be a Professor.